

N 69 38608

**NASA TECHNICAL
MEMORANDUM**

Report No. 53942

**CASE FILE
COPY**

NUCLEATE POOL BOILING OF SATURATED FREON 113
IN A REDUCED GRAVITY ENVIRONMENT

By Jerrol Wayne Littles
Astronautics Laboratory

August 22, 1969

NASA

*George C. Marshall Space Flight Center
Marshall Space Flight Center, Alabama*

1. REPORT NO. NASA TM X-53942		2. GOVERNMENT ACCESSION NO.		3. RECIPIENT'S CATALOG NO.	
4. TITLE AND SUBTITLE Nucleate Pool Boiling of Saturated Freon 113 In a Reduced Gravity Environment				5. REPORT DATE August 22, 1969	
				6. PERFORMING ORGANIZATION CODE	
7. AUTHOR(S) Jerrol Wayne Littles				8. PERFORMING ORGANIZATION REPORT #	
9. PERFORMING ORGANIZATION NAME AND ADDRESS George C. Marshall Space Flight Center Marshall Space Flight Center, Alabama 35812				10. WORK UNIT NO.	
				11. CONTRACT OR GRANT NO.	
12. SPONSORING AGENCY NAME AND ADDRESS				13. TYPE OF REPORT & PERIOD COVERED NASA Technical Memorandum	
				14. SPONSORING AGENCY CODE	
15. SUPPLEMENTARY NOTES Work performed by Astronautics Laboratory, Science and Engineering Directorate					
16. ABSTRACT <p>Pool boiling of Freon 113 was investigated in a body force field less than standard gravity using the four-second drop tower at Marshall Space Flight Center (MSFC). Emphasis was placed on the behavior of the nucleate portion of the pool boiling curve. The growth and departure of individual bubbles was also investigated.</p> <p>A transient calorimeter technique was used to obtain boiling curve information. This technique allowed the use of a heater of sufficient size to eliminate the problem of heater geometry influencing the boiling behavior while avoiding the necessity of achieving steady state during the short drop time available.</p> <p>The results of the study indicate that the location of the pool boiling curve is a function of both acceleration level and surface orientation. Individual bubble departure diameters were predicted reasonably well by existing theories. However, the growth rate equations available in the literature did not predict the behavior of the Freon 113 bubbles. A new calculation procedure was developed which gave growth rates in agreement with the experimental data.</p>					
17. KEY WORDS			18. DISTRIBUTION STATEMENT STAR Announcement <i>J. Wayne Littles</i> J. Wayne Littles		
19. SECURITY CLASSIF. (of this report) U		20. SECURITY CLASSIF. (of this page) U		21. NO. OF PAGES 178	22. PRICE

TABLE OF CONTENTS

	Page
SUMMARY	1
INTRODUCTION	3
Statement of the Problem.....	3
Literature Survey.....	5
EXPERIMENTAL APPARATUS	23
Test Facility.....	23
Test Package	24
Test Container	33
Test Specimen	36
Instrumentation	41
EXPERIMENTAL PROCEDURES	47
Standard Gravity Boiling Curves	47
Bubble Tests.....	49
Nucleate Boiling Tests-Predrop and Reduced Gravity..	49
EXPERIMENTAL RESULTS AND ANALYSIS	53
Bubble Growth Rate Data	53
Comparison of Bubble Growth Rate Data With Existing Theory and With a Proposed Calculation Procedure ..	57
Coalescence of Bubbles.....	75
Bubble Departure Diameters.....	81
Reduced Gravity Nucleate Boiling Data.....	81
Standard Gravity Nucleate Boiling Data	98
Comparison of Nucleate Boiling Data with Previous Data and Existing Theories.....	102
SUMMARY AND CONCLUSIONS.....	113

Preceding Page Blank

TABLE OF CONTENTS (Concluded)

	Page
APPENDIX A - EXPERIMENTAL DATA	117
APPENDIX B - ERROR ANALYSIS	163
Heat Flux	163
Surface Temperature	167
Bubble Diameters	167
APPENDIX C - FROUDE NUMBER CALCULATION	169
REFERENCES	171

LIST OF ILLUSTRATIONS

Figure	Title	Page
1.	Heat Flux Versus Superheat for Liquid Hydrogen at One-g and Zero-g	7
2.	Boiling Heat Transfer to Liquid Nitrogen at One g and Reduced g	8
3.	Saturated Nucleate Pool Boiling of Water at 1 atm in Standard and Low Gravity	10
4.	Effect of Gravity Upon Pool Boiling	13
5.	Variation of Boiling Curve with Surface Orientation . . .	16
6.	View of Aeroshield	25
7.	External View of Catch Tube	26
8.	Internal View of Catch Tube	27
9.	View of Test Package Inside Aeroshield	28
10.	Test Package Mounted on Balancing Platform	29
11.	View of Top Floor of Test Package	30
12.	Typical Nozzle Calibration Curve	32
13.	Test Container Mounted on Package	34
14.	View of 2 × 2 In. Heater Plate and Nichrome Heating Wire	38
15.	View of 2 × 2 In. Heater Plate After Heating Element and Thermocouples Were Installed	38
16.	View of 2 × 2 In. Test Heater	39

LIST OF ILLUSTRATIONS (Continued)

Figure	Title	Page
17.	View of 2 × 4 In. Test Heater	39
18.	Calibration System for Test Heater Thermocouples . . .	43
19.	Photographic Arrangement.	45
20.	Block Diagram of Electrical System	46
21.	Sequence of Operations for a Typical Test	51
22.	One g Bubble Growth Data	56
23.	Low g Bubble Growth Data	58
24.	Comparison of 1g and Low g Bubble Diameters at 0.02 g.	59
25.	Calculation of Bubble Growth Rates for Pool Boiling of Saturated Freon 113	61
26.	Bubble Growth Model	64
27.	Reduced Gravity Data Compared with Theories	70
28.	One g Data Compared with Theories	72
29.	Comparison of Low g Data of Schwartz With Theory	73
30.	Coalescence of a Small Bubble by a Larger Bubble Growing on a Horizontal Surface	76
31.	Coalescence of a Bubble Growing on a Horizontal Surface by a Bubble Moving Away from the Surface.	78
32.	Bubbles Growing and Sliding Up a Vertical Surface	79

LIST OF ILLUSTRATIONS (Continued)

Figure	Title	Page
33.	Bubble Coalescence on a Vertical Surface at a Heat Flux Near the Incipient Point.	80
34.	Comparison of Observed Bubble Departure Diameters with Theory	82
35.	Comparison of Standard Gravity and Reduced Gravity for Horizontal Heated Face Up - Test 10F32, Thermocouple No. 4	84
36.	Comparison of Standard Gravity and Reduced Gravity for Horizontal Heated Face Down - Test 10F34, Thermocouple No. 2	85
37.	Comparison of Standard Gravity and Reduced Gravity for Horizontal Surface.	87
38.	Comparison of Standard Gravity and Reduced Gravity for Vertical Heated Surface	88
39.	Comparison of Temperature Gradient at Standard Gravity and Reduced Gravity for Vertical Heater.	90
40.	Difference in Enthalpy Change Rate Between Reduced Gravity and Standard Gravity Versus $T_w - T_{sat}$ for Horizontal Heated Surface Facing Downward.	93
41.	Enthalpy Change Rate Difference of Figure 40 Added to Standard Gravity Boiling Curve	94
42.	Difference in Enthalpy Change Rate Between Reduced Gravity and Standard Gravity Versus Time from Release.	95
43.	Difference in Enthalpy Change Rate Between Reduced Gravity and Standard Gravity Versus Time from Heater Power Turn Off	97
44.	One g Boiling Results Versus Orientation.	99

LIST OF ILLUSTRATIONS (Concluded)

Figure	Title	Page
45.	One g Boiling Results Versus Orientation	100
46.	Comparison of Standard Gravity Data for Heaters	101

DEFINITION OF SYMBOLS

a	Acceleration
a'	Constant defined in text
A	Area of heater surface
A_b	Area occupied by base of bubble
A_m	Imaginary surface area of bubble extending below heated surface
A_s	Surface area of bubble
A_w	Cross-sectional area of wire
A_δ	Surface area of bubble in contact with thermal layer
c	Specific heat
D_d	Bubble diameter
f	Bubble frequency
g	Standard gravitational acceleration
GR_r	Grashof number
h	Heat transfer coefficient
H	Heater enthalpy
I	Current
k	Thermal conductivity
L	Length of heater

DEFINITION OF SYMBOLS
(Continued)

L_w	Length of wire
l	Thermal layer thickness defined by equation (4)
M	Mass of heater surface
Nu_r	Nusselt number
P_l	Pressure of liquid
Pr	Prandtl number
P_v	Pressure of vapor
q_b	Heat flux in Zuber analysis
q_c	Heat transfer through cap of bubble
q_l	Heat flux from thermal layer
q_s	Heat flux from wall to vapor
q_w	Heat flux from wall to microlayer
q_{wire}	Heat leak through wire
R	Bubble radius
\dot{R}	Bubble growth rate
r_c	Nucleation cavity radius
t	Time
t_p	Heater thickness
T	Temperature

DEFINITION OF SYMBOLS
(Concluded)

T_s	Saturation temperature
T_{tc}	Thermocouple temperature
T_w	Wall temperature
T_∞	Bulk fluid temperature
U	Velocity
V	Bubble volume
V_h	Heater voltage
W	Width of heater
α	Thermal diffusivity
δ	Thermal layer thickness
Θ_w	$T_w - T_\infty$
Θ_{bt}	Temperature of bubble - T_∞
Θ_{sat}	$T_s - T_\infty$
λ	Heat of vaporization
ν	Viscosity
ρ_l	Density of liquid
ρ_v	Density of vapor
σ	Surface tension
φ	Contact angle

TECHNICAL MEMORANDUM X-53942

NUCLEATE POOL BOILING OF SATURATED FREON 113
IN A REDUCED GRAVITY ENVIRONMENT

By

Jerrold Wayne Littles

SUMMARY

The effects of surface orientation and reduced gravity on nucleate boiling of saturated Freon 113 at one atmosphere of pressure were investigated. Reduced gravity was obtained by using a drop tower at the Marshall Space Flight Center (MSFC) with a free-fall distance of 294 feet which resulted in approximately 4 seconds of free-fall time. Two test heaters, one 2 inches wide and 4 inches long and one 2 inches wide and 2 inches long, made of 0.063 inch thick copper were used to investigate the nucleate portion of the pool boiling curve at heat fluxes from 5,500 BTU/hr-ft² to 21,500 BTU/hr-ft² and at an acceleration level of 0.01 g. High-speed motion picture coverage at approximately 400 frames per second was employed with a heater 2 inches wide and 4 inches long to study bubble growth rates and bubble departure diameters for isolated bubbles and to investigate bubble coalescence during the heat transfer tests.

The location of the nucleate boiling curve was found to be dependent on acceleration level and on the orientation of the surface with respect to the acceleration vector. At an acceleration level of 0.01 g, the boiling curve shifted upward for the heated surface in the horizontal position with the heated face upward and shifted downward for the vertical surface and the horizontal surface with the heated face downward. The magnitude of the downward shift was less for the vertical surface than for the horizontal surface with the heated face downward. The magnitude of the changes for the boiling curve decreased as the heat flux was increased. At standard gravity the efficiency of the boiling mechanism increased as the surface was rotated from the horizontal heated face upward to the vertical position and then increased again as the surface was rotated from the vertical position to the horizontal heated face downward position.

Bubble growth rates in saturated Freon 113 at atmospheric pressure were found to be poorly predicted by existing theories. A new calculation procedure was outlined that used some recent data on the thermal layer thickness and the nature of bubbles growing on a heated surface and which assumed that the bubble grows through the thermal layer. The new calculation procedure predicted the growth rates of bubbles in Freon 113 better than existing theories and also predicted growth rates for bubbles growing on a heated surface at reduced gravity in saturated water quite well.

A large variation was seen in bubble departure diameters at reduced gravity. In general, the departure diameters were between the values predicted by Fritz and by Zuber. Several types of bubble coalescence were discussed. The coalescence of bubbles sliding up a vertical surface at reduced gravity produced large vapor accumulations near the surface, and it was surmised that this vapor accumulation was the cause of the decrease in heat transfer coefficient for the vertical surface at reduced gravity. The heat transfer coefficient was increased for the horizontal surface with the heating face upward in reducing the acceleration level from 1 g to 0.01 g. A reduction in acceleration level to near zero and the resulting increased vapor accumulation might cause a reversal of this trend.

INTRODUCTION

Statement of the Problem

As a result of the interest in space flight during the past decade, researchers have focused attention on the behavior of the pool boiling curve when subjected to force fields other than the standard gravity force field normally encountered in earth-bound systems. Space vehicles in flight or in orbit about the earth, or other planets, experience effective accelerations considerably lower than the gravity force encountered on earth. Proper design of the various systems associated with such space vehicles requires an understanding of the influences of low gravity on the physical mechanisms likely to be encountered during their operation. One of these mechanisms is pool boiling. Most investigators in the area have considered the problem of the effects of reduced gravity levels, while a few investigators have concerned themselves with the effects of increased accelerations on the pool boiling curve.

Due to the low heat flux levels associated with some systems currently being planned for space missions, the nucleate boiling region of the pool boiling curve is of particular interest. The purpose of this work is to investigate further the behavior of this region at reduced gravity levels.

Although there have been investigations in this region, much of the data are questionable with regard to application to general engineering surfaces due to the size and configuration of the surfaces used in the investigations.

The objective of the present work is to eliminate questions concerning the effect of the size of the test specimen by employing a heater whose surface area is large with respect to the bubbles produced both at standard gravity and at reduced gravity. Prior investigations have also left some doubt about the influence of the acceleration vector with respect to the surface orientation, and an effort was made to eliminate this variable by changing the orientation of the surface from test to test. It should be noted that some investigators have assumed by using surfaces such as small wires and spheres, that either the orientation variable was negligible, or that if a shift in the boiling curve occurred it would be in the same direction for any orientation. The results of this investigation suggest that these assumptions are subject to question.

In addition to the primary objective of investigating the behavior of the nucleate boiling region, it was desirable to observe the behavior of individual bubbles and the interaction of groups of bubbles. In order to accomplish this, high-speed motion pictures were taken of bubble formation.

Literature Survey

Introductory Comment

Considerable research has been done in the area of nucleate pool boiling heat transfer during recent years and much of it is applicable to the current effort. Due to the amount of material available, it seems impractical to review all of it here; instead, only that material directly applicable to this research will be discussed, and the reader is referred to Reference 1 for a more complete review of the general field.

Reduced Gravity Investigations

One of the earliest attempts to detect an influence of reduced gravity on the nucleate boiling region of the pool boiling curve was reported by Usiskin and Siegel [2, 3]. Their test specimen consisted of 0.0453 inch diameter platinum wires and flat nickel ribbons up to 0.2 inch wide and 0.010 inch thick. Tests were conducted using a 9 foot drop tower which produced reduced gravity time of approximately 0.7 second. Water was used as the test fluid. The authors could not detect a shift in the boiling curve. However, they noted that the instrumentation could not detect a temperature shift of the heated surfaces of less than 6 °F and this could represent a significant shift in the nucleate boiling region. Perhaps a stronger objection to the tests is that the size of the test section is approximately the same as the bubbles at reduced gravity levels in water as reported by Schwartz [4].

Sherley [5] conducted tests both with a 1 second drop tower and using a KC-135 aircraft at reduced gravity times of approximately 15 seconds. The test fluid was liquid hydrogen and the test specimen was a horizontal thin film of lead deposited on an insulating material. The heated surface was in an upward position and had an effective area of 2 square inches. There was a fairly large statistical scatter for both standard gravity and reduced gravity. A least-squares curve fitted through each set of data indicated a slight upward shift in the boiling curve (Figure 1).

Merte and Clark [6] conducted tests in a 1.4 second drop tower using liquid nitrogen as a test fluid. Test specimen for these tests were 1 inch and 1/2 inch copper spheres. In order to avoid the problems of reaching steady state during the drop time available, the authors treated the spheres as dynamic calorimeters and produced a boiling curve by monitoring the temperature history of the sphere as it cooled in liquid nitrogen. The resulting data indicated an insignificant shift of the boiling curve at reduced gravity. In contrast to the work of Sherley [5], the indicated direction of the shift was downward (Figure 2). The primary objection to this data is that, since the heater was a sphere, no preferred orientation of the acceleration vector with respect to the test surface existed. This seems to assume that if there is a shift in the boiling curve with reduced gravity level it will be in the same direction for all orientations of the surface with respect to the acceleration vector. The effects of this assumption will be discussed in more detail as the results of the present investigation are presented.

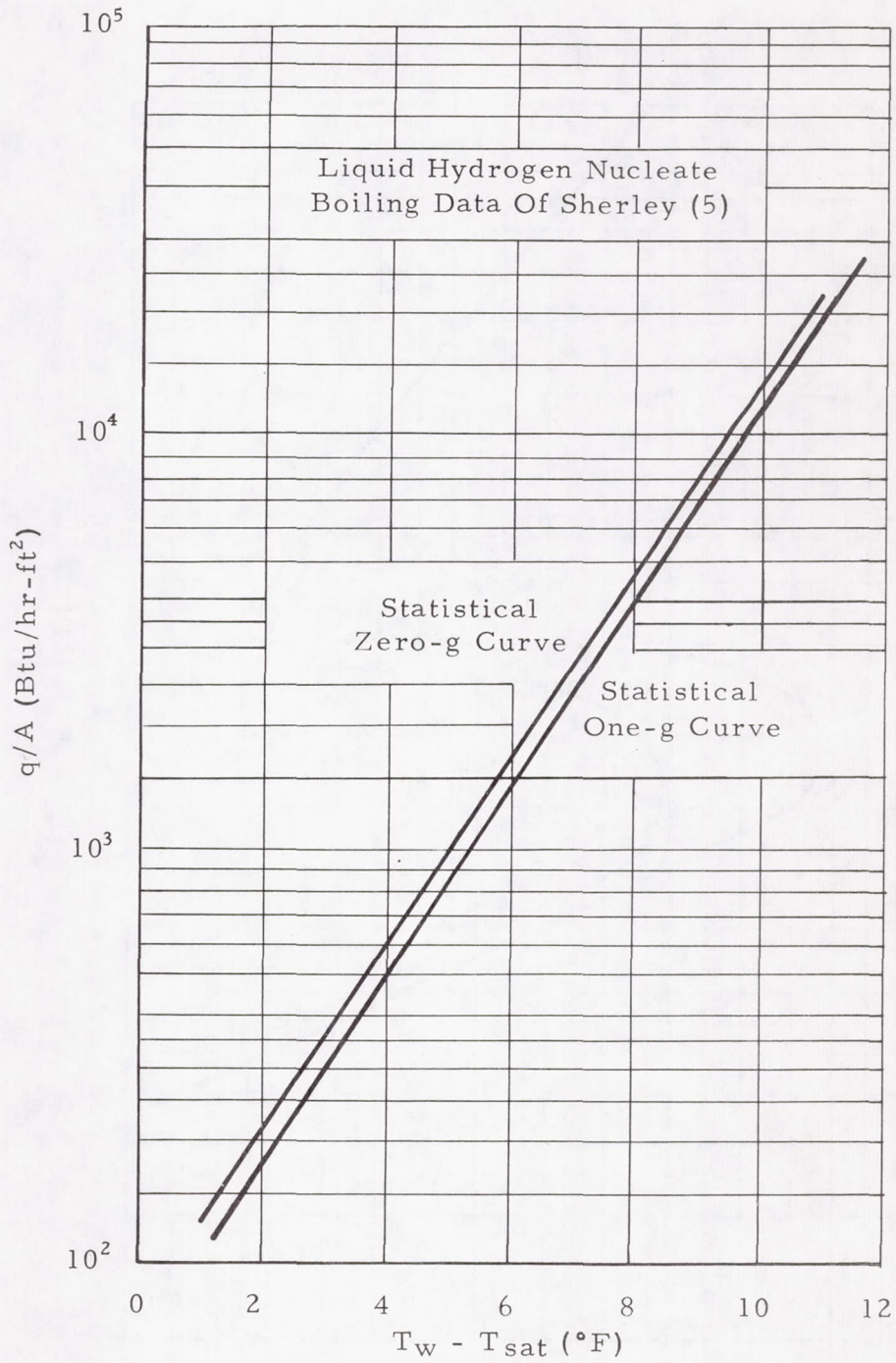


FIGURE 1. HEAT FLUX VERSUS SUPERHEAT FOR LIQUID HYDROGEN AT ONE-g AND ZERO-g [SHERLEY (5)]

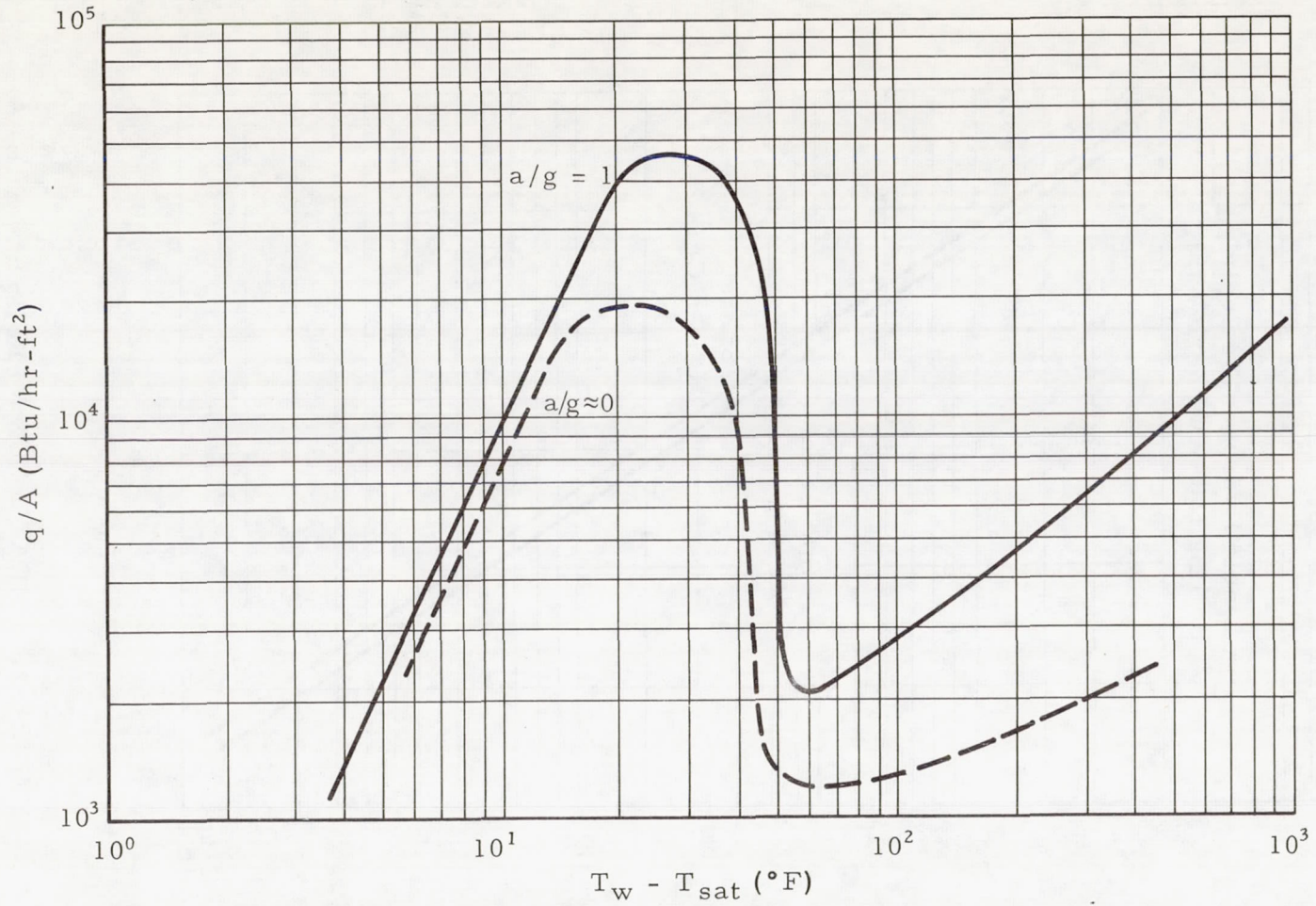


FIGURE 2. BOILING HEAT TRANSFER TO LIQUID NITROGEN AT ONE g AND REDUCED g [MERTE AND CLARK (6)]

Clodfelter [7] has conducted reduced gravity tests for water using a 1.8 second drop tower. The test specimen included horizontal 0.02 inch platinum wires and 1/8 inch and 1/4 inch platinum ribbons. A decrease in the test heater temperature of approximately 4 °F was seen in the heat flux range of 1.28×10^4 to 6.87×10^4 BTU/hr-ft², and this represents an upward shift of the boiling curve. A similar study was conducted by Siegel and Keshock [8] using horizontal and vertical wires, 0.0197 inch in diameter, with similar results. It was noted in the study of Siegel and Keshock, however, that the direction of shift of wire temperature was upward for vertical wires. As was the case with the test specimen of Usiskin and Siegel, the size of the test surfaces for the work of Clodfelter and Siegel and Keshock was approximately the same as the bubbles at reduced gravity.

Schwartz [4] has used an Aero Commander aircraft to obtain reduced gravity times of 8 to 10 seconds to study nucleate boiling of water. The test heater was a horizontal ribbon 0.25 inch wide and 2.75 inches long. The ribbon was insulated on one side and the heated surface faced upward. The author concludes that no significant shift of the boiling curve was seen. The combined low gravity and standard gravity data presented in Figure 3, however, suggest an upward shift of the curve. As was the case with some of the previous investigations, one dimension of the heater was approximately the same size as the bubbles at reduced gravity.

Hedgepeth and Zara [9] conducted tests using water and a vertical tube as the heater surface. The reduced gravity time of approximately

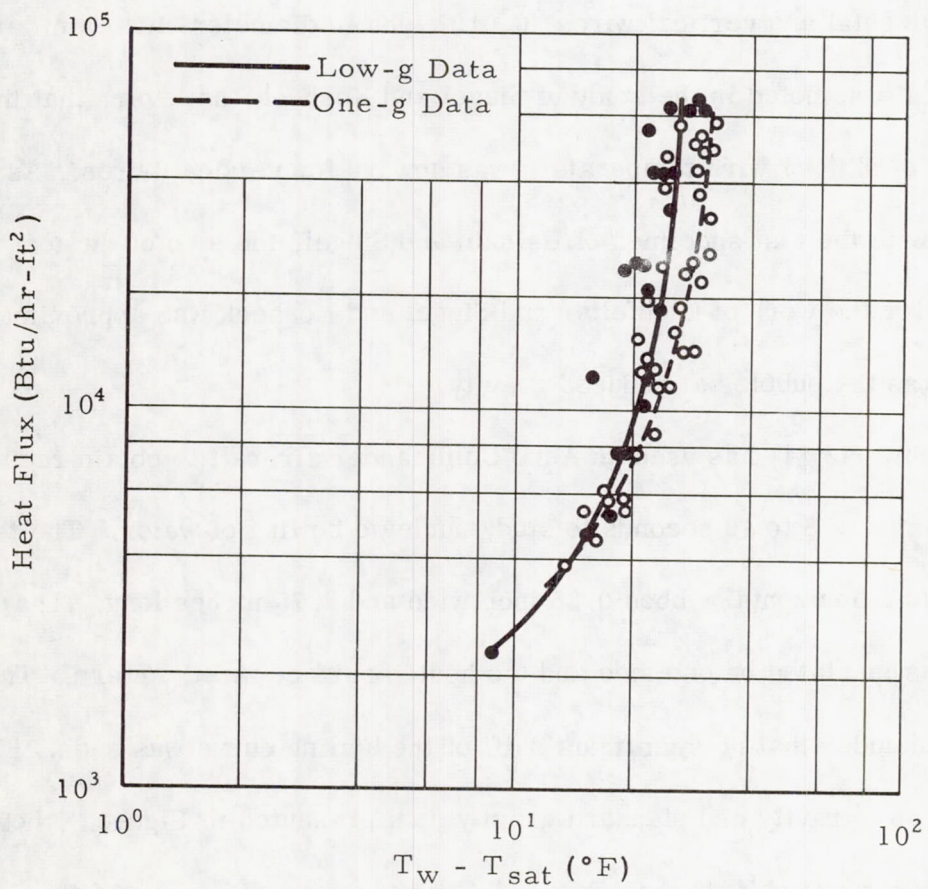


FIGURE 3. SATURATED NUCLEATE POOL BOILING OF WATER AT 1 atm IN STANDARD AND LOW GRAVITY [SCHWARTZ (4)]

15 seconds was produced with a KC-135 aircraft. Due to the relative size of the test heater and the test container and the amount of vapor produced, the pressure of the system increased with time during the tests. The result was a system which was subjected to varying amounts of subcooling during a test. The authors declined to advance any conclusions with regard to an increase or decrease of boiling coefficients in reduced gravity.

Rex and Knight [10] conducted a reduced gravity boiling experiment with propane in a heated spherical tank 25.4 centimeters in diameter. Reduced gravity was produced for approximately 4 minutes by use of a ballistic missile. As was the case with the tests of Hedgepeth and Zara [9], the pressure increased with time during the test and there is some question regarding the comparison of their data with constant pressure standard gravity data. According to the data presented by the authors, the tank pressure increased from approximately 125 psig to approximately 250 psig over a 4-minute test period. In addition, the authors compared their data to 1-g data taken by other investigators for another heater, and since the shape of the boiling curve is known to be sensitive to the heater surface condition, this is questionable. The authors concluded that, for the same value of $T_w - T_{sat}$, the heat flux at reduced gravity was approximately 1/3 of the value seen by other investigators at standard gravity.

Papell and Faber [11] used a magnetic field to produce low gravity in normal heptane with a horizontal ribbon 1/16 inch wide and 1 inch long. The technique used eliminates some of the objections connected with drop tower

or aircraft tests in that steady-state conditions can be obtained. Using this system, a decrease of approximately 5 ° F was observed at the incipient point between standard gravity and reduced gravity for the horizontal strip with the heated surface in the upward position.

Increased Acceleration Investigations

A few investigations have been conducted to determine the effect of high accelerations on pool boiling, and these investigations yield valuable information in explaining the overall effect of acceleration level on the pool boiling mechanism. Four investigations have been conducted where the increased acceleration was directed toward the heated surface. Three investigations, those of Graham and Hendricks [12], Merte and Clark [13], and Costello and Tuthill [14], were conducted using water as a test fluid. The other investigation was that of Graham, Hendricks, and Ehlers [15] using hydrogen as a test fluid. The results of the tests using water all indicated that in the lower portion of the nucleate boiling region (Merte and Clark established an upper limit of approximately 50,000 BTU/hr-ft²) the boiling curve was shifted upward with an increase in acceleration. After that point, Merte and Clark found that the effect of acceleration was not as pronounced, but that a downward shift of the curve was indicated. The data provided by Costello and Tuthill were in the latter region and verified the downward shift quite well (Figure 4). Graham, Hendricks and Ehlers [15] concluded that for liquid hydrogen, acceleration has little effect on the nucleate boiling region.

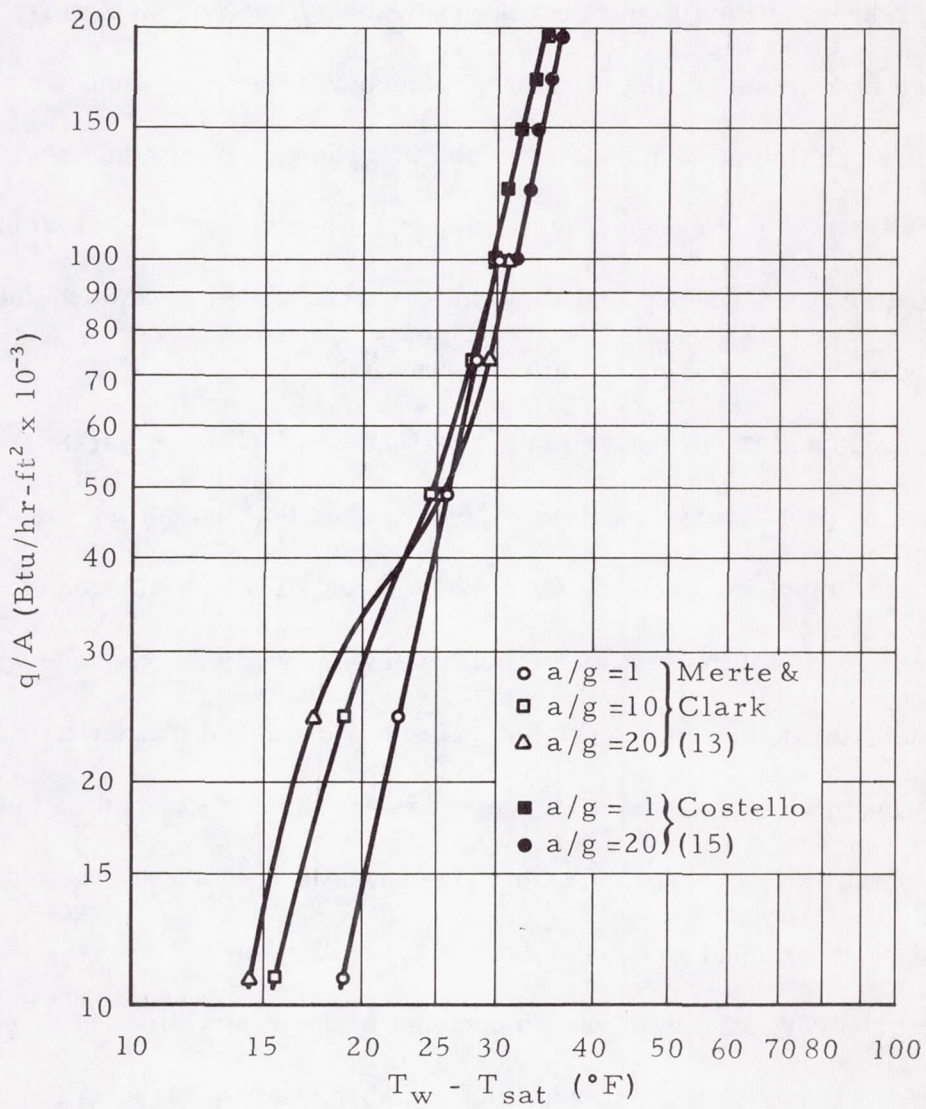


FIGURE 4. EFFECT OF GRAVITY UPON POOL BOILING

Standard Gravity Investigations

The influence on the boiling curve at standard gravity of surface orientation with respect to the acceleration vector has been investigated by a few researchers. Githinji and Sabersky [16] studied the effects of surface orientation in nucleate boiling of isopropyl alcohol. They found that the boiling curve shifted upward as the surface was changed from a horizontal facing upward to a vertical position. However, when the horizontal facing upward heater was turned so that the heating surface faced downward, the opposite was true and the curve shifted downward.

Marcus and Dropkin [17] have investigated the effect of surface orientation on pool boiling in water. They reported that the boiling heat transfer coefficient increased as the surface orientation was changed from horizontal to vertical in the nucleate boiling region, while the opposite was true in the saturated convection region. The authors noted that the number of nucleating sites was substantially decreased as the angle of inclination to the horizontal was increased. Coeling [18] investigated boiling in liquid hydrogen and also found an upward shift in the boiling curve between the horizontal and vertical positions. In contrast to the observations of Marcus and Dropkin, however, an increase in the number of sites was seen for the vertical surface. It was also noted by Coeling that at high heat fluxes the horizontal surface had the higher heat transfer coefficient.

Class, Dehann, Piccone, and Cost [19] investigated both the effects of orientation and surface condition on the nucleate boiling region for liquid

hydrogen. They learned that for a smooth surface, an upward shift of the boiling curve was seen as the surface was changed from horizontal to a 45-degree inclination and then to the vertical orientation. For a greased surface, the shift was in the same direction but more pronounced (Figure 5). When the smooth surface was roughened with emory paper, however, the heat transfer coefficient decreased as the surface was rotated from horizontal to vertical. This last set of data contradicts the trend seen by other investigators.

Bubble Growth Rate Investigations

Since the mechanism of energy removal in the nucleate boiling region must ultimately be connected to the growth of bubbles, the ability to predict bubble growth rates is of fundamental importance. Attempts to predict the growth rates of bubbles fall into two primary categories. The first category makes the fundamental assumption that the bubble is growing in an infinite fluid with no surface present, while the second assumes that the bubble grows on a heated surface. The latter group of theories is of primary interest, but the first group will also be reviewed.

One of the first to predict the growth rates of bubbles was Bosnjakovic [20], who investigated the case of a bubble growing in a superheated liquid. The growth process was assumed to be supported by vaporization at the bubble interface due to energy transport from the superheated fluid. Experimental verification was obtained for this theory by Jacob [21].

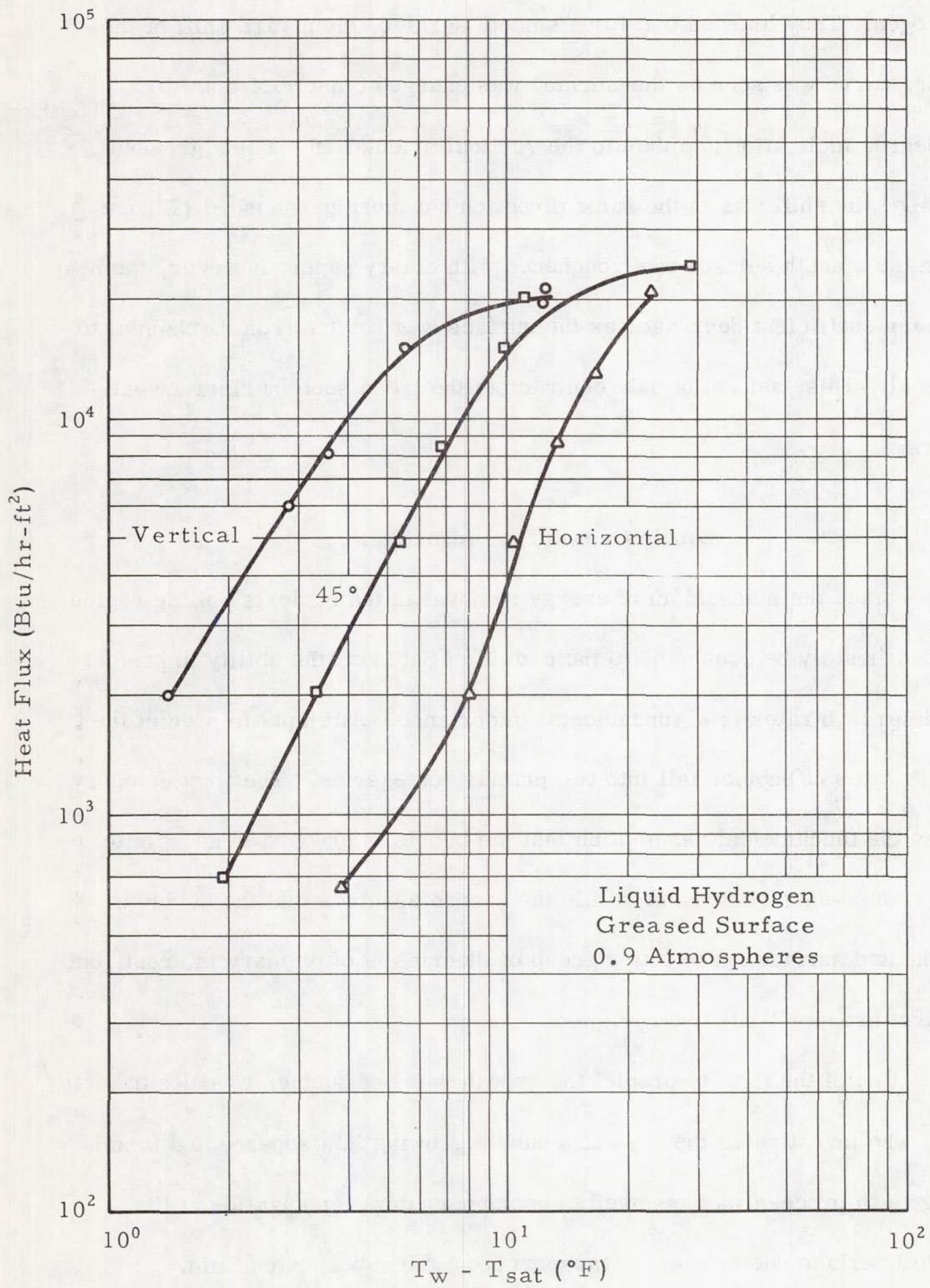


FIGURE 5. VARIATION OF BOILING CURVE WITH SURFACE ORIENTATION [CLASS (19)]

Fritz and Ende [22] used the same basic model as Bosnjakovic and treated the heat transfer through the boundary of the bubble as being similar to one dimensional transient conduction. The equation obtained for bubble growth was

$$R = \frac{2 k (T_{\infty} - T_s)}{\lambda \rho_v \sqrt{\pi \alpha}} t^{\frac{1}{2}} \quad (1)$$

Fritz and Ende presented data which showed agreement with their theory. Other investigators have found varying degrees of agreement with the theory. Siegel and Keshock [23] reported good agreement for bubbles growing on a heated surface in saturated water at reduced gravity levels. Schwartz [4] reported good agreement at low values of $T_w - T_{\infty}$ with less agreement at higher values. Where there was disagreement, the Fritz and Ende equation produced bubble diameters which were too large in the latter growth stages. Schwartz's data were for pool boiling of saturated water at both 1 g and for low g.

Plesset and Zwick [24] included the effects of liquid inertia and surface tension by formulation of the problem from Rayleigh's equation of motion, the energy equation, and the Clausius-Clapeyron equation. It was learned that the inertia and surface tension were not important and that the growth equation reduced to one which differed from the Fritz and Ende equation by $\sqrt{3}$. The lack of agreement with the previously cited experimental data is obvious since the resulting growth rate is larger than that produced by the

Fritz and Ende relation. However, Dergarabedian [25] found that the Plesset and Zwick equation agree quite well with data which he obtained with superheated water at 1 g, and Hewitt and Parker [26] found that their data for growth of bubbles in superheated liquid nitrogen were correlated quite well by the equation. The bubbles observed in the experiments of Dergarabedian and Hewitt and Parker were not on a heat transfer surface but were observed in the bulk liquid. Dergarabedian used gas impurities for nucleation sites and radiant energy was used to heat the liquid. Hewitt and Parker generated their bubbles with an electrical heater and viewed them as they grew or collapsed in superheated or subcooled liquid nitrogen after they had moved from the generating surface into the fluid.

Forster and Zuber [27], in a formulation similar to that of Plesset and Zwick, verified the insignificance of the inertia and surface tension terms and obtained an expression which differs from the Fritz and Ende equation by $\pi/2$. It is explained by Zuber [28] that the primary difference between the above three relationships is that the Fritz and Ende equation treats the conduction through the bubble wall as a one-dimensional cartesian problem, while the other two account for the sphericity of the bubble.

Griffith [29] assumed a laminar flow field, constant properties in the fluid surrounding a growing bubble, and that the energy input to the bubble wall by conduction was responsible for vaporization. In addition, he assumed an initial linear temperature distribution through the superheated layer on the surface and that the bubble was hemispherical and attached to a heated

surface. The computer solution developed by Griffith from the above assumptions agreed with the experimental results of Dergarabedian. It would seem that the agreement is fortuitous, however, since the conditions of Dergarabedian's experiments are not the same as the boundary conditions used in the Griffith analysis.

Bankoff and Mikesell [30] have used the same basic model of Plesset and Zwick, but have varied the assumptions regarding the temperature distribution surrounding the vapor bubble.

Zuber [28] has examined the case of a bubble growing on a heated surface. Zuber's analysis extended the theory Bosnjakovic to include the rate of growth for a bubble growing in a nonuniform temperature field. The analysis assumes that the equation for bubble growth can be obtained by the addition of a term which accounts for the heat transfer to the bulk liquid. The equation is then

$$\dot{R} = \frac{1}{\lambda \rho_V} \left[\frac{k (T_\infty - T_S)}{\sqrt{\pi \alpha t}} - q_b \right] \quad (2)$$

The value of q_b was assumed to be the heat transfer rate from the heating surface. Even though this is a drastic assumption, as pointed out by Zuber, it predicted the experimental data of Zmola for pool boiling of saturated water quite well when the value predicted by equation (2) was multiplied by $\pi/2$ in order to account for sphericity.

In order to remove Zuber's major assumptions, Hsu and Graham [31] derived a growth rate equation which includes the heat flux from the base of the bubble and calculates the energy exchange between the vapor bubble and the thermal layer surrounding it. It was assumed that all energy input to the bubble caused vaporization and bubble growth. In addition, it was assumed that the thermal layer surrounds the bubble during its entire growth period, has an initial linear profile, and is subjected to a constant temperature, Θ_b , at the liquid-vapor interface. The value used for this temperature was obtained from the Clausius-Clapeyron equation as

$$\Theta_b = \Theta_{\text{sat}} + \frac{2 \sigma T_s}{1.25 r_c \rho_v \lambda} \quad (3)$$

Utilizing these assumptions, the transient cartesian one-dimensional conduction equation was solved to obtain the energy exchange between the vapor and thermal layer. The thermal layer thickness used in the analysis was

$$l = \frac{k \Theta_b}{q_b} + 2 r_c \quad (4)$$

where r_c is the radius of the cavity. As will be shown later, the Hsu and Graham equations are extremely sensitive to the value of r_c chosen. In comparing their experimental data with Zuber's theory and their own, Hsu and Graham found that Zuber's equation fits the data very well, while their

equation with no modification for sphericity agreed with the data in the early growth stage and gave higher values in the latter stage.

Bubble Force Investigations

Forces which act on bubbles during their growth have been calculated by Cochran, Aydelott, and Frysinger [32], Rehm [33], and Keshock and Siegel [34]. These analyses consider the bouyancy, inertia, and pressure unbalance because the bubble is attached to a wall as the primary removal mechanisms and the drag and surface tension forces as the retentive mechanisms. In addition to these forces, the work of McGrew and Larkin [35] has suggested that the retentive force due to the surface tension gradient present around a bubble growing on a heated wall could be large enough to be considered.

Bubble Departure Size Investigations

The first available work on the change in the bubble departure size with gravity level was a qualitative study by Siegel and Usiskin [2]. They photographed vapor removal from horizontal and vertical ribbons in water near the saturation temperature. It was observed that the vapor remained near the heating surface. No bubble measurements were made and the exact acceleration level was not known. Later, Usiskin and Siegel [3] conducted a series of tests using a counterweighted platform so that the effective gravity

level could be determined; these tests were also conducted in water. Measurement of bubble departure diameters showed that the diameters increased with gravity to a $-1/3.5$ exponent, rather than the exponent of $-1/2$ as predicted by Fritz [36]. In another set of experiments for saturated water, Siegel and Keshock [23] found that for cases where the reduced gravity level was greater than 10 percent of standard gravity the departure diameters increased with gravity to a $-1/3$ exponent, while for gravity levels of less than 10 percent of standard the exponent was approximately $-1/2$. In a more recent investigation, with water at gravity levels between 0.01 g and 0.02 g, Schwartz [4] has found that the Fritz equation is valid. An investigation using saturated aqueous-sucrose solutions ranging from 20 to 60 percent sucrose by weight, Keshock and Siegel [34] found no dependence of departure diameter on gravity level. In this case, the bubbles had an inertia force during growth which was much larger than the buoyancy force, and as a result, the buoyancy change with a reduction in gravity level had no effect.

EXPERIMENTAL APPARATUS

The primary objective of this investigation was to determine the effects of reduced gravity level and surface orientation on the nucleate boiling region of the pool boiling curve with a secondary objective of investigating bubble behavior. The test fluid used was saturated Freon 113 at atmospheric pressure.

In the sections which follow, the test facility, test package, test specimen, and the related data acquisition system will be described. The test procedures used to obtain the data will also be discussed.

Test Facility

A drop tower located in the Saturn V Dynamic Test Stand at Marshall Space Flight Center in Huntsville, Alabama was used to obtain the reduced gravity levels. The facility has a free-drop distance of 294 feet, which provides a free-fall time of approximately 4.1 seconds. The basic facility consists of an aeroshield which is held in position by guide rails as it falls to a pneumatic catch tube. The aeroshield is approximately 24 feet long and 7 feet in diameter. The test bay area of the aeroshield is 6 feet 6 inches in

diameter and 8 feet 8 inches high. The aeroshield is equipped with a reverse and direct thruster system and a removable drag plate in order to provide control of the aeroshield displacement versus time. The catch tube consists of a 40-foot orificed cylinder with a 1.5-inch radial clearance between the aeroshield and cylinder wall. The deceleration g level imposed on the aeroshield is approximately 25 times standard gravity. Figures 6, 7, 8, and 9 are views of the aeroshield, catch tube, and the package inside the aeroshield.

The test package, described in detail in the following section, is equipped with a calibrated high-pressure gas thruster system which is used to provide the desired acceleration level. The package thruster is turned on approximately 2 seconds prior to release of the aeroshield. At the time of aeroshield release, the package separates from the aeroshield test bay floor. Ideally, the aeroshield drag plate and thruster system are operated such that, for a given package acceleration level, the package will reposition itself on the test bay floor prior to aeroshield deceleration by the catch tube.

Test Package

Two views of the test package which were used are shown in Figures 10 and 11. The test equipment was mounted on a two floor metal angle framework 3 feet by 3 feet by 30 inches tall. Total weight of the test package was 473 pounds. The major on-board equipment is identified in the figures. The major equipment items carried on board included: (1) a 30-volt alkaline

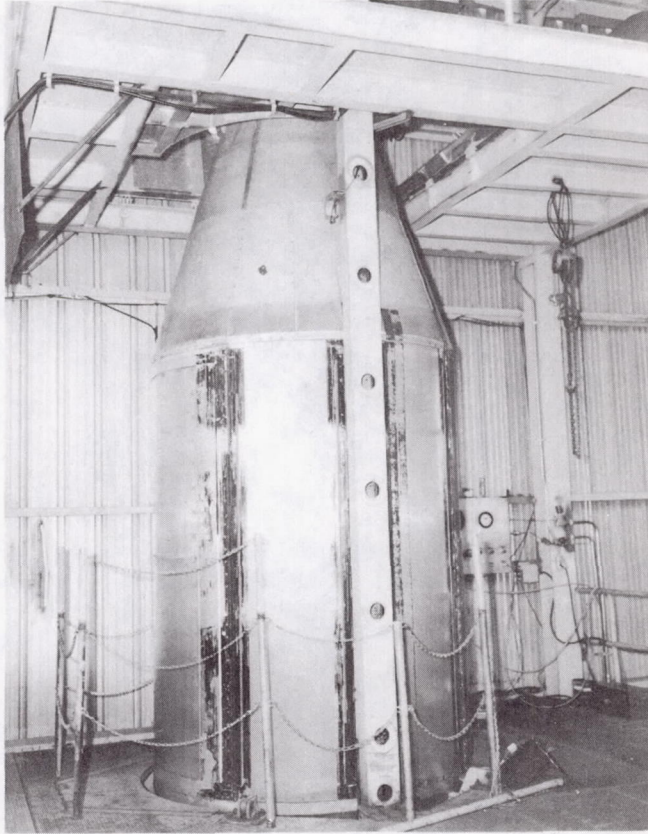


Figure 6. View of Aeroshield



Figure 7. External View of Catch Tube

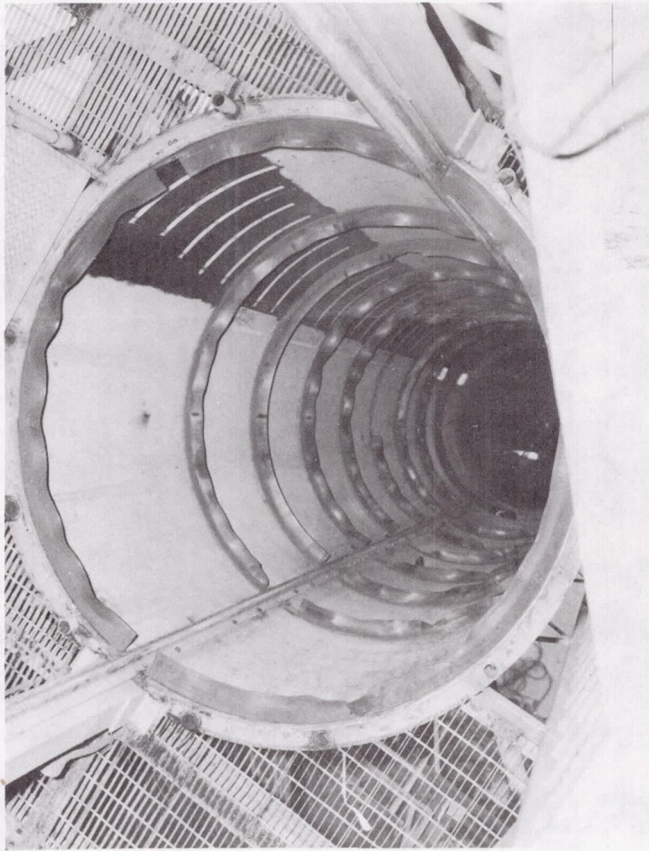


Figure 8. Internal View of Catch Tube



Figure 9. View of Test Package Inside Aeroshield

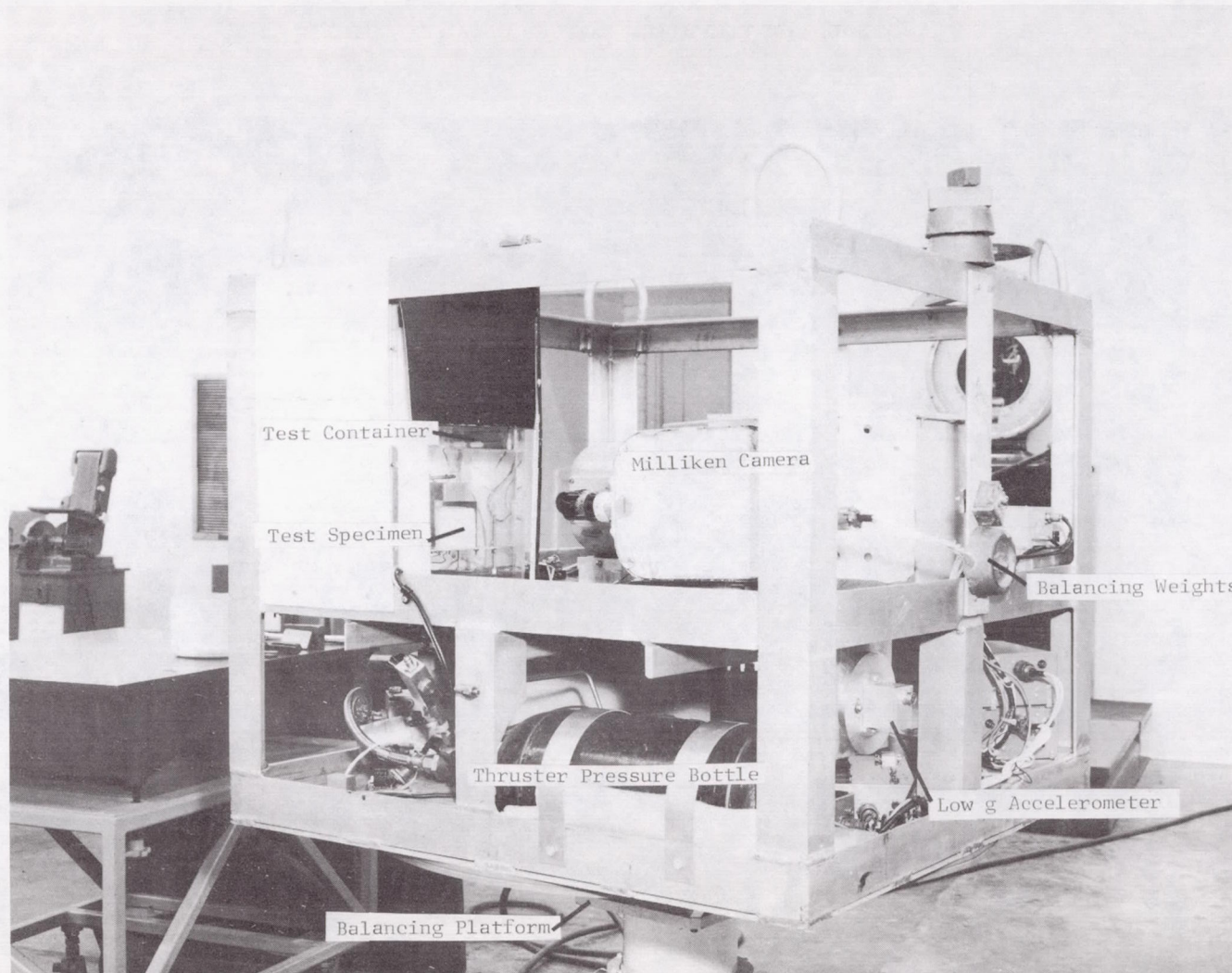


Figure 10. Test Package Mounted on Balancing Platform

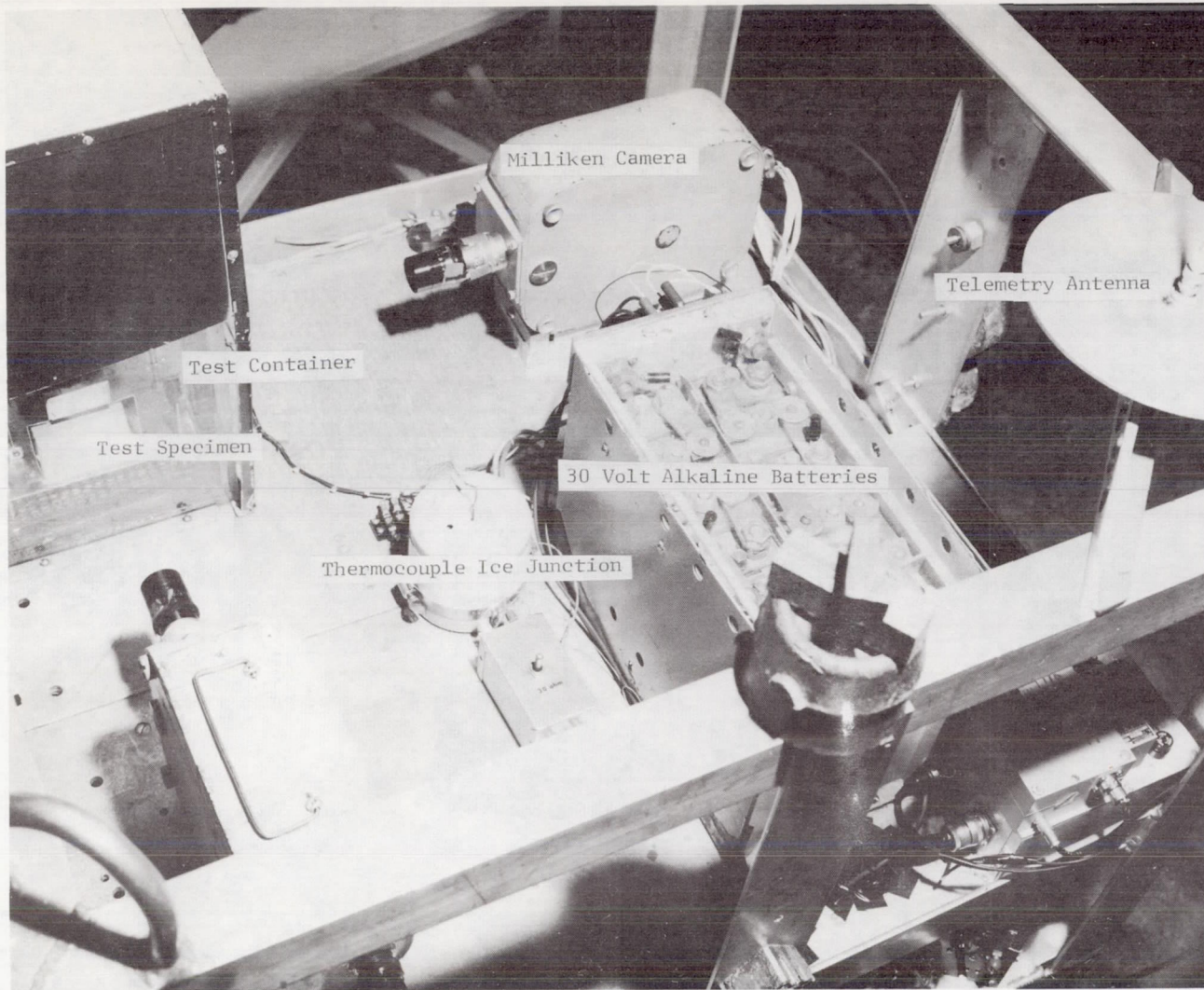


Figure 11. View of Top Floor of Test Package

battery which provided all power during tests, (2) a GN₂ pressure bottle; pressure regulator, and calibrated sonic nozzle for g-level control, (3) two 16-mm high-speed Milliken cameras, (4) a universal timer for control of sequenced operations, (5) high- and low-g accelerometers, (6) a test container which housed the test specimen and its associated equipment, and (7) a telemetry unit and the associated control equipment. The operation of this equipment will be discussed in the following paragraphs.

In order to prevent package rotation during the time that it was separated from the aeroshield floor, it was necessary that the package be balanced about the axis of thrust of the sonic nozzle. A strain gage balancing system had been set up for previous packages tested in the MSFC facility and that system was used for the test package. The view of the test package given in Figure 10 shows the test package mounted on the balancing platform. The instrumentation system associated with the strain-gage system allows the package to be balanced within 0.0625 inch-pounds.

The package thruster nozzle was calibrated under simulated operating conditions by use of a set of balance scales and weights. A typical calibration curve is shown in Figure 12. Prior to each test, the upstream nozzle pressure was set using a Heise Gage (temporarily connected to the system for this purpose), and the upstream pressure regulator to give the desired acceleration level during the test. The acceleration level monitored by the low-g accelerometer during the test usually fell within 10 percent of the predicted value. As an additional check, a pressure transducer was installed upstream

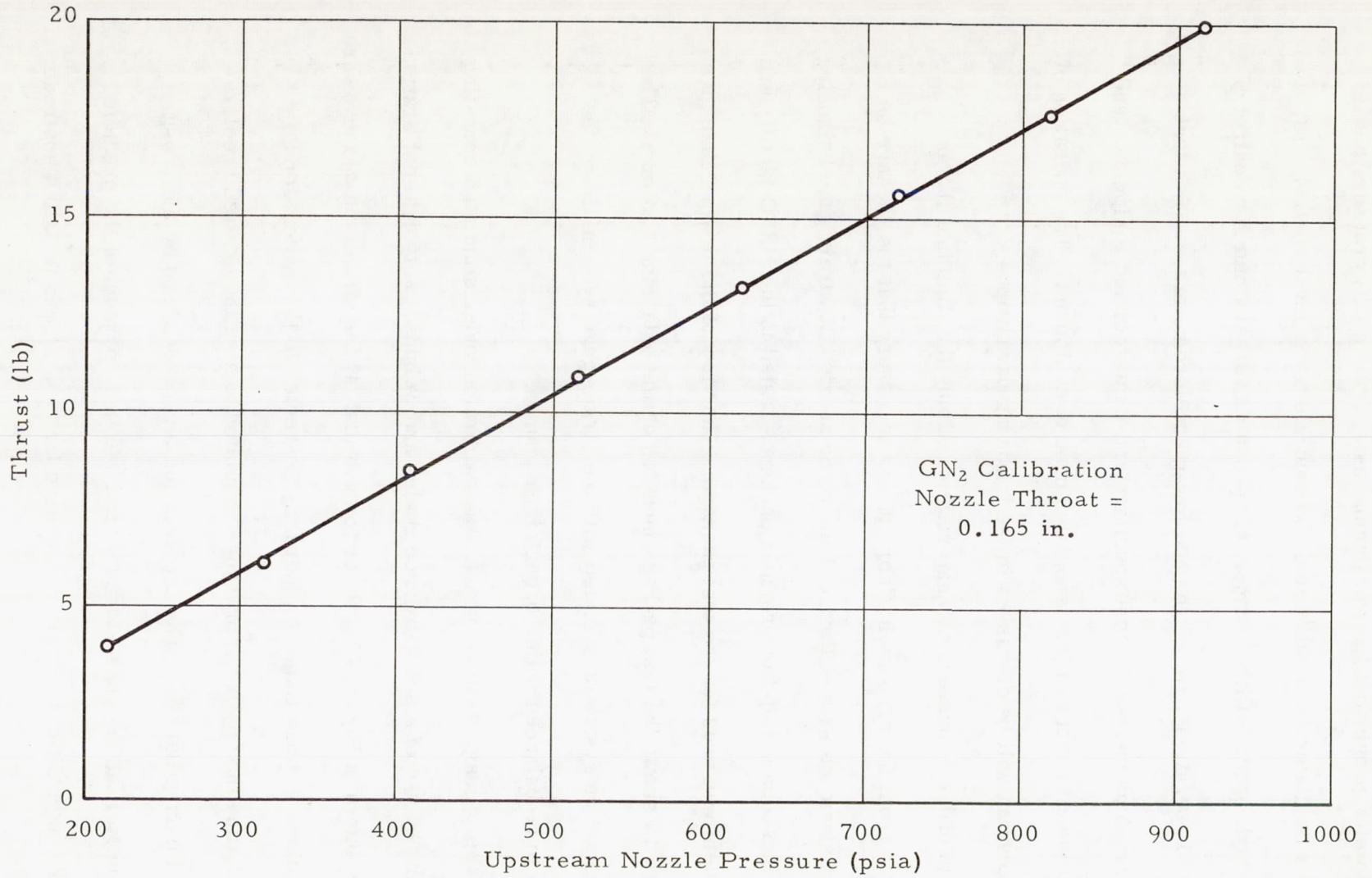


FIGURE 12. TYPICAL NOZZLE CALIBRATION CURVE

of the nozzle and the pressure was monitored through the telemetry system during the test. Operation of the thruster system was controlled by a solenoid valve in the upstream pressure line which was actuated through the universal timer.

Test Container

Figure 13 is a photograph of the test container mounted on the package. The container is 8 inches wide, 9 inches long, and 10 inches high. It is made of 1/2-inch-thick plexiglass for viewing purposes. The container lid is provided with a vent to keep the fluid inside the container at atmospheric pressure.

A 200-watt preheater was installed in the bottom of the tank to bring the Freon 113 to saturation temperature initially. During tests, the energy dissipated by the test specimen was sufficient to maintain the fluid at the saturation temperature. An option was available for the power source for the auxiliary heater. It could be run by the on-board batteries or by an externally powered AC-DC converter. The converter was not a part of the test package.

The test specimen was mounted on support rods attached to the bottom of the container when the heater was tested in the horizontal position with the heated face either upward or downward. Adapters were made which could be fastened to two of the support rods and then to the test specimen support plate for testing the heater in the vertical position.

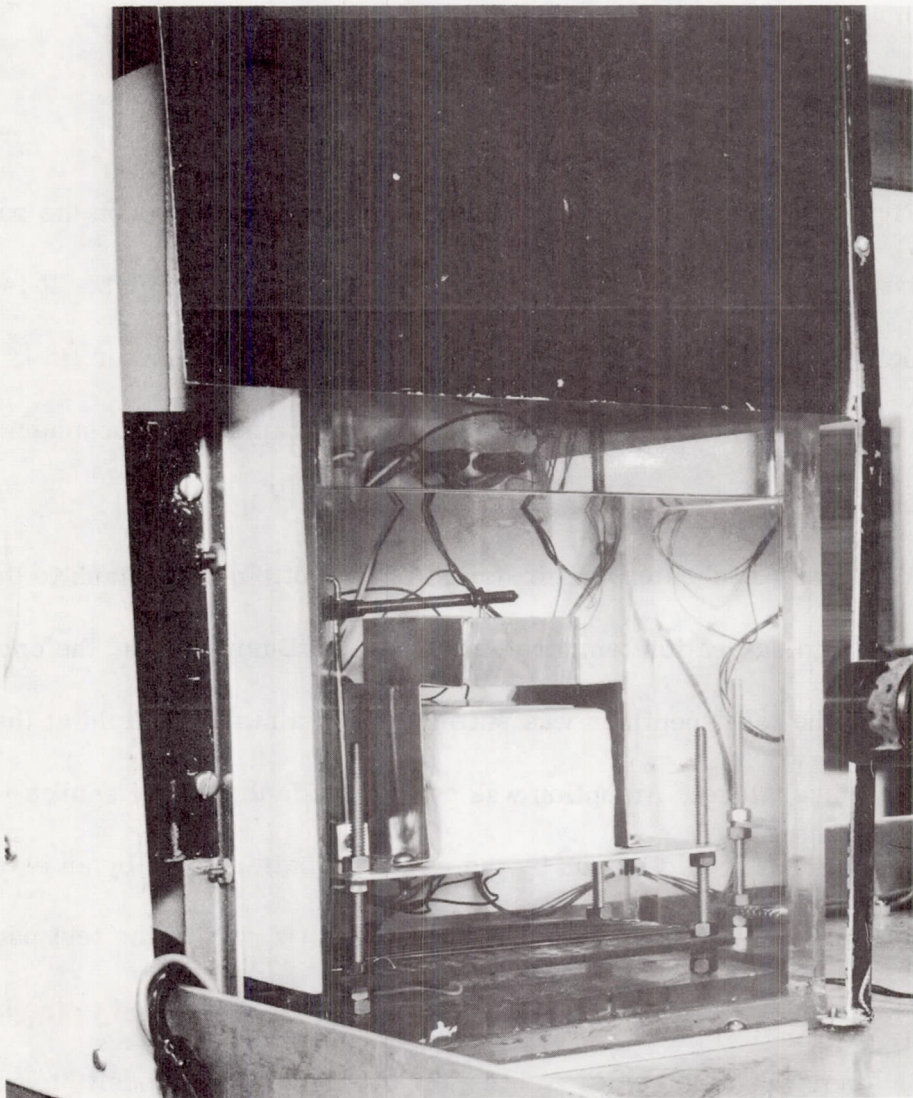


Figure 13. Test Container Mounted on Package

A thermistor was mounted on the test specimen support plate and was used to monitor the Freon temperature both before and during tests through the telemetry system. The thermistor was calibrated prior to installation and had an accuracy of ± 0.2 °F. Frequent checks were made of the thermistor by use of a thermometer prior to tests.

The heater thermocouple wires were pulled directly through the container lid, and thence to the thermocouple reference junction which was mounted on the first floor of the package (Figure 11). The test specimen power leads, auxiliary heater power leads, and thermistor wires were pulled through plugs mounted on the side wall of the container 1 inch from the top.

For balance purposes, the Freon level was maintained 1.5 inches from the top of the container, and when it was necessary to replenish the Freon supply after closing the container, this was accomplished through the vent.

Normally, the test specimen was not shielded. However, in order to investigate the possible effects of sloshing or excess convection currents on the behavior of the test specimen, some standard and reduced gravity tests were run with a shield around the specimen. No change in the operating characteristics of the heater was seen with the shield in place. Similar results were obtained by Schwartz [4].

Test Specimen

One of the primary objectives of this study was to obtain data on test specimens whose dimensions were large when compared to the size of the bubbles generated at both 1 g and low g. This fact, when coupled with the reduced gravity time available, made the design of test specimen which would reach steady state impractical. As a result, it was decided to adopt the philosophy of Merte and Clark [6] and treat the heat transfer surface as a dynamic calorimeter. The test specimen used, however, is not as amenable to such a treatment as were the spheres used by Merte and Clark. The problems encountered are primarily those of heat leak through the insulation behind the heater surface and a residual energy source which is present when the heater is turned off. These items will be discussed in more detail in the section devoted to test results and in the thermal analysis of the test specimen in Appendix C.

Three test specimens were used during the course of the experimental work. The majority of the investigation of the nucleate boiling curve was performed using a 2 inch by 4 inch by 0.063 inch thick flat copper surface. One face of the plate was insulated with 2 inches of polyurethane foam. The heating element was 48 inches of No. 25 Nichrome wire coiled on the back side of the heater surface. The second heater used in the boiling work was a 2 inch by 2 inch by 0.063 inch thick surface heated by 20 inches of coiled Nichrome wire and insulated in the same manner as the first. The heater

used for the bubble studies was identical to the first heater except that the copper was 0.030 inch thick, the Nichrome wire used was No. 16 wire, and no thermocouples were installed. The copper used in constructing the heaters was analysed by the Materials Division at MSFC and found to be electrolytic copper containing less than 0.05 percent total impurities.

With the exception of the fact that no thermocouples were installed beneath the bubble study heater, the heaters were constructed in an identical manner. A thin coat of cement (Saurisen No. 14) was brushed onto one side of the copper. The plate was then baked in an oven for 1/2 hour at 125 °F and then for 1 hour at 175 °F. The Nichrome wire was then placed over the cement and a second thin layer of cement was brushed over the wire and surface. The baking procedure was then repeated. The thermocouple wires were installed at that point by drilling small holes through the cement and into the copper surface. The holes were slightly smaller than the thermocouple bead and deep enough so that the bead was completely embedded in the copper. The thermocouple wires and power leads were threaded through 2 inches of polyurethane insulation and the insulation was placed over the heater element. Finally, the insulation was completely covered with Armstrong A-2 epoxy to prevent leakage. Figure 14 is a photograph of the 2 inch by 2 inch heater surface and Nichrome wire prior to assembly, and Figure 15 is a photograph taken just prior to installation of the insulation. The 2 inch by 2 inch heater in its final form is depicted in Figure 16, and the 2 inch by 4 inch heater is shown in Figure 17.

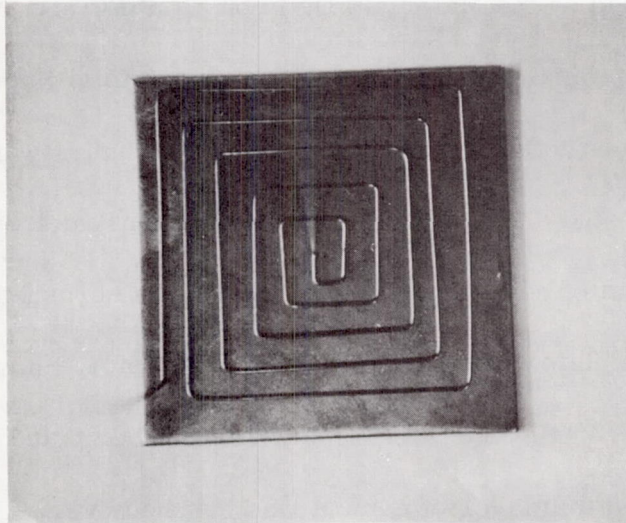


Figure 14. View of 2 × 2 In. Heater Plate and Nichrome Heating Wire

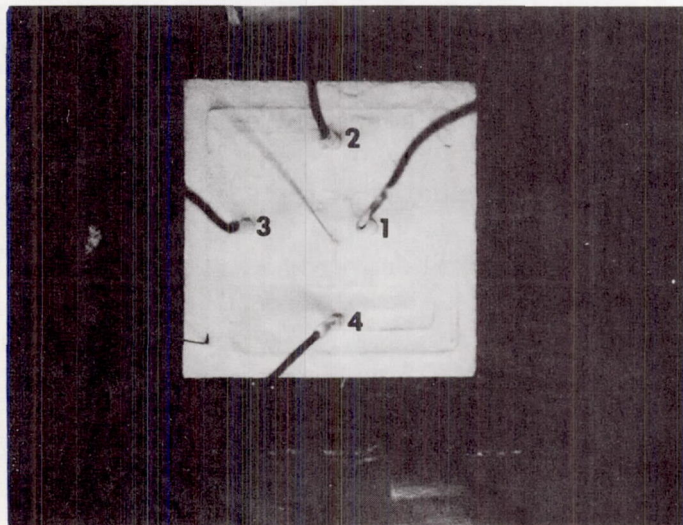


Figure 15. View of 2 × 2 In. Heater Plate After Heating Element and Thermocouples Were Installed

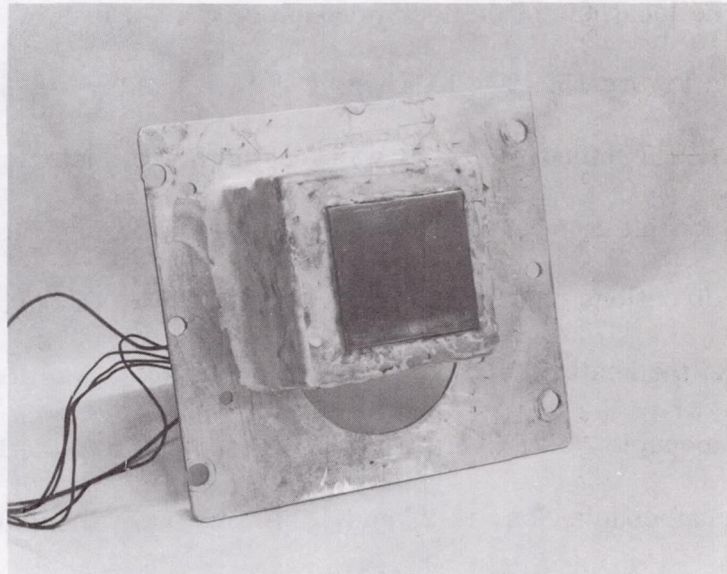


Figure 16. View of 2 × 2 In. Test Heater

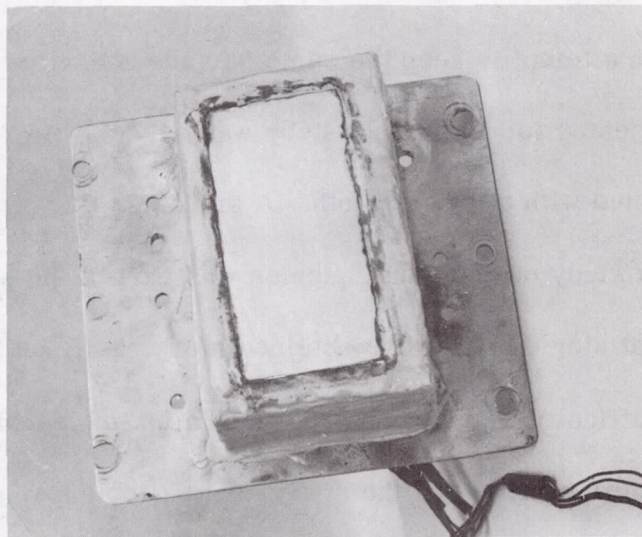


Figure 17. View of 2 × 4 In. Test Heater

Four thermocouples were installed on each heater. The thermocouples used were of copper-constantan gage 36 wire. The beads were made by arc welding. The locations of the thermocouples on the 2 inch by 2 inch heater are shown in Figure 15. The locations for the 2 inch by 4 inch heater are as follows: (1) Thermocouple No. 1 was located in the center of the heater, (2) Thermocouple Nos. 2 and 3 were located 1 inch from Thermocouple No. 1 in opposite directions on a line passing through the No. 1 position and running lengthwise to the heater, and (3) Thermocouple No. 4 was located $3/4$ inch from Thermocouple No. 1 in a direction perpendicular to the line passing through Thermocouple Nos. 1, 2, and 3. An ice bath, located as depicted in Figure 11, was used as a reference junction. Calibration of the thermocouples will be discussed in the instrumentation section.

The surface of the heaters used in the boiling curve study were prepared by sanding with a 400-grit emery paper. The surfaces were resanded frequently in an attempt to keep the same surface finish for all tests. The surface of the heater for the bubble study was sanded with 600-grit emery paper and finished with a crocus cloth. A smoother finish was used on this surface since a study of individual bubbles was part of the objective, and it was learned that single sites were obtained more easily on the smooth surface. Considerable difficulty was encountered in eliminating bubbles at the joint between the heater surface and the epoxy. The problem was compounded by the fact that the Freon 113 attacks most sealants which would normally be used. The final solution was to use a rubber compound (Silicone 140) to

seal the joint. This compound is affected by the Freon (an increase in volume occurs), but proper cleaning of the surface prior to application and allowing a suitable curing time (48 hours) yielded a reasonable bond.

Instrumentation

Two types of instrumentation systems were used. An on-board telemetry system was used to monitor the following items: (1) thruster pressure, (2) Freon temperature, (3) package acceleration level during free fall (low g), (4) package acceleration at impact (high g), (5) test heater current, (6) test heater voltage, (7) an impulse signal to signify package release, and (8) an impulse signal to signify test heater turn off. The signals were transmitted to a recording station approximately 1 mile away and, except for the two impulse signals, were recorded on both oscillograph recorders and by a digital system. An attempt was made to use the telemetry system to record the output of the test heater thermocouples. However, the output of the copper-constantan thermocouples in the range of interest was between 1.75 and 3.25 millivolts. The only variable frequency oscillators available (5 volt) made it necessary to amplify the output signal approximately 2000 times and the resulting signal was too noisy for the digital system. The span available on the oscillograph recorder was too small to read the data with any reasonable degree of accuracy. As a result, it was decided to connect cables to the aeroshield and measure the thermocouple output directly. Three four-conductor cables (one was a spare) were used and the

output was monitored at a recording station at the base of the test stand. The results with this system were quite good. The Bristol strip-chart recorders used were run at a speed of 1 inch per second during the tests and produced a timing pip every second. The paper used was 6.8 inches wide from 0 to 100 percent of full scale and was divided into 100 equal increments. With the 2 inch by 4 inch test heater, the recorders were set for 1.75 millivolts at 0 percent to 2.75 millivolts at 100 percent, and when the 2 inch by 2 inch heater was used, the setting was for 1.75 millivolts at 0 percent and 3.25 millivolts at 100 percent.

All instrumentation channels were calibrated prior to each day's testing. Particular attention was given to calibration of the test heater temperature measuring system. Each recorder span setting was calibrated by imposing known millivolt values on the thermocouple lead connected to that channel with a Rubicon potentiometer. The thermocouples themselves were calibrated using the system shown in Figure 18. The test heater was immersed in a silicone oil bath whose temperature was controlled by a Rosemount 910A controller. The temperature of the oil bath was monitored by a highly accurate platinum resistance thermometer and Mueller Bridge. After calibration of the recorders, the output of each thermocouple using the calibration system described above was channeled to its recorder and the deviation of the thermocouple determined at a number of points in the temperature range of interest.

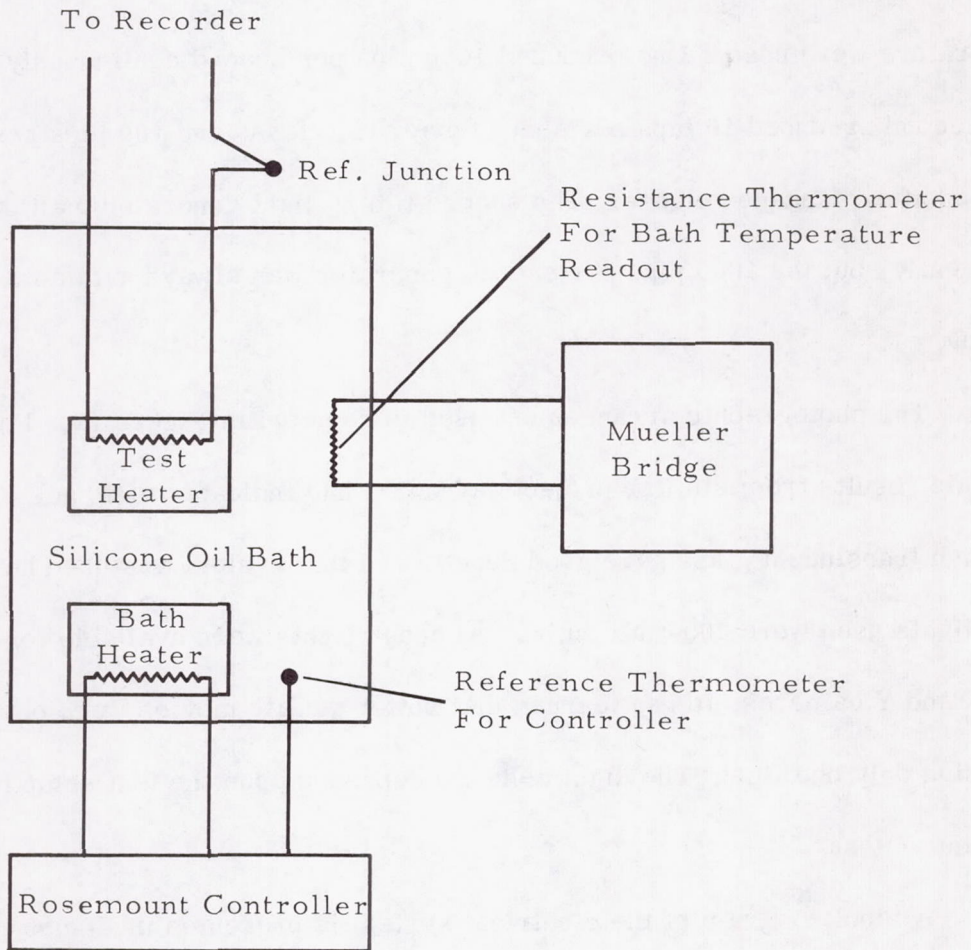


FIGURE 18. CALIBRATION SYSTEM FOR TEST HEATER THERMOCOUPLES

Two 16-mm Milliken cameras were used to obtain movies of the boiling phenomenon during the tests. The cameras were set at 400 frames per second and the lens opening was usually set at f4. Two sets of pulse-timing light generators were used. One produced 1000 pips per second continuously while the second produced 10 pips per second prior to release and 100 pips per second after package release. The second timing light generator malfunctioned frequently, but the 1000 pips per second generator was always available for timing.

The photographic arrangement used is depicted in Figure 19. Photographic results from similar projects at MSFC had indicated that back lighting through translucent glass gave good results and that system was used here. The lights used were 200-watt bulbs. Although lights were available for both the X and Y cameras, it was learned that better quality movies were obtained by using only one light. The light selected depended upon the test setup for a particular test.

A block diagram of the electrical system is presented in Figure 20. The operation of the system will be discussed in detail in the section on experimental procedures.

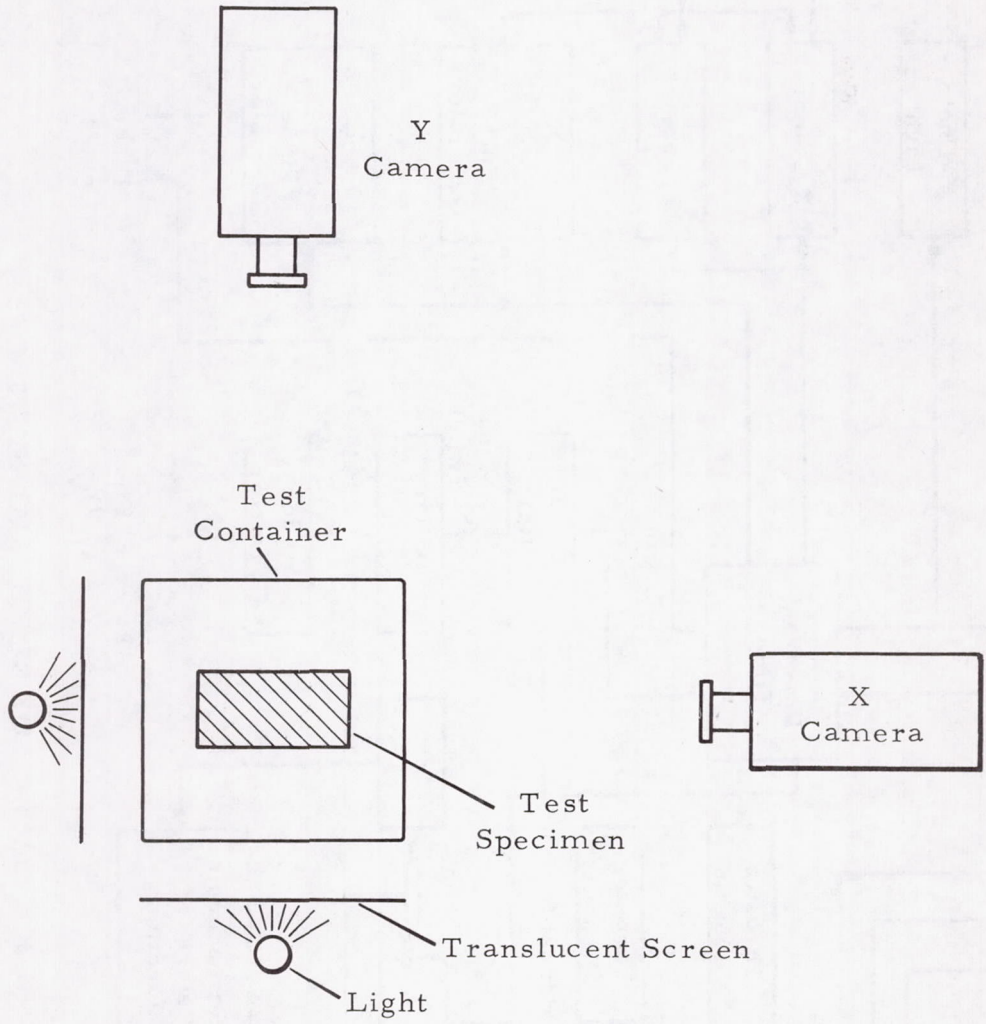


FIGURE 19. PHOTOGRAPHIC ARRANGEMENT

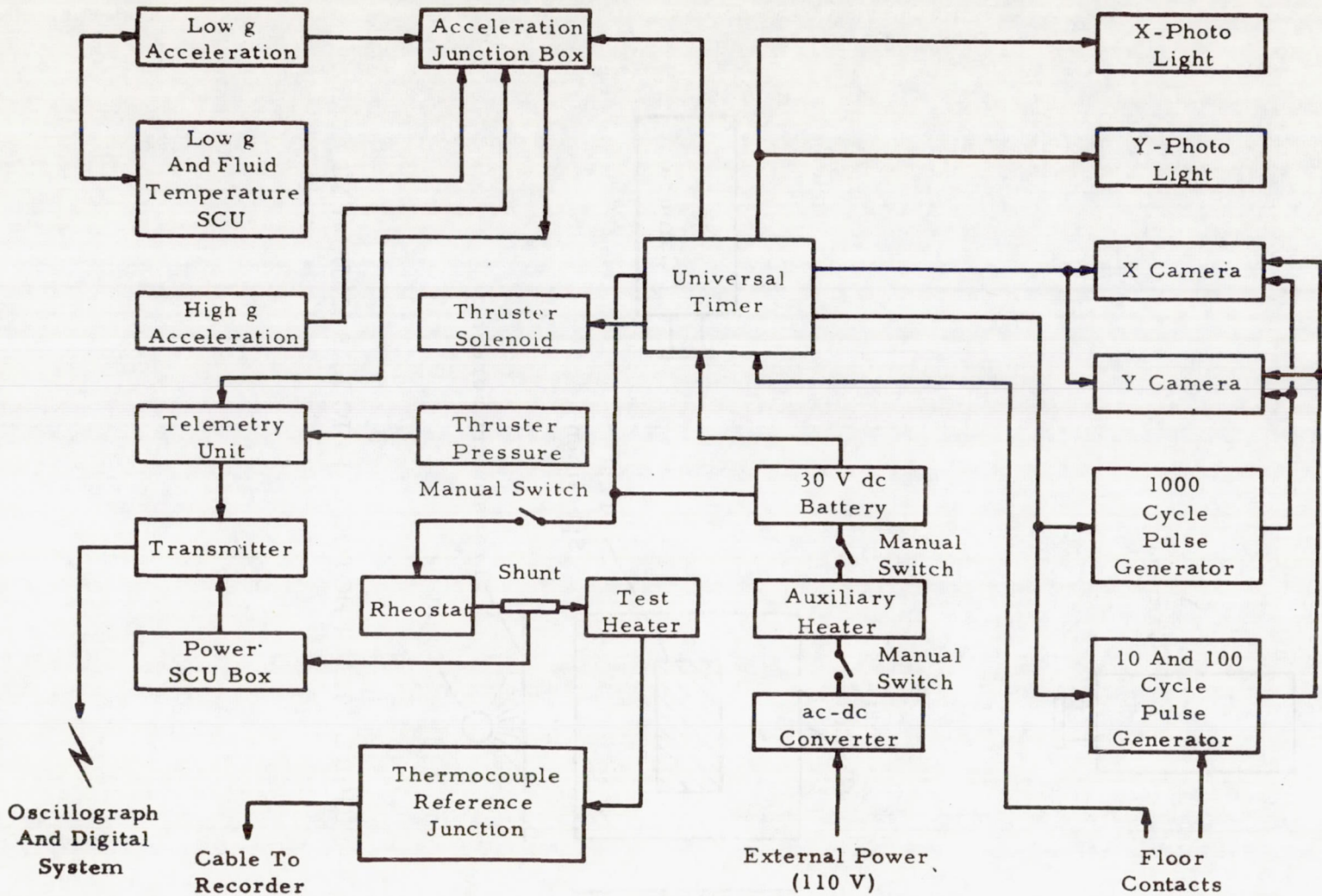


FIGURE 20. BLOCK DIAGRAM OF ELECTRICAL SYSTEM

EXPERIMENTAL PROCEDURES

Four types of tests were run during the course of the investigation. Due to the similarity of the predrop and reduced gravity tests, which were conducted to investigate the effects of acceleration level and surface orientation on the nucleate boiling curve, the procedures for these tests will be discussed concurrently. The procedures for the tests to investigate bubble behavior and the tests to create 1-g boiling curves will be discussed in separate sections.

Standard Gravity Boiling Curves

The test container was first filled with Freon 113. All electrical connections were then made and the recording equipment was calibrated. The auxiliary heater was turned on to bring the test fluid to its saturation temperature. The test heater was installed in the test container and turned on at a moderate heat flux. Depending upon the initial fluid temperature, the time required for both heaters to bring the fluid to saturation varied from 15 to 30 minutes.

In order to have a basis for comparison of the effect of orientation

on the reduced gravity boiling curve, 1-g boiling curves were created for vertical, horizontal heating face up, and horizontal heating face down positions of the heater face. After the fluid had reached the saturation temperature, both heaters were turned off to allow fluid motion to dissipate. The test heater was then turned on and allowed to come to steady state. Usually, the first point selected was a low heat flux. However, after data for a complete set of curves had been obtained, several intermediate points were rerun for comparison purposes. Data for the three positions were accumulated both concurrently and separately. For the concurrent tests, after the heater had reached steady state in the initial position (e. g. , horizontal heating face up) , a data point was taken. Then, without turning the power off, the heater was turned to a second position, allowed to assume its new steady state temperature, and the next data point taken. The procedure was repeated for the third orientation and then the power level was changed in order to obtain a new set of data points. This procedure was repeated for a few points. However, since it was necessary for the author to adjust the position of the heater manually by immersing his hands in the Freon, most of the data points were taken with the heater in a given orientation and then the orientation was changed for the next set of data points. The Freon temperature was monitored continuously, and the auxiliary heater used intermittently to maintain the saturation temperature of the Freon.

During most of these tests, the current and voltage were read directly with ammeter and millivolt meters. For some points, the telemetry system

was used along with the meters as a check on that system. Agreement between the two sets of readings was good.

Bubble Tests

The procedure outlined in the previous section to bring the Freon to its saturation temperature was repeated. All equipment was calibrated and the cameras were loaded and installed on the test package. In order to ensure proper operation of all equipment, a full sequence of test operations was run. With the exception of the fact that the package thruster solenoid was disconnected to prevent excess noise, the sequence was identical to that which occurred during the drop. The package thruster pressure bottle was then pressurized from an external GN₂ source. The Freon temperature was brought back to its saturation value and the test heater power level was set near the incipient boiling point so that the number of nucleation sites on the surface was small. The aeroshield door was closed and the test was conducted. For this investigation, the heater remained on throughout the test.

Nucleate Boiling Tests - Predrop and Reduced Gravity

Since the primary objective of the investigation was to establish the effect of reduced gravity on the 1-g nucleate boiling curve, care was taken to ensure the same test conditions on the predrop 1 g and the reduced gravity tests. In all cases, the 1 g test with which a reduced gravity test was compared was run immediately prior to the reduced gravity test. In several

cases, more than one standard gravity test was run prior to the reduced gravity test to ensure repeatability.

The test container was filled with Freon 113, and the fluid was brought to its saturation temperature with both heaters as described in an earlier section. The loaded cameras were installed and pretest calibrations were conducted. The test heater was turned on at the peak power level for the heater and allowed to come to steady state. The standard gravity tests were then conducted under simulated drop conditions. On some tests, the package thruster was allowed to run and the connection to the floor contacts was broken so that the only difference between these tests and the reduced gravity test was that the aeroshield was not released. Since no effect of the package thruster and floor contact connections was seen, however, most tests were run with the package on the floor contacts and the package thruster solenoid disconnected.

After the 1 g test was conducted, the heater was turned back on at the same power setting. The aeroshield door was closed and the reduced gravity test was conducted. The time lapse between the standard gravity test and the reduced gravity test was usually approximately 10 minutes.

A typical sequence of operations for a test is shown in Figure 21. On some tests, the heater was sequenced to turn back on after the aeroshield was in the catch tube.

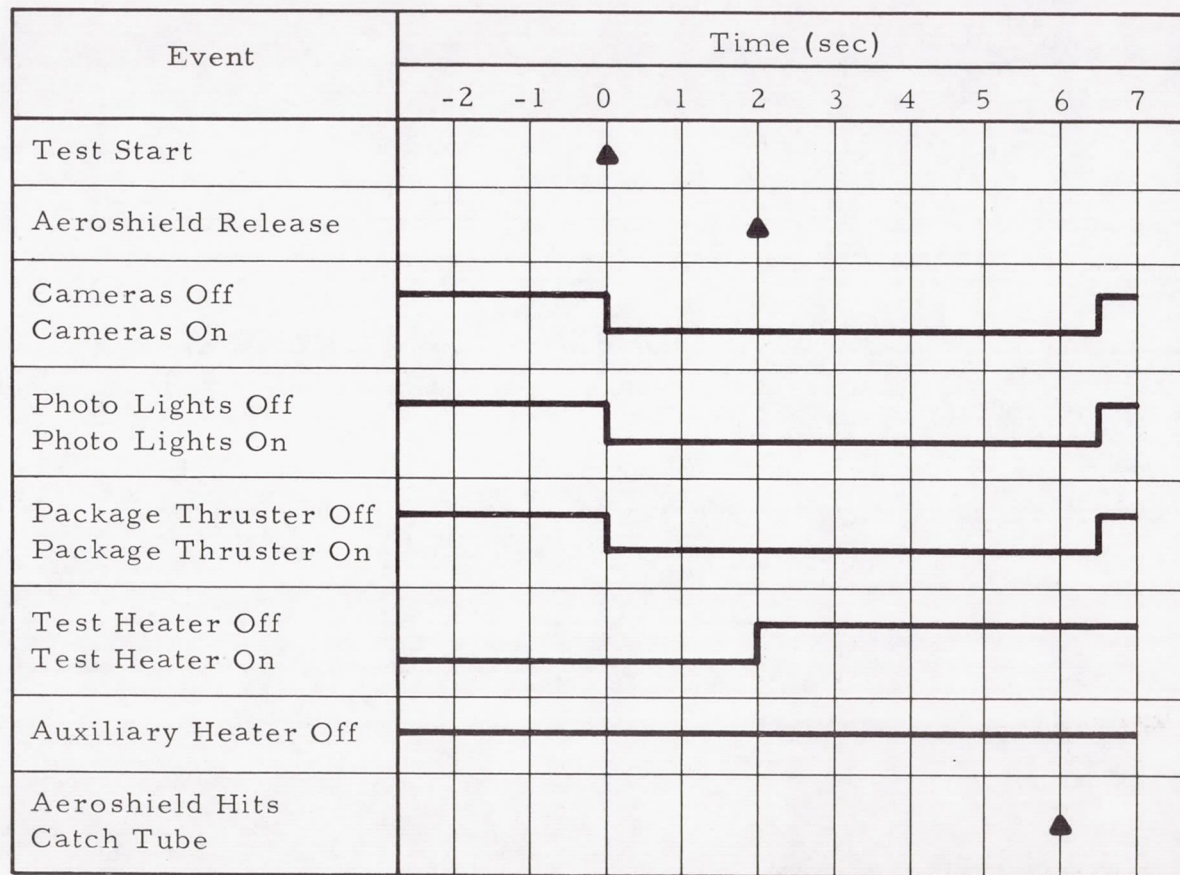


FIGURE 21. SEQUENCE OF OPERATIONS FOR A TYPICAL TEST

EXPERIMENTAL RESULTS AND ANALYSIS

The results and accompanying analysis fall into the two major categories of bubble phenomena at reduced gravity and the behavior of the nucleate boiling curve at reduced gravity. The information on the bubble studies will be presented in the first part of this section and the presentation of the nucleate boiling material will follow. The data reduction procedures will be discussed as the data are presented.

Bubble Growth Rate Data

Growth rates for isolated bubbles were obtained both at 1 g and at reduced gravity levels of 0.01 g and 0.02 g. The motion pictures were analyzed frame by frame using a Vanguard Motion Analyzer. The motion analyzer is equipped with calibrated cross-hairs which were used to determine the bubble diameters. A direct readout, graduated in 1000 counts per inch, is given as the cross-hairs are moved. An 0.040-inch probe was located in the field of view of the cameras and was used for calibration purposes. For each roll of film analyzed, five readings were made of the probe and the results averaged to obtain the calibration. The deviation from reading to

Preceding Page Blank

reading was always within three percent for the probe diameter. Since two cameras were available, an isolated bubble could be viewed from two locations 90 degrees apart. A comparison of bubble diameters for a given bubble taken from both cameras showed good agreement. As a result, the bubble diameters were usually taken from one view. The magnification used in most of the measurements was approximately five times.

As has been indicated previously, two timing light generators produced timing pips on the film edge. For the section of film of interest for a particular bubble, these pips were counted and correlated with the frame numbers to obtain relative time data. The time associated with a given frame was determined to approximately 0.001 seconds by using the 1000-cycle timer. At the frame rate of the cameras (approximately 400 frames per second), an average of 2.5 pips appeared per frame after the cameras had achieved full speed. The pip nearest the top of the frame was taken as the time for the frame.

At reduced gravity levels, the bubbles were spherical. The bubbles observed at 1 g were slightly elongated during their early growth stage and slightly flattened during the latter stage of their growth. For purposes of comparing the growth rates, however, the diameter of the bubble axis parallel to the heated surface was taken as the bubble diameter. It would have been possible to measure both the major and minor diameters of the bubbles or to divide the bubble into segments to determine an average diameter or a diameter associated with the volume of the bubble; however, it was felt that

the wide variation in bubble size and the large variation in growth rates made the worth of such refinements questionable.

Since the growth rate of bubbles is quite large initially, the 0.0025-second increment between frames was too long to obtain detailed data during the early growth stage. In addition, the time lapsed since the initiation of growth of a bubble appearing for the first time was unknown. As a result, the time associated with the first frame of a bubble growth sequence was somewhat arbitrary. After looking at a good sample of bubbles, it was decided to assign a time for the bubble as it first appeared based on the size of the bubble at that time. For bubbles which were relatively large, a time of 0.0025 second was assigned, whereas for smaller bubbles, the time associated with one-half frame (0.00125 second) was assigned. The resulting error for bubbles at reduced gravity which remained on the surface for times of 0.2 to 0.4 second was negligible, but for bubbles growing in the 1-g field which remain on the surface for approximately 0.015 second, the error was more significant. However, the only way to avoid the error would be to use a higher speed camera, and the magazine sizes associated with cameras of sufficient speed was prohibitive with the test package.

Bubble growth rate data at a wall superheat of 11 ° F and a heat flux of approximately 1500 BTU/hr-ft² were taken from several sites at 1 g. The data, along with a faired curve, are presented in Figure 22. Since no thermocouples were installed beneath the surface of the bubble study heater, the value of wall superheat was obtained from two thermocouples mounted

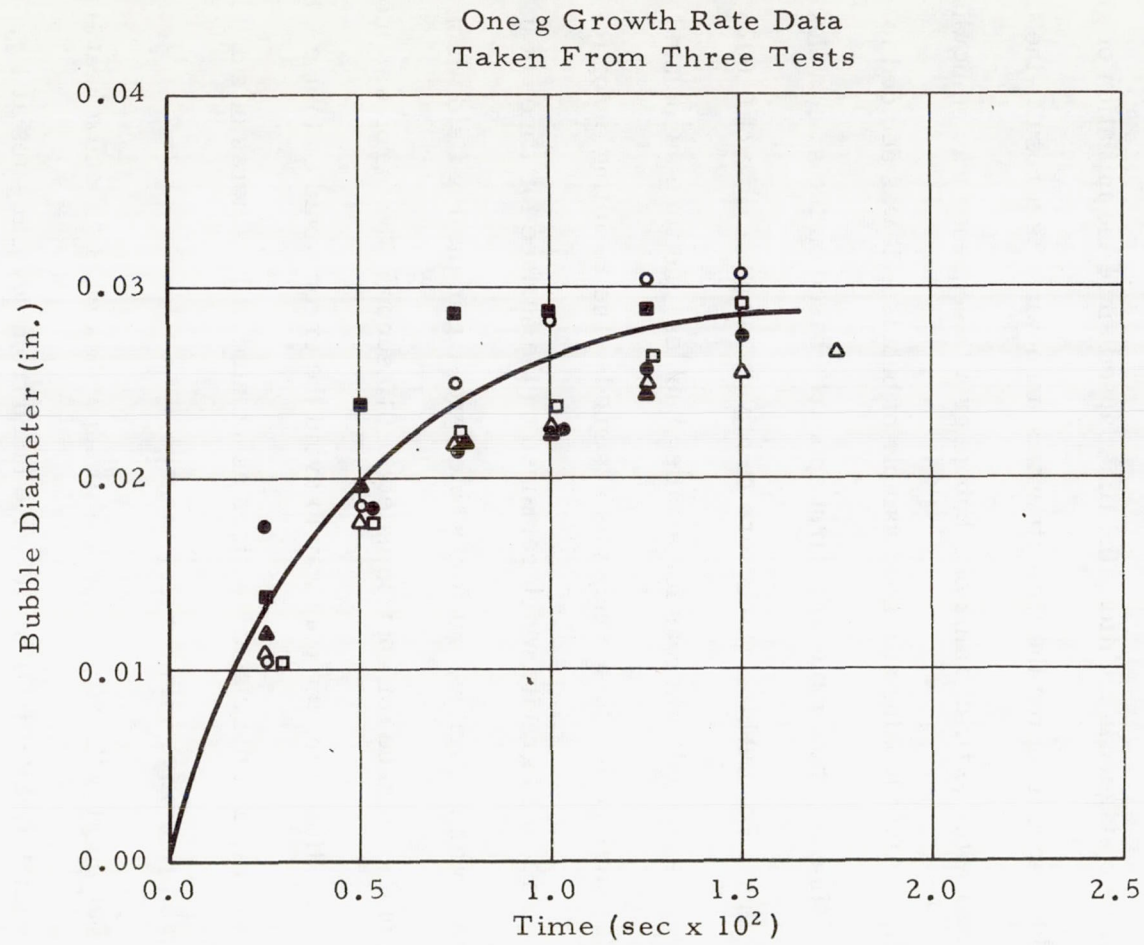


FIGURE 22. ONE g BUBBLE GROWTH DATA

directly to the heat transfer surface. The thermocouples were covered with epoxy to prevent boiling from their surface. The power level was obtained from direct ammeter and millivolt meter readings.

Reduced gravity bubble growth rate data for acceleration levels of 0.01 g and 0.02 g is presented in Figure 23. The wall superheat and power level for this data is approximately the same as for the 1 g data. The data presented were taken from eight sites. A faired curve is presented so that the data can be compared with existing growth rate theories and with a new calculation procedure which will be presented in the following section.

In order to illustrate the difference between standard gravity bubble diameters and bubble diameters in the range of interest of this investigation, two frames (presented in Figure 24) were taken from one of the rolls of film to obtain bubble growth rates at reduced gravity. The bubble growing at reduced gravity originated from the same site as the one seen on the frame taken from the 1 g portion of the film. The acceleration level for this test was 0.02 g. The reduced gravity bubble is presented just prior to departure from the surface.

Comparison of Bubble Growth Rate Data With Existing Theory and With a Proposed Calculation Procedure

As will be shown, the bubble growth analyses discussed in the literature survey section do not agree with the experimental data obtained for pool boiling of Freon 113 at 1 g and at reduced g levels. Recent experimental data

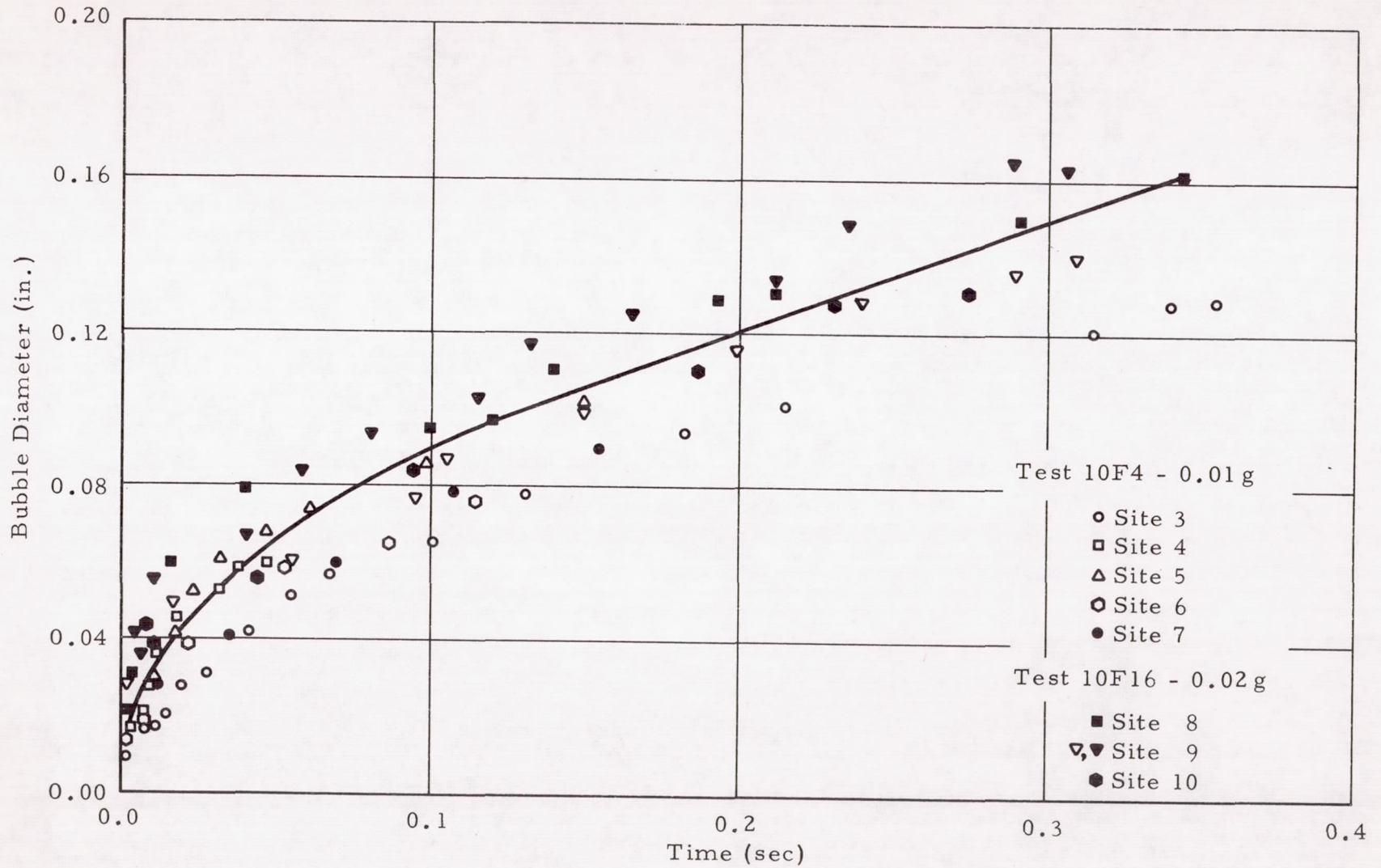
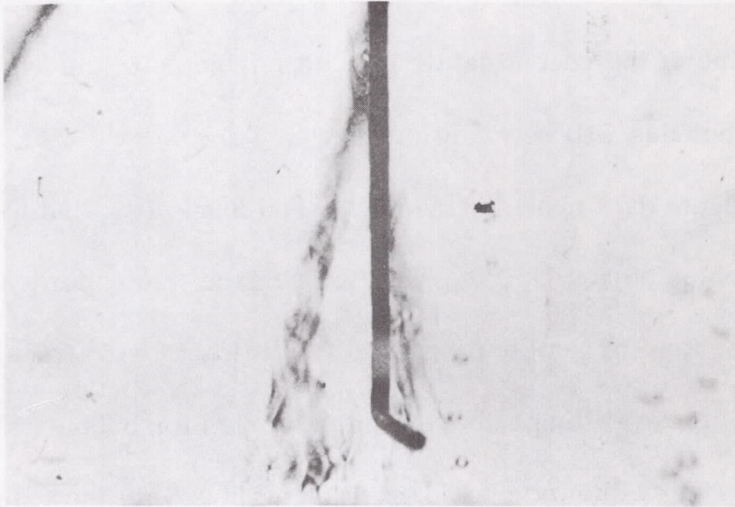
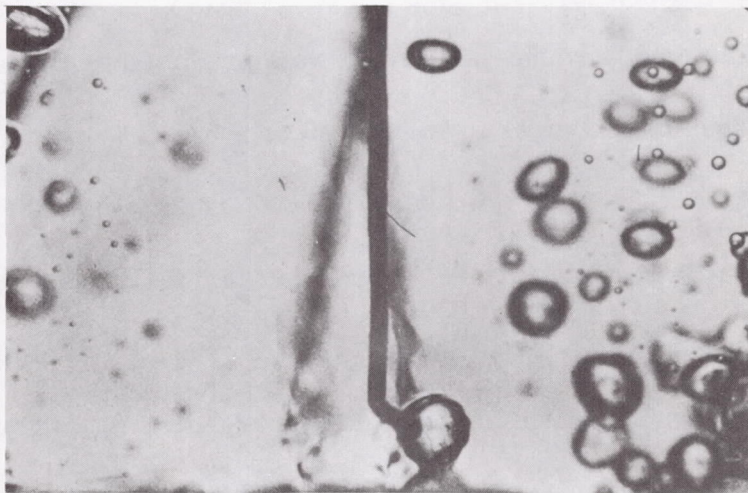


FIGURE 23. LOW g BUBBLE GROWTH DATA



a. Standard Gravity



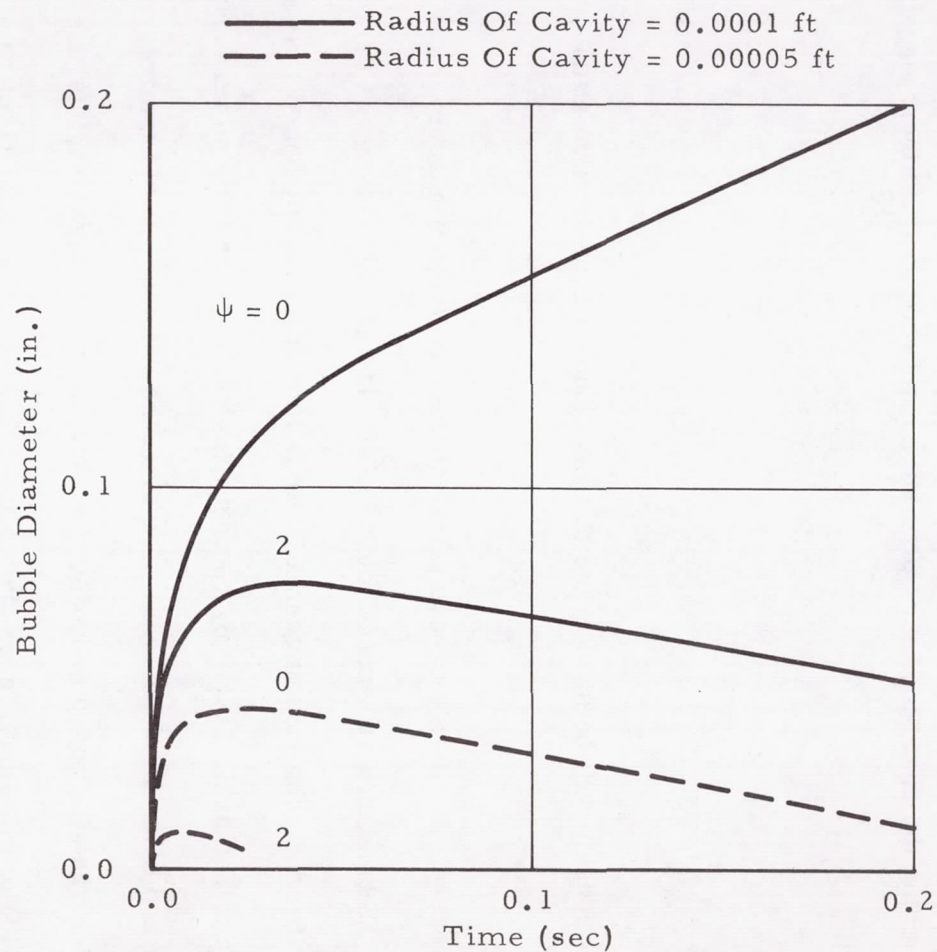
b. Reduced Gravity

Figure 24. Comparison of 1g and Low g Bubble Diameters at 0.02 g

have been provided which indicates that some of the basic assumptions contained in several of these theories are subject to question. Before comparing the data with theory, a calculation procedure will be outlined which attempts to use some of the recent data. In addition, some of the assumptions made in existing theories will be modified.

Recent data provided by Jacobs and Shade [37] indicated that the vapor inside bubbles departing from a heated surface was superheated. The data were presented for pool boiling of carbon tetrachloride for a wide range of heat flux. Several temperature-time histories for bubbles were presented and the majority showed considerable superheat with the values varying from 2 to 11 degrees. The authors suggested that the probable reason for some bubbles not being superheated was that in those cases the thermocouple failed to break through the bubble wall. The presence of superheated vapor inside a bubble would tend to reduce the growth rate predicted by the existing theories which all assume the vapor to be saturated.

A knowledge of the thickness of the thermal layer surrounding the bubble, as it is initially formed, is an important factor in determining the heat flux into the bubble from the layer, if the energy is assumed to be transferred by conduction. As explained in equation (4) Hsu and Graham assume that this layer is a function of the nucleation site radius, r_c . In general, this quantity is not known. In addition, the analysis is quite sensitive to the value of cavity radius chosen. This fact is illustrated in Figure 25. Two sets of calculations were made for the growth rate of bubbles in saturated



HSU And Graham
(Ref. 31), $C = 1$

$\psi = \text{Vapor Superheat} (^{\circ}\text{F})$

Fluid - Freon 113

$Q_w = 1150 \text{ Btu/hr-ft}^2$

$T_w - T_{\infty} = 11 ^{\circ}\text{F}$

FIGURE 25. CALCULATION OF BUBBLE GROWTH RATES FOR POOL BOILING OF SATURATED FREON 113

Freon 113. As shown in Figure 25, a change of cavity radius from 0.0001 foot to 0.00005 foot produced a significant change in the predicted growth rate. The effect of adding superheat is also shown in the figure and is seen to reduce the growth rate of the bubble.

Experimental data provided by Lippert and Dougall [38] indicate that the thermal layer thickness can be predicted if the heat transfer coefficient is known. Using the data which they presented for Freon 113 and their suggested correlation,

$$\delta = \left(\frac{3.4 \times 10^{-4}}{h} \right)^{\frac{1}{2.6}} \quad (5)$$

This relationship will be used in the proposed bubble growth calculation method.

Several investigators have proposed the existence of a liquid micro-layer at the base of a growing bubble [39, 40, 41, 42, 43]. Perhaps the best evidence for the existence of such a layer is that presented by Sharp [39] and Torikai and Yamazaki [40]. By photographing bubbles growing on transparent surfaces and using a suitable optical system the existence of the microlayer was demonstrated. Sharp proposes, as have other investigators, that the evaporation of this liquid layer probably accounts for the major fraction of heat transfer in nucleate boiling.

In addition to demonstrating the existence of the liquid layer, Torikai and Yamazaki noted that a portion of the area beneath a growing bubble was

not covered by the liquid microlayer. The ratio of this dry area to the total area in contact with the heated surface was approximately 0.1 over a wide range of heat fluxes.

The analyses of Zuber and of Hsu and Graham assume that the thermal layer always remains around the growing bubble. While this may be true in some cases, it seems likely that in other cases the bubble grows through the thermal layer and moves a portion of the layer aside rather than moving it uniformly toward the bulk liquid. This seems especially likely at reduced gravity, since the bubble grows to sizes of much more than an order of magnitude larger than the thermal layer and remains on the surface for times of an order of magnitude longer than in 1 g. Several investigators have proposed that the evaporation of the liquid microlayer between the growing bubble and the heated surface accounts for a major portion of the heat transfer in nucleate boiling. It is proposed here that it also accounts for a major portion of the energy for bubble growth as it is continuously vaporized, and that at low gravity levels where the bubble remains on the surface for long periods of time and grows to large sizes, it accounts for almost all of the growth after the bubble becomes significantly larger than the thermal layer.

The model to be adopted is depicted in Figure 26. During the early growth of the bubble, the thermal layer completely surrounds the bubble. During this stage, the bubble receives energy from the microlayer and from the thermal layer which covers its entire surface area. All of this energy is assumed to vaporize fluid and contribute to bubble growth. It will also be

assumed that the dry portion of the area beneath the bubble transmits energy to the bubble and that this energy serves to superheat the vapor inside the bubble. It will be assumed that the mechanism of energy transmittal for the dry area is conduction through the vapor.

It will be assumed that as the bubble grows, it grows through the thermal layer and that after its cap passes through the layer, energy is transmitted to the bulk fluid by free convection. This energy is removed from the vapor by condensation. The energy associated with the condensation mechanism is very small when compared to the other mechanisms outlined in the case of a saturated bulk liquid.

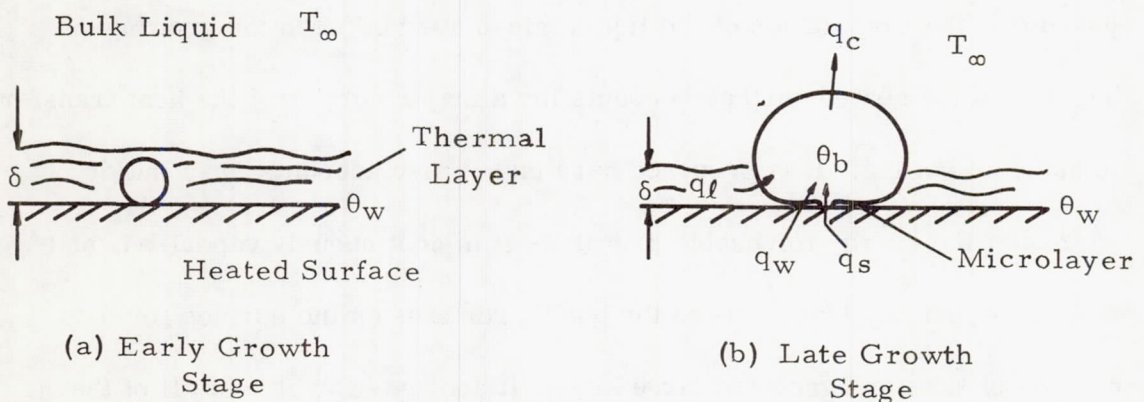


FIGURE 26. BUBBLE GROWTH MODEL

An energy balance for the bubble can be made which accounts for the energy transports discussed above, yielding,

$$\lambda \rho_v \frac{dV}{dt} = 0.9 A_b q_w + C_2 A_s q_l - C_3 A_s q_c \quad (6)$$

The constants, C_2 and C_3 , account for the fractions of bubble inside and outside of the thermal layer, respectively, and the factor of 0.9 is the ratio of dry area to wetted area beneath the bubble discussed in Reference 40.

Assuming that the bubble is spherical equation (6) yields

$$\frac{dR}{dt} = \frac{1}{\lambda \rho_v} \left(0.9 \frac{A_b}{A_s} q_w + C_2 q_\ell - C_3 q_c \right) \quad (7)$$

In order to evaluate q_ℓ , it will be assumed that the thermal layer can be represented as a plate of thickness δ , as determined by equation (5). It will be assumed that the thermal layer thickness is constant for the portion of the bubble which it contacts. After a portion of the bubble grows beyond the thermal layer, the contribution from the thermal layer to that portion of the bubble is replaced by convection from the bubble to the bulk fluid. The transient conduction equation to be used is

$$\frac{\partial^2 \Theta}{\partial x^2} = \frac{1}{\alpha} \frac{\partial \Theta}{\partial t} \quad (8)$$

and the boundary conditions will be assumed to be

$$\begin{aligned} \Theta(x, 0) &= \Theta_w \left(\frac{x}{\delta} \right) && \text{for } 0 < x < \delta \\ \Theta(0, t) &= 0 && \text{for } t \geq 0 \\ \Theta(\delta, t) &= \Theta_{bt} && \text{for } t \geq 0 \text{ where } \Theta_{bt} = f(t) \end{aligned}$$

In order to obtain a solution for the heat flux, q_l , at any time, it will be assumed that the value of Θ_{bt} at that time has been constant since growth was initiated. For values of superheat determined in the calculations, this assumption produces small errors.

The solution can be obtained by separation of variables and application of the above boundary conditions. The solution obtained is

$$\Theta = \Theta_{bt} \frac{x}{\delta} + \frac{2}{\pi} \sum_{n=1}^{\infty} \frac{\Theta_{bt} \cos(n\pi)}{n} \sin \frac{n\pi x}{\delta} e^{-\frac{\alpha n^2 \pi^2 t}{\delta^2}} + \frac{2}{\pi} \sum_{n=1}^{\infty} \sin \frac{n\pi x}{\delta} e^{-\frac{\alpha n^2 \pi^2 t}{\delta^2}} (-1)^{n+1} \frac{\Theta_w}{n} \quad (9)$$

Evaluating the heat flux at $x = \delta$ as $q_l = -k \left. \frac{\partial \Theta}{\partial x} \right|_{\delta}$

$$q_l = -\frac{k \Theta_{bt}}{\delta} + \left(2 \frac{\Theta_w k}{\delta} - 2 \frac{k \Theta_{bt}}{\delta} \right) \sum_{n=1}^{\infty} e^{-\frac{\alpha n^2 \pi^2 t}{\delta^2}} \quad (10)$$

The heat flux, q_w , will be assumed to be the same as the average heat flux over the heated surface. This is consistent with the assumption of Hsu and Graham [31].

The heat flux, q_c , for the portion of the bubble outside the thermal layer will be obtained by using an empirical free convection correlation recommended by McAdams [44],

$$\overline{Nu}_r = 0.53 (GR_r Pr)^{1/4} \quad (11)$$

The heat flux, q_c , is then

$$q_c = h \Theta_{bt} \quad (12)$$

As previously stated, the energy transferred through the dry portion of the bubble base will be assumed to superheat the vapor, and it will be assumed that the mechanism is conduction. Equation (8) will be used with the boundary conditions:

$$\Theta(x, 0) = 0 \quad \text{for } 0 < x < 2R$$

$$\Theta(0, t) = 0 \quad \text{for } t \geq 0$$

$$\Theta(2R, t) = \Theta_w - \Theta_{bt} \quad \text{for } t \geq 0$$

Solving again by separation of variables,

$$\begin{aligned} \Theta = & (\Theta_w - \Theta_{bt}) \frac{x}{2R} + \frac{2}{\pi} \sum_{n=1}^{\infty} (\Theta_w - \Theta_{bt}) \frac{\cos(n\pi)}{n} \\ & \cdot \sin \frac{n\pi x}{2R} e^{-\frac{\alpha n^2 \pi^2 t}{4R^2}} \end{aligned} \quad (13)$$

$$\text{Evaluating } q_s = -k \left. \frac{\partial \Theta}{\partial x} \right)_{2R},$$

$$q_s = - \frac{k (\Theta_w - \Theta_{bt})}{2R} - \frac{(\Theta_w - \Theta_{bt}) k}{R} \sum_{n=1}^{\infty} e^{-\frac{\alpha n^2 \pi^2 t}{4R^2}} \quad (14)$$

Equations (7), (10), (12), and (14) may be solved in order to determine bubble radius as a function of time. Due to the nature of Θ_{bt} , the equation for bubble growth, equation (7), cannot be integrated directly. Instead, a finite difference solution was obtained using the IBM 1130 digital computer.

Additional relationships include equation (5) for the thermal layer thickness, δ , and the following relationships for C_2 and C_3 :

$$C_2 = \frac{A_\delta}{A_s} = \frac{\delta}{2R} \quad (15)$$

$$C_3 = \frac{A_s - (A_\delta + A_M)}{A_s} = 1 - \frac{\delta + (1 - \cos \varphi) R}{2R} \quad (16)$$

The temperature difference between the vapor inside the bubble and the saturated bulk fluid as a result of the curvature of the vapor-liquid interface can be obtained from the Gibbs equation for the static equilibrium of the bubble,

$$P_v - P_l = \frac{2\sigma}{R} \quad (17)$$

and the Clausius-Clapeyron equation in the form

$$\frac{P_v - P_l}{T_v - T_l} = \frac{\lambda \rho_v}{T_{sat}} \quad (18)$$

These equations can be combined to yield,

$$\Theta_b = \Theta_{\text{sat}} + \frac{2 \sigma T_s}{R \rho_v \lambda} \quad (19)$$

At each time step, the contribution from equation (19) to the temperature of the vapor inside the bubble must be re-evaluated since the bubble radius, R , is a function of time.

A final relationship needed is one for the ratio of base area to surface area, $\frac{A_b}{A_s}$. Bashford and Adams [45] determined the geometric shape of bubbles as a function of bubble volume and, as explained by Hsu and Graham, it is possible to use the tables furnished to compute $\frac{A_b}{A_s}$. However, Hsu and Graham found that little error would be introduced if it was assumed that $\frac{A_b}{A_s} = 0.5$ for $R < 0.04$ inch and $\frac{A_b}{A_s} = 0.25$ for $R > 0.04$ inch. Observations of bubbles growing in saturated Freon 113 from the present data show that the hemispherical phase of bubble growth extends only to approximately $R = 0.01$ inch. Consequently, in both the calculations using the equations of Hsu and Graham, and in the calculations using the derived equations $\frac{A_b}{A_s} = 0.5$ was used for $R < 0.01$ inch. The relationship $\frac{A_b}{A_s} = 0.25$ for $R > 0.01$ inch agreed well with the data and was used in both sets of calculations.

In Figure 27, the reduced gravity data curve of Figure 23 is compared with several growth theories. It can be seen that the actual bubble growth rate is much nearer the curve predicted by equations (7), (10), (12), and (14) than the curves predicted by the other theories. The deviation of the data from the predicted values in the latter growth stage could be due to many

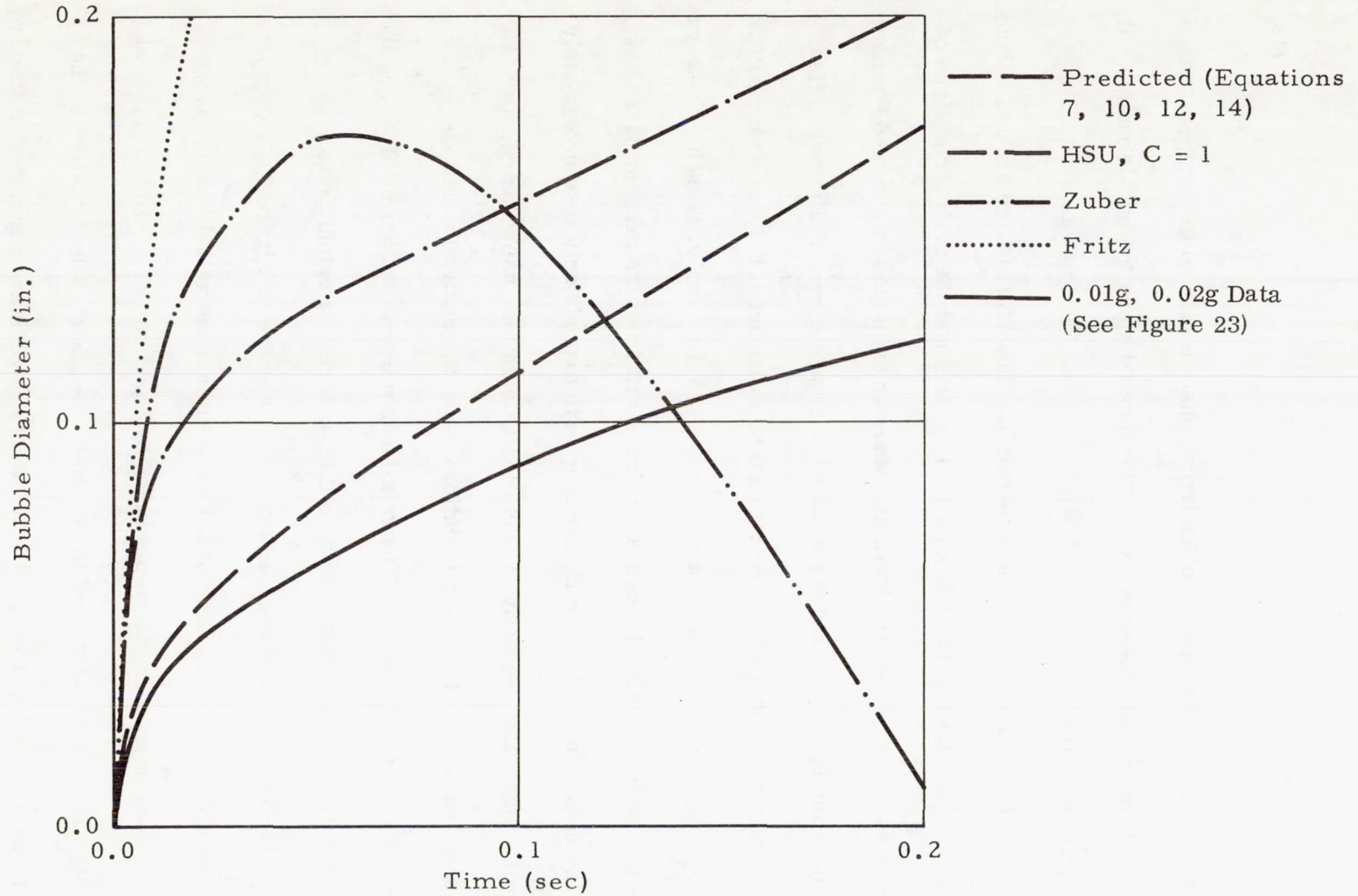


FIGURE 27. REDUCED GRAVITY DATA COMPARED WITH THEORIES

reasons. The bubble superheat predicted by the stepwise integration of equation (14) produced only approximately 4 °F during more than 0.3 second of growth and during the early growth the superheat was quite low when compared with the values measured by Jacobs and Shade [37]. An increased superheat would decrease the growth rate. It is possible that, contrary to what has been assumed, all of the energy transmitted from the thermal layer and from the heated wall does not produce vapor, but instead, part of the energy superheats the vapor.

A comparison of the standard gravity data of Figure 27 with the Hsu and Graham theory, and with the values predicted by the equations presented here, is made in Figure 28. Again, the values predicted by the proposed equations yield the best argument.

In order to compare the theory developed here with a second set of data, a group of bubble growth rates was selected from the work of Schwartz [4]. The data were found in Table D-7 of Reference 4. Data for bubbles which remained on the surface longer than 0.1 second are presented in Figure 29. Schwartz's data were taken at reduced gravity levels during flights of an Aero Commander aircraft which produced low gravity periods of 8 to 10 seconds by flying a Keplerian trajectory. The data presented in Figure 29 were taken at g levels ranging from 0.15 g to 0.32 g . The bubbles grew on a heated surface in saturated water. The thermal layer thickness data were again taken from the work of Lippert and Dougall [38].

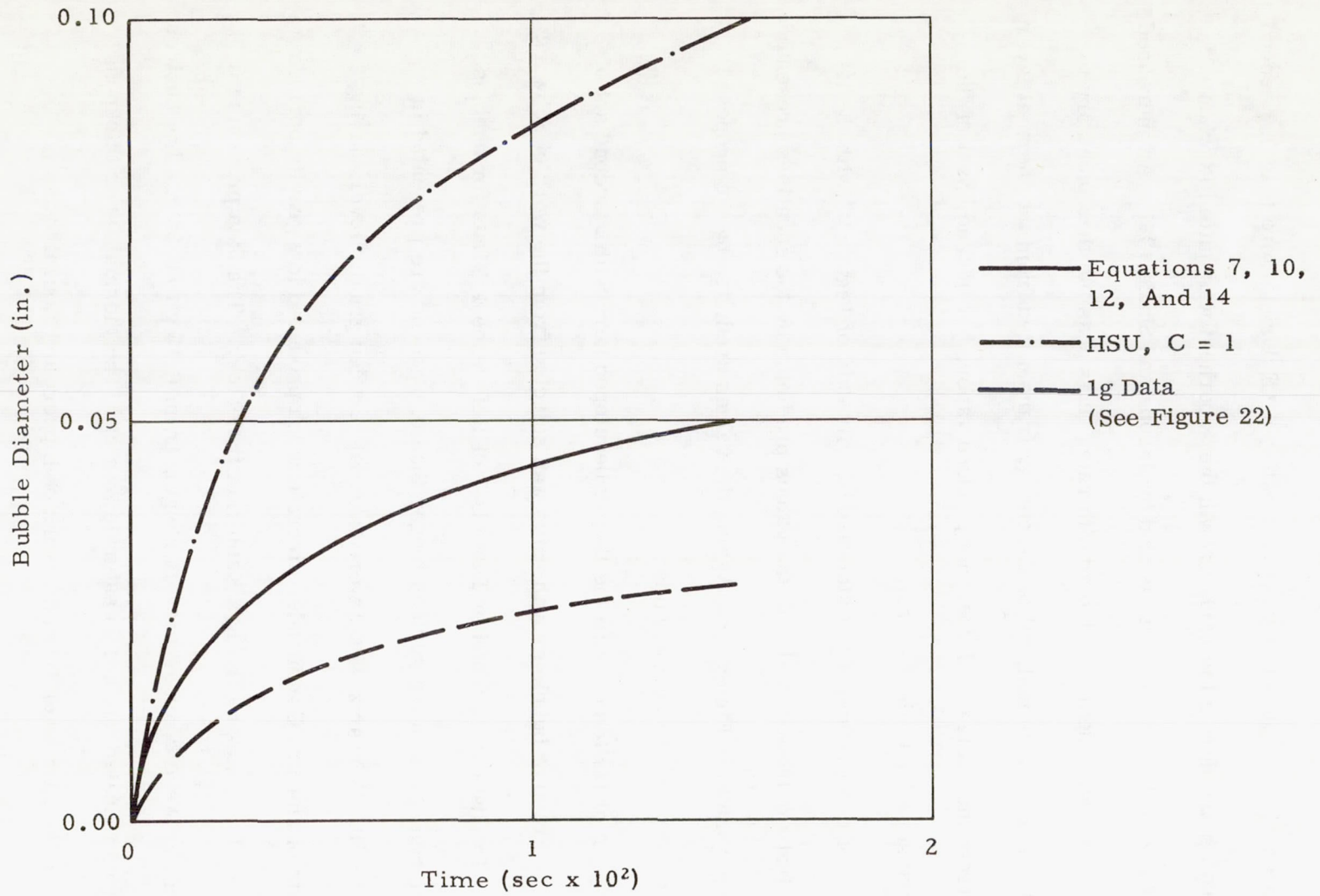


FIGURE 28. ONE g DATA COMPARED WITH THEORIES

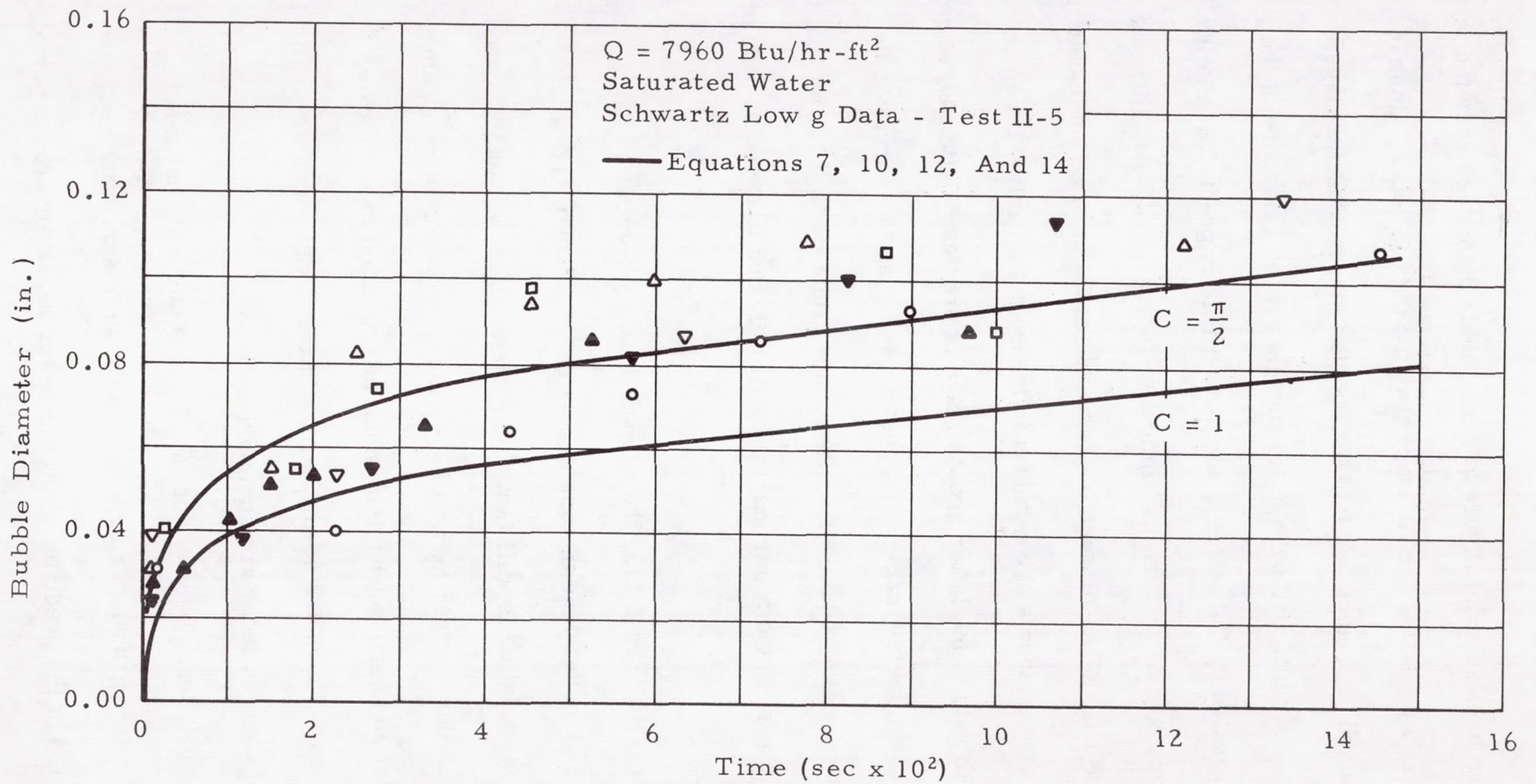


FIGURE 29. COMPARISON OF LOW g DATA OF SCHWARTZ WITH THEORY

As can be seen from Figure 29, the bubble diameter predicted is slightly lower in the latter growth stage than the data indicate. However, if the equation used to predict flux into the bubble from the thermal layer, equation (10), is multiplied by $\pi/2$ to account for the curvature of the bubble as suggested by Zuber [28], the growth rate is predicted quite well. It is interesting to note that the multiplication factor, $\pi/2$, has little effect during the majority of the lifetime of the bubble since most of the bubble moves beyond the thermal layer and beyond its influence quite early. It can be seen that the growth rate in the latter growth stage is predicted quite well either with or without the factor $\pi/2$, since the slopes of the two curves in the stage are approximately equal. This fact lends credence to the hypothesis that the growth rate in the latter stage is primarily due to evaporization of the microlayer.

In the case of Freon 113, the proposed theory correlates the experimental data better than the other methods of calculation available. However, the correlation is still far from perfect. The fact that the proposed calculation procedure agrees as well as it does with the Freon and water data tends to support an actual mechanism which is simulated to some extent by the model chosen. There are several areas in the model which are subject to question and some of these are summarized below.

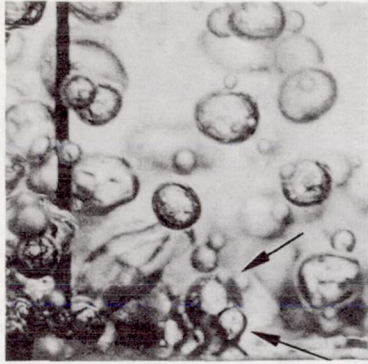
1. The relationships used for A_b/A_s are certainly not exact throughout the entire growth period and an error in this quantity would be strongly reflected in the predicted growth rate for the latter growth period.

2. The assumption that the bubble grows through the thermal layer, rather than moving it toward the bulk fluid, is probably too conservative for some fluids. The fact that the proposed equations overpredict the growth rates for Freon 113, and underpredict the growth rates for water, suggests that the actual mechanism might vary from fluid to fluid. It seems reasonable that the actual mechanism with respect to the behavior of the bubble with regard to moving the thermal layer or growing through it might be somewhere in between the two extremes and that it might not be the same for all fluids.

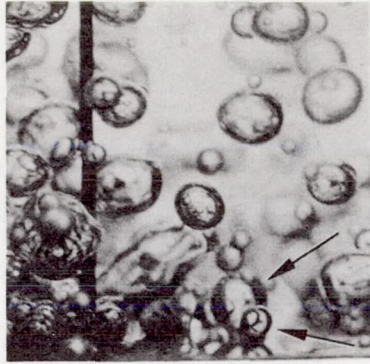
3. The method used to predict vapor superheat is certainly subject to question. The bubble superheat is relatively low during the early stage of growth and it is at this time that the vapor superheat has the greatest effect on the heat flux from the thermal layer.

Coalescence of Bubbles

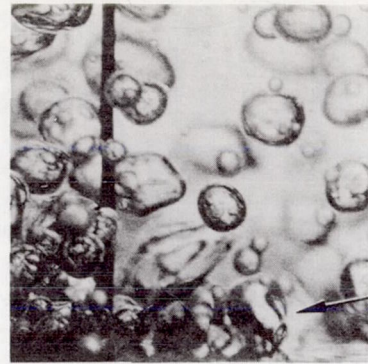
Several types of coalescence were observed at reduced gravity levels which are not present or occur infrequently at 1 g. The type most frequently observed involves coalescence of bubbles growing on the surface. In several instances, bubbles growing on a horizontal surface were seen absorbing smaller bubbles adjacent to them. A sequence of photographs showing this is given in Figure 30. Occasionally, bubbles leave the surface at diameters somewhat smaller than normal. The rise velocity of these bubbles is smaller than average due to the lower buoyancy force associated with the smaller volume of the bubble. In this case, the next bubble growing at the nucleation



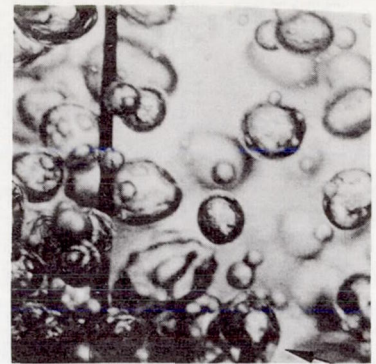
$t = 0 \text{ Sec}$



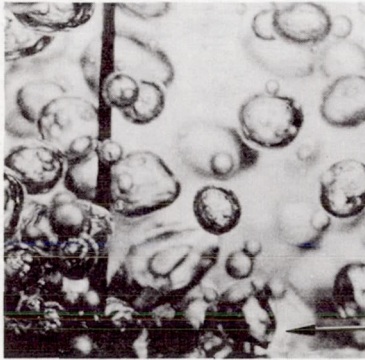
$t = 0.003 \text{ Sec}$



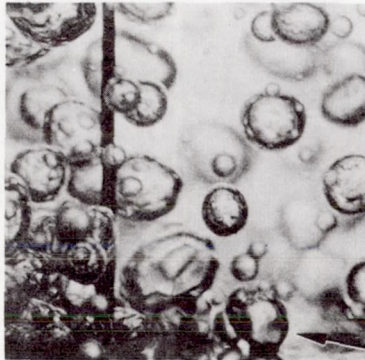
$t = 0.006 \text{ Sec}$



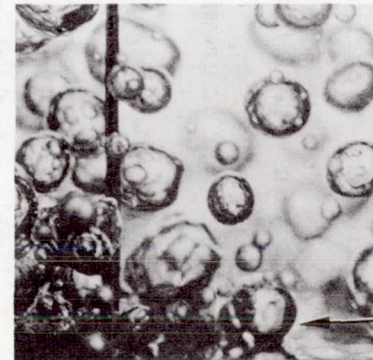
$t = 0.009 \text{ Sec}$



$t = 0.012 \text{ Sec}$



$t = 0.015 \text{ Sec}$



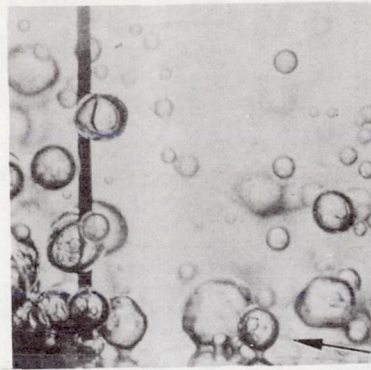
$t = 0.018 \text{ Sec}$

Figure 30. Coalescence of a Small Bubble by a Larger Bubble Growing on a Horizontal Surface

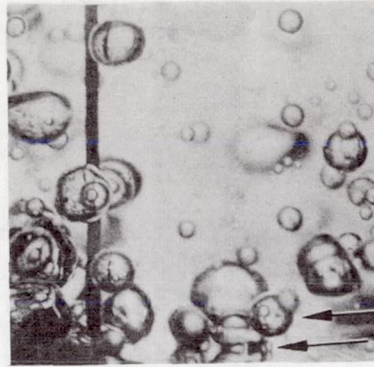
site vacated by the departed bubble will sometimes be absorbed. The photographs of Figure 31 illustrate this phenomenon. Siegel and Keshock [23] reported the same types of coalescence as described above in their reduced gravity work with water.

A final type of coalescence found in boiling from a horizontal surface was seen after the bubbles had departed from the surface and were rising through the fluid. Bubbles whose rise trajectories brought them close together would frequently merge. This happened several times so that the bubble became quite large.

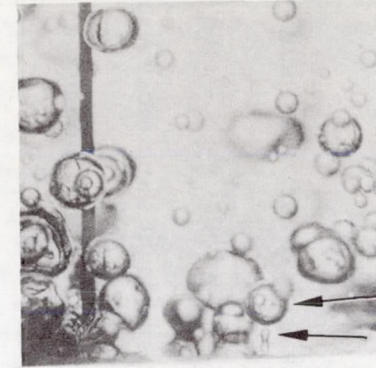
For the vertical surface, bubbles do not grow and depart in the same manner as on the horizontal surface with Freon 113. After a short time, the bubbles would leave their nucleation site and slide up the surface (Figure 32). For 1 g, the bubble moved away from its site almost immediately and was usually seen to have moved on the second frame on which the bubble was visible. At reduced gravity, several frames were usually required to detect movement up on the surface. At both 1 g and at reduced gravity, the bubbles remained very close to the surface and infrequently moved away from the influence of other bubbles growing on the surface. The result with the slow moving, large bubbles at reduced gravity was pronounced coalescence and vapor accumulation near the surface (Figure 33). This vapor accumulation seems to have an effect on the heat transfer characteristics of the surface, as will be pointed out in a subsequent section.



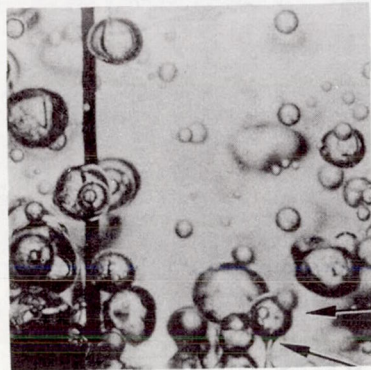
$t = 0 \text{ Sec}$



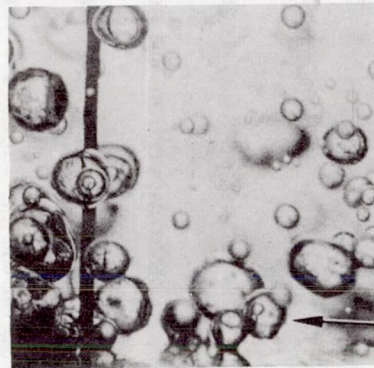
$t = 0.087 \text{ Sec}$



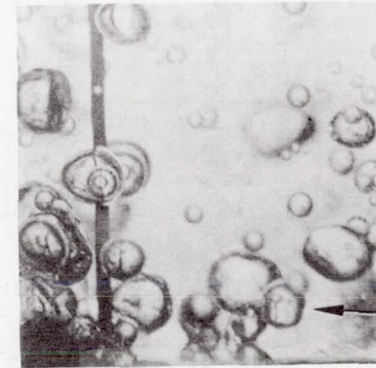
$t = 0.090 \text{ Sec}$



$t = 0.093 \text{ Sec}$

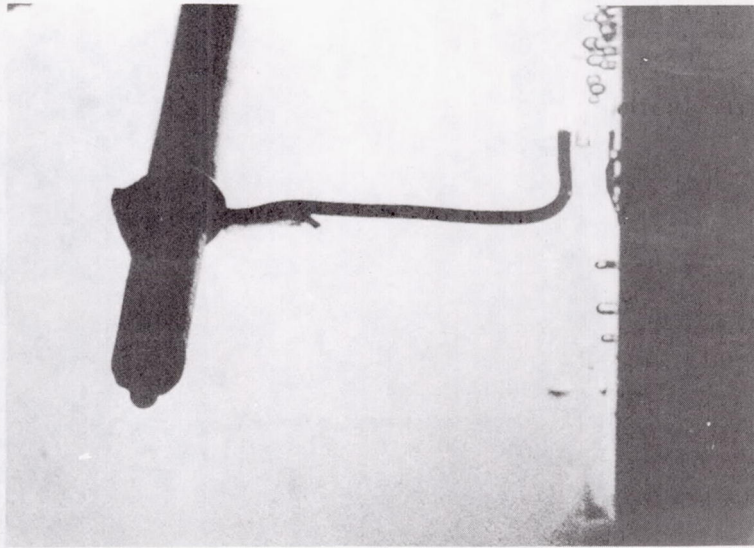


$t = 0.096 \text{ Sec}$

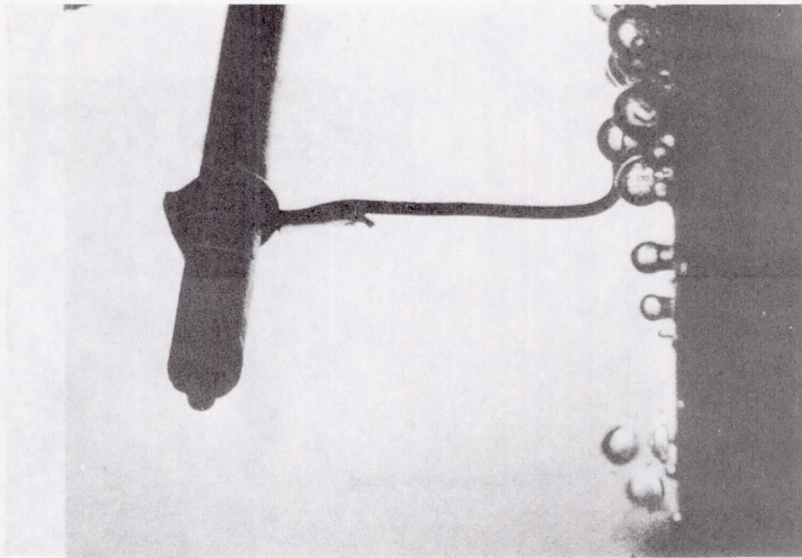


$t = 0.099 \text{ Sec}$

Figure 31. Coalescence of a Bubble Growing on a Horizontal Surface by a Bubble Moving Away From the Surface

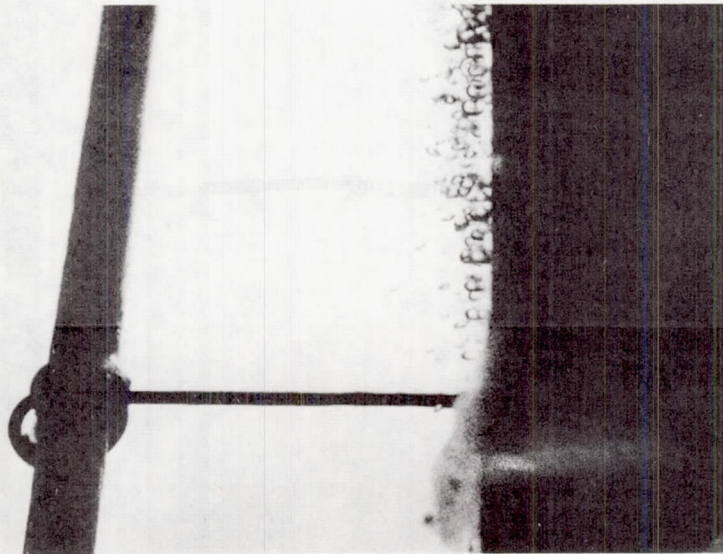


a. Standard Gravity

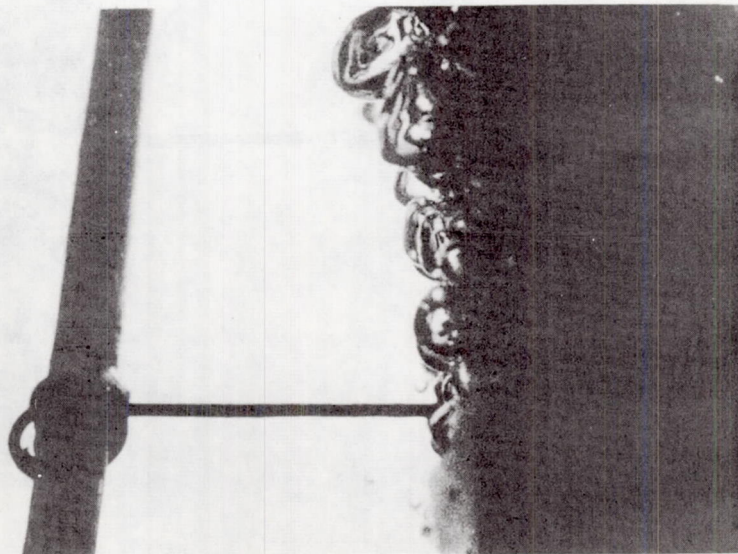


b. Reduced Gravity

Figure 32. Bubbles Growing and Sliding Up a Vertical Surface



a. Standard Gravity



b. Reduced Gravity

Figure 33. Bubble Coalescence on a Vertical Surface at a Heat Flux Near the Incipient Point

Bubble Departure Diameters

The ratio of bubble departure diameters at 0.01 g and 0.02 g to the bubble departure diameters observed at standard gravity are shown in Figure 34. It can be seen that a wide scatter of ratios were observed. This scatter is produced by a variation in departure diameter at the reduced gravity level. The departure diameters at standard gravity were reasonably consistent and varied from 0.027 inch to 0.32 inch. Also shown in the figure are lines which indicate the departure diameter ratios predicted by Fritz [36] and Zuber [28]. It can be seen that the data points fall, in general, above the Zuber predictions and below the Fritz predictions. In previous investigations, Siegel and Keshock [23] and Schwartz [4] had found the Fritz equation to be valid for water in the acceleration range of this investigation, although Siegel and Keshock found that the Zuber equation was better for acceleration levels greater than 10 percent of standard gravity.

Reduced Gravity Nucleate Boiling Data

As explained previously, the primary purpose of this investigation was to determine the influence of reduced gravity and surface orientation on the nucleate portion of the pool boiling curve. A number of tests were conducted with the two test heaters previously described, and the results of these are presented in reduced form in Appendix A. In order to compare the results at reduced gravity with standard gravity, a standard gravity test was always

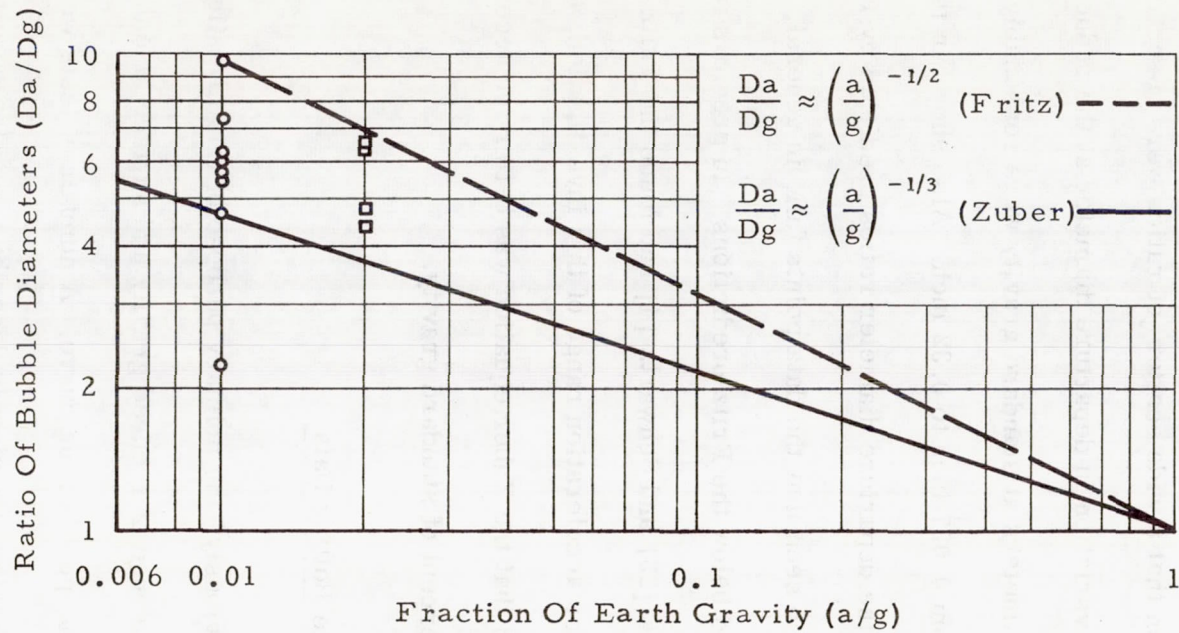
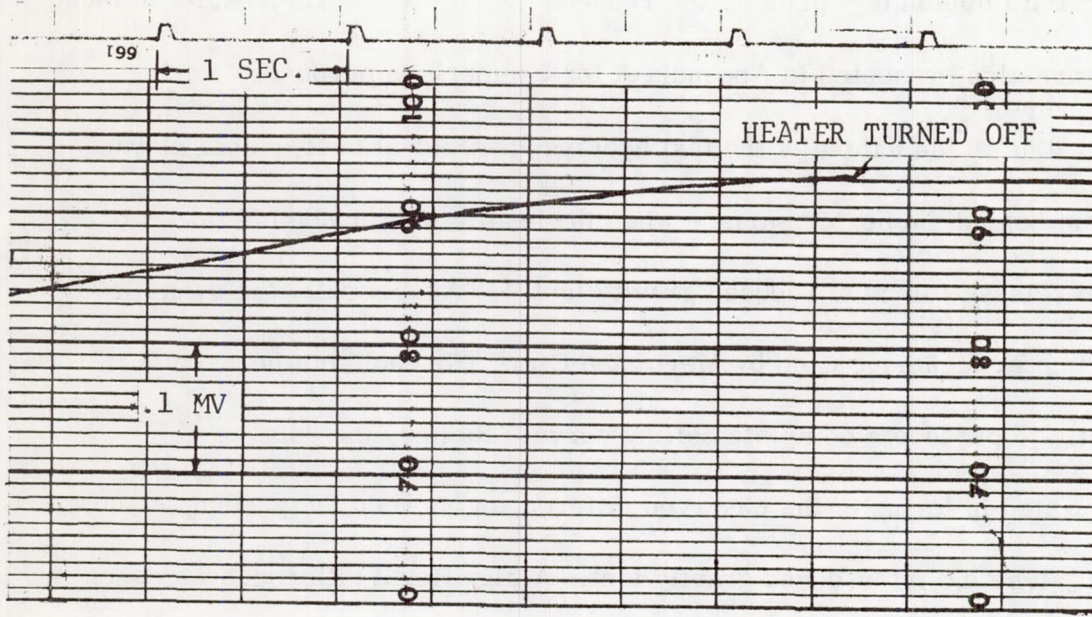


FIGURE 34. COMPARISON OF OBSERVED BUBBLE DEPARTURE DIAMETERS WITH THEORY

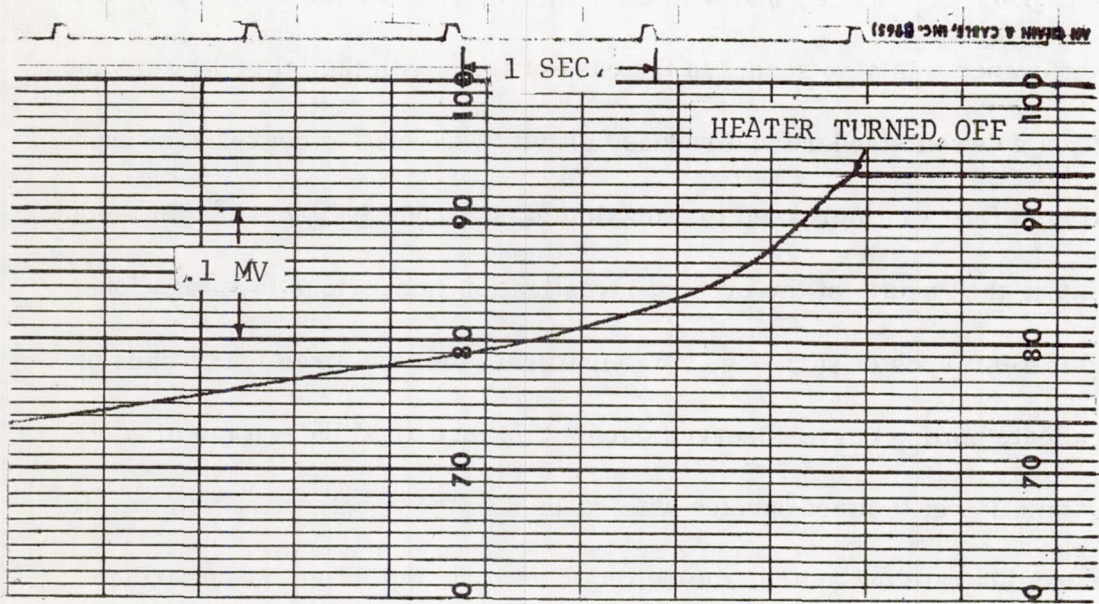
conducted immediately prior to the reduced gravity test. The results of these tests are also presented in Appendix A for comparison purposes.

Due to the nature of the test heaters, a residual energy source was present behind the heater surface when the heater was turned off (at aeroshield release for most reduced gravity tests). As a result, the dynamic calorimeter technique used by Merte and Clark [6] could not be used directly to produce a complete boiling curve. Rather, the data were interpreted in terms of the observed differences between the predrop standard gravity test and the reduced gravity test. A significant difference was seen in all cases with the 2 inch by 4 inch heater operating at maximum heat flux (5500 to 6000 BTU/hr-ft²) and with the 2 inch by 2 inch test heater, a significant difference was also seen. In the case of tests with the latter heater, the variation between standard and reduced gravity was seen to decrease as the initial heat flux was increased to a maximum of 21,500 BTU/hr-ft². In terms of relating the results of the present investigation to previous investigations with different types of surfaces, it is significant that the direction of shift of the nucleate boiling curve observed during this investigation is a function of the orientation of the test surface with respect to the acceleration vector. In order to illustrate the shift in the boiling curve and the influence of surface orientation, some of the raw data will now be presented.

The variation with acceleration level and the influence of surface orientation are illustrated by the data shown in Figures 35 and 36. Figure 35 is a comparison of the surface temperature versus time for the heated

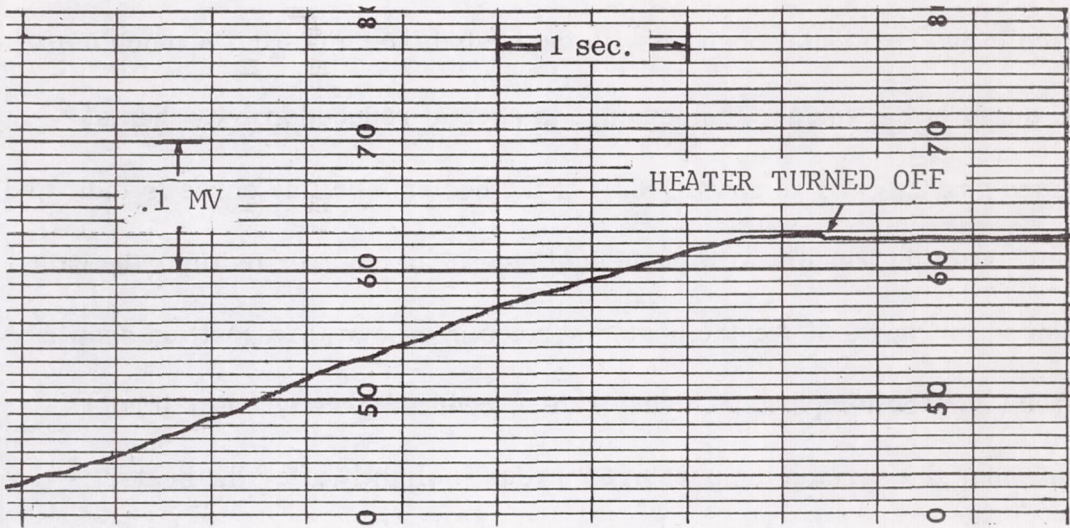


a. Standard Gravity

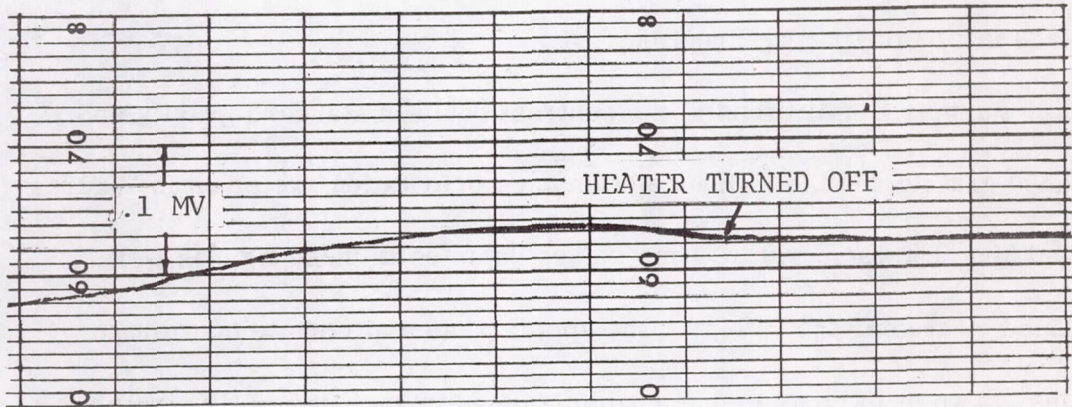


b. Reduced Gravity, 0.01 g

FIGURE 35. COMPARISON OF STANDARD GRAVITY AND REDUCED GRAVITY FOR HORIZONTAL HEATED FACE UP - TEST 10F32, THERMOCOUPLE NO. 4



a. Standard Gravity



b. Reduced Gravity, 0.01 g

FIGURE 36. COMPARISON OF STANDARD GRAVITY AND REDUCED GRAVITY FOR HORIZONTAL HEATED FACE DOWN - TEST 10F34, THERMOCOUPLE NO. 2

surface in the horizontal position with the heated face upward. A much more rapid decay of the surface temperature is seen at reduced gravity than at standard gravity, and an upward shift of the nucleate boiling curve is indicated. In contrast to the results with the heated face in an upward position, the data presented in Figure 36 for the heated surface in a downward position show a retarded surface temperature decay rate at reduced gravity. For this orientation, the surface temperature increases slightly after the heater is turned off and does not decay below its original temperature for approximately 2 seconds. The indicated shift for the boiling curve for the downward facing surface is in a downward direction.

Further illustrations of the contrast between standard gravity and reduced gravity and the influence of surface orientation are given in Figures 37 and 38. The temperature time traces depicted in these figures were obtained by tracing the raw data and applying the appropriate coordinate scales. Two of the four thermocouple traces are included to illustrate the consistency in temperature gradient seen over the surface. The data of Figures 35 and 37 for the horizontal surface facing upward are from the same test and the data of Figures 36 and 37 for the horizontal surface facing downward are from the same test. The data of Figure 38 for the surface in the vertical orientation indicate that the boiling curve for this orientation shifts downward, but the shift is not as pronounced as for the horizontal surface with the heated surface facing downward.

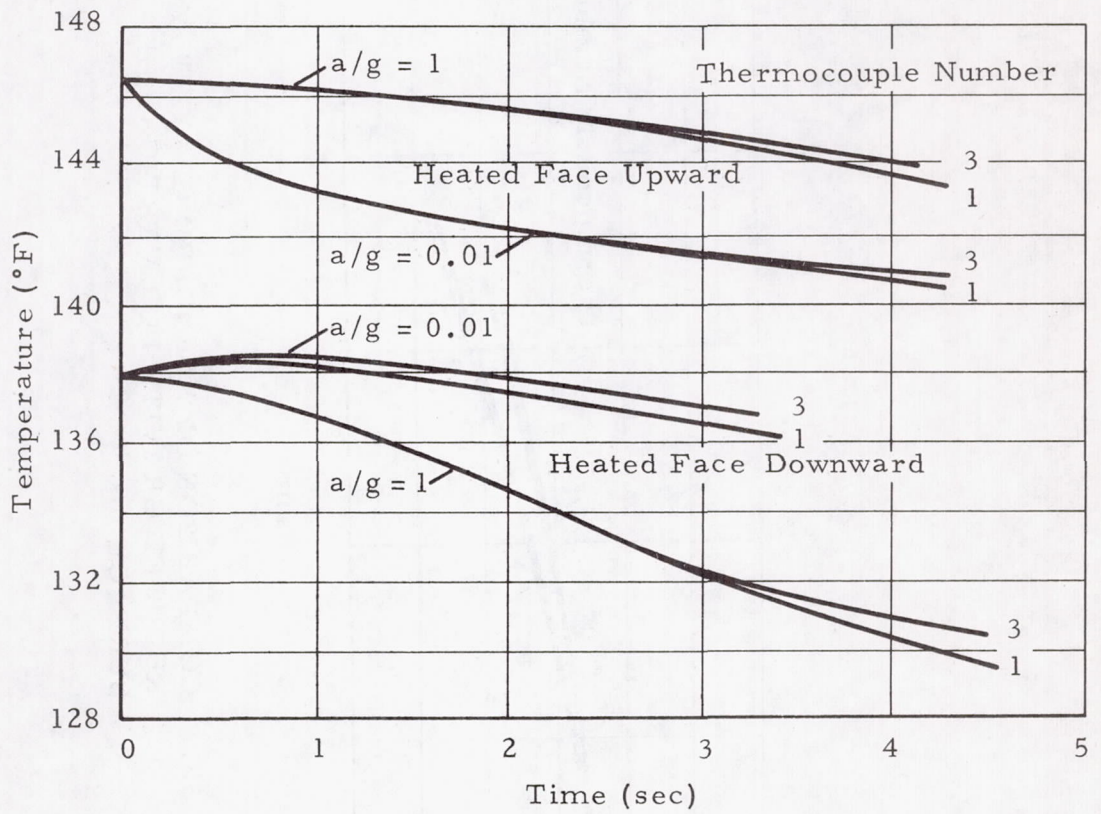


FIGURE 37. COMPARISON OF STANDARD GRAVITY AND REDUCED GRAVITY FOR HORIZONTAL SURFACE

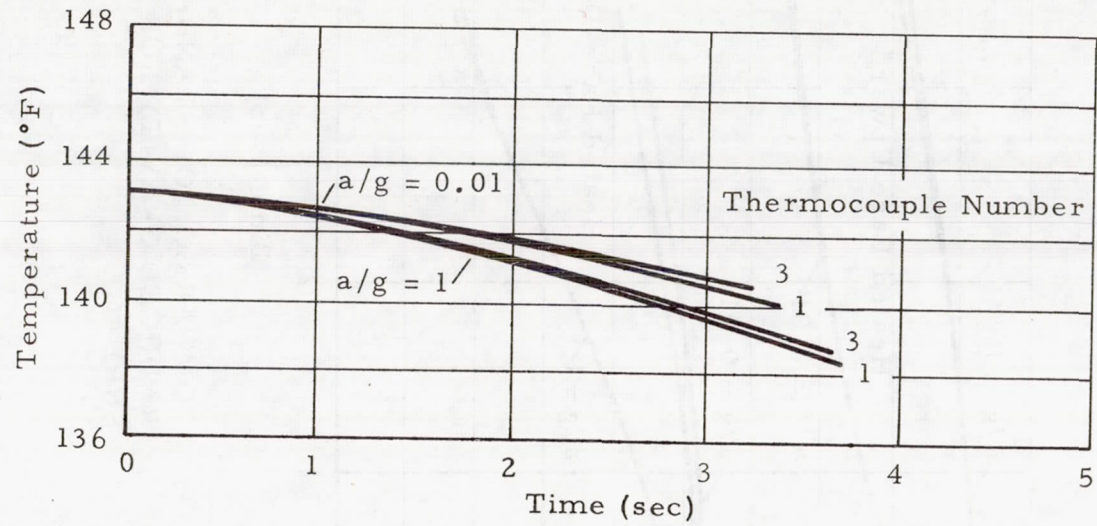


FIGURE 38. COMPARISON OF STANDARD GRAVITY AND REDUCED GRAVITY FOR VERTICAL HEATED SURFACE

The results presented in the preceding figures were taken from three sets of data for the various orientations. Several tests were conducted for the three different orientations, and the trend was always in the same direction for each orientation as that presented in the figures.

The universal timer, which controls the time of turnoff for the test heater, malfunctioned during one test with the heater in the vertical orientation. On this test, the heater was turned off approximately 2 seconds prior to aeroshield release rather than at the time of release. The result was an interesting verification of the results presented previously for the vertical orientation. As seen in Figure 39, the decay rate of the heater surface temperature experienced a marked change after the time of package release, which again indicates a shift of the boiling curve in the downward direction.

The most desirable way to present the results of the investigation would be to present a complete standard gravity pool boiling curve and then a complete reduced gravity boiling curve so that they could be compared directly. As explained previously, however, the Nichrome heating element behind the heater surface constitutes a residual energy source after the heater power has been turned off. The time rate of change of enthalpy of the heater mass does not, then, represent the boiling heat flux. Instead, an energy balance for the heater surface must include the energy source and the heat leak through the insulation must also be considered. The system involved has a Biot Number of approximately 0.005 and may therefore be treated as a lumped system.

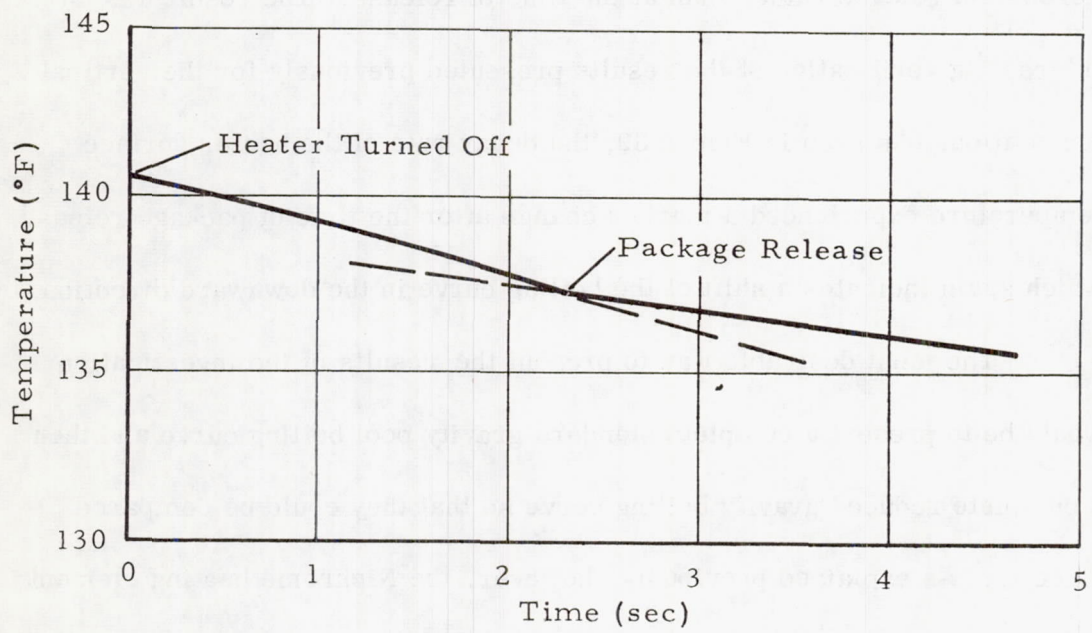


FIGURE 39. COMPARISON OF TEMPERATURE GRADIENT AT STANDARD GRAVITY AND REDUCED GRAVITY FOR VERTICAL HEATER

Considering the energy source and heat leak through the insulation, an energy balance for the heater surface may be written as,

$$\left(\frac{m}{A} \frac{dH}{dt} \right)_{\text{heater mass}} = \left(\frac{q}{A} \right)_{\text{heater element}} - \left(\frac{q}{A} \right)_{\text{boiling}} - \left(\frac{q}{A} \right)_{\text{leak}} \quad (20)$$

The heat leak through the insulation has been estimated (Appendix B) to be much less than 2 percent of the energy dissipation by boiling and could be neglected. The heat leak to the heater mass from the heater element is, however, an unknown function of time. At the time when the heater is turned off, it should have the same value for both the reduced gravity test and the standard gravity test since both tests started at the same power level and were initially at steady state. At the time of power cutoff, equation (20) can be written for both standard gravity and reduced gravity and the two equations subtracted yielding,

$$\left(\frac{m}{A} \frac{dH}{dt} \right)_{\text{heater } 1 \text{ g}} - \left(\frac{m}{A} \frac{dH}{dt} \right)_{\text{heater } \text{low g}} = - \left(\frac{q}{A} \right)_{\text{boiling } 1 \text{ g}} + \left(\frac{q}{A} \right)_{\text{boiling } \text{low g}} \quad (21)$$

This relationship can be used to obtain a value for the shift of the boiling curve near the beginning of tests. Its use after the first portion of tests is completely valid only if no shift of the boiling curve occurs and the energy input from the heater element is assumed to be the same function of time for both standard gravity and reduced gravity.

The time rate of enthalpy change of the heater mass was calculated for all tests from the reduced time versus surface temperature data and is presented in Appendix A. The specific heat versus temperature data for the copper used was taken from Reference 46. The mass of each heater was determined by weighing the copper prior to heater assembly. In order to avoid the large number of hand calculations involved, a digital computer program was written to reduce the data.

Equation (21) was used to obtain the shift of the boiling curve and sample results for the 2 inch by 4 inch horizontal heater facing upward are presented in Figure 40 plotted versus the difference between the surface temperature and the Freon saturation temperature. As explained previously, only the initial difference (at the highest value of $T_w - T_{sat}$) is completely valid. The difference between standard gravity and reduced gravity, at that point, ranges between 3000 and 5500 BTU/hr-ft². Since the initial power level of this heater was approximately 5500 BTU/hr-ft², this represents a shift in the boiling curve between 50 and 100 percent in an upward direction. The data of Figure 40 have been added to the standard gravity boiling curve and are presented with the more conventional log-log plot in Figure 41.

Since the surface temperature changed very little for the vertical and horizontal heated face downward orientations, the values obtained from equation (21) for those orientations cannot be presented versus $T_w - T_{sat}$. Instead, Figure 42 gives the change seen versus time. The data for the horizontal surface with the heated face upward are also shown for comparison.

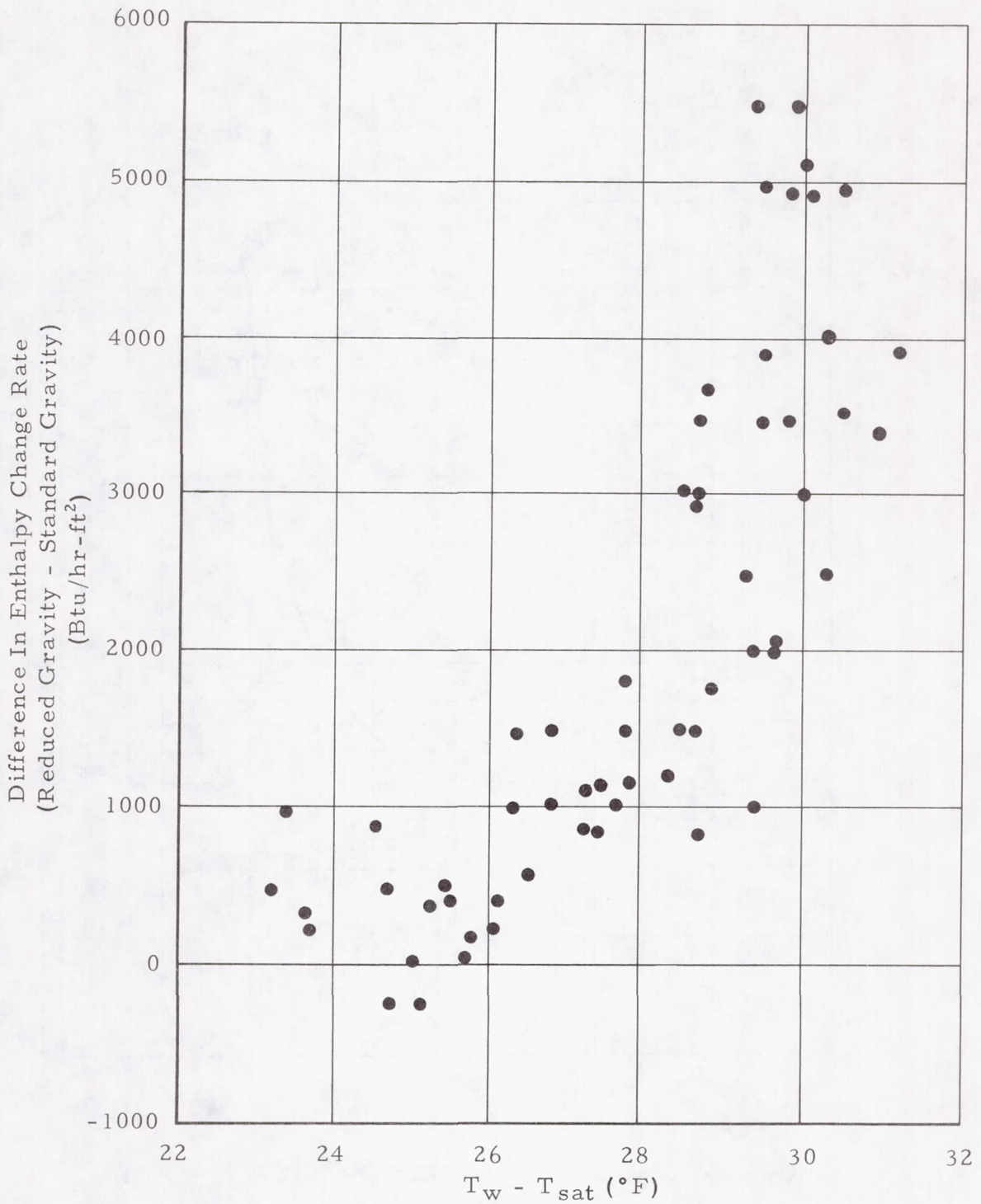


FIGURE 40. DIFFERENCE IN ENTHALPY CHANGE RATE BETWEEN REDUCED GRAVITY AND STANDARD GRAVITY VERSUS $T_w - T_{sat}$ FOR HORIZONTAL HEATED SURFACE FACING UPWARD

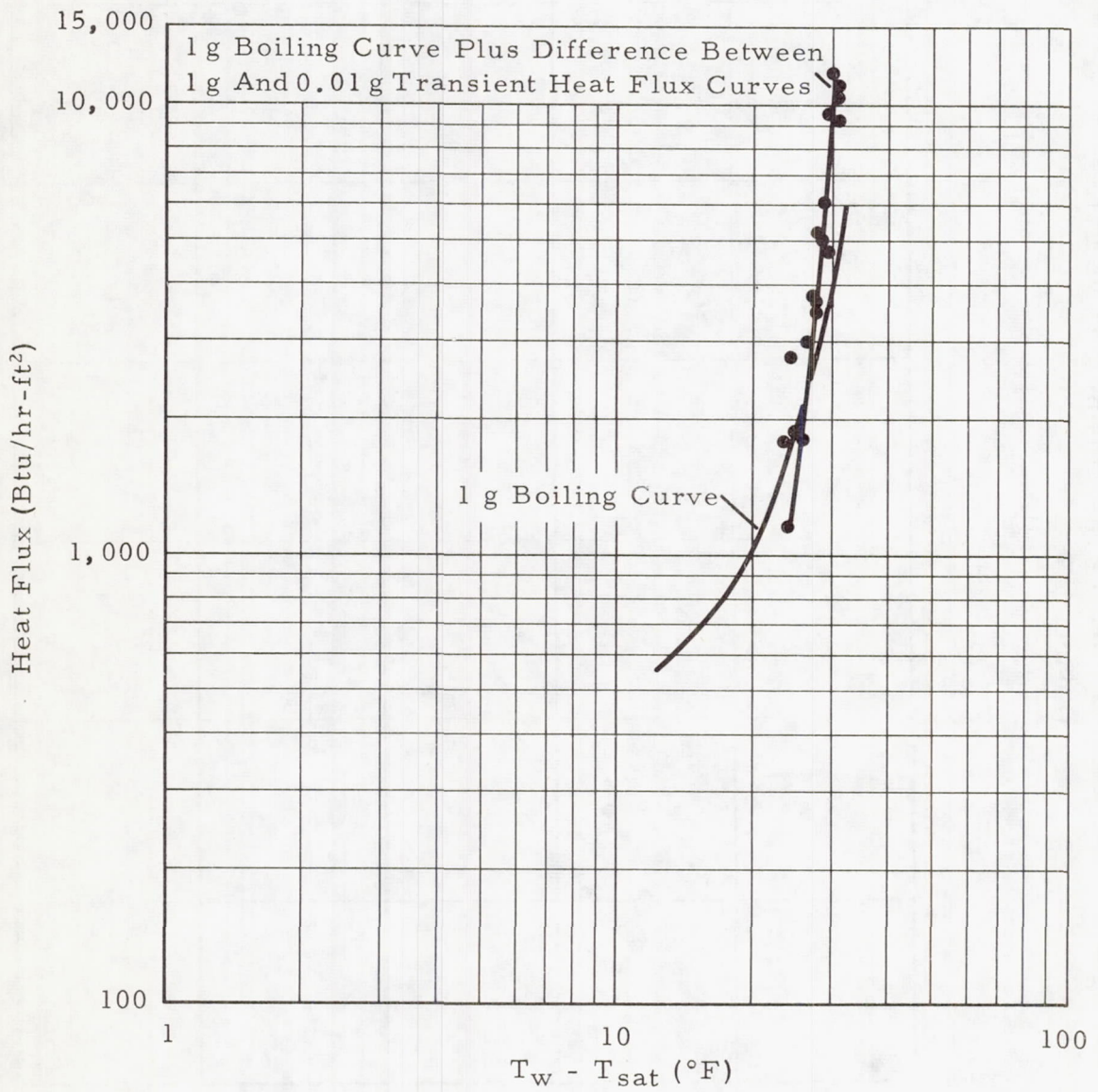


FIGURE 41. ENTHALPY CHANGE RATE DIFFERENCE OF FIGURE 40 ADDED TO STANDARD GRAVITY BOILING CURVE

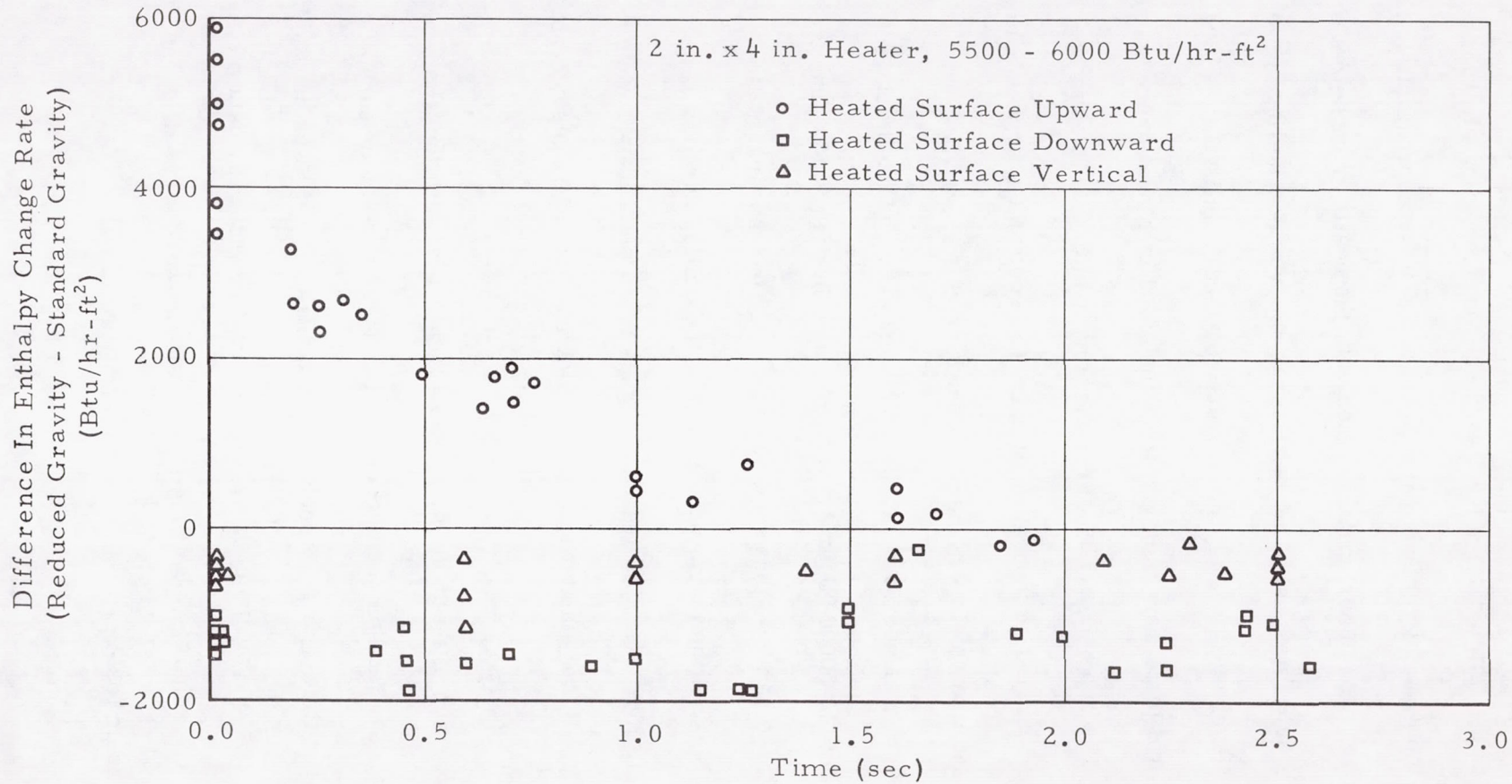


FIGURE 42. DIFFERENCE IN ENTHALPY CHANGE RATE BETWEEN REDUCED GRAVITY AND STANDARD GRAVITY VERSUS TIME FROM RELEASE

In contrast to the latter data, a downward shift of approximately 10 percent is seen for the vertical surface and a downward shift of approximately 25 percent is seen for the horizontal surface with the heating face downward.

In order to investigate the behavior of the nucleate boiling curve at higher heat fluxes and to verify the results obtained with the 2 inch by 4 inch heater, several tests were run with the 2 inch by 2 inch heater previously described. The upper power limit for the first heater was fixed by the battery power carried on the test package. The second heater was made smaller in order to obtain a higher heat flux per unit area.

The data obtained with the second heater at power levels of 7100 BTU/hr-ft² and 21,500 BTU/hr-ft² are presented in Figure 43. The trend of the data is the same as that shown in Figure 42 for the first heater. It is also interesting that the magnitude of shift of the boiling curve is reduced as the heat flux is increased. This fact assumes more significance when considered along with the standard gravity boiling curves to be presented in the following section.

Comparison of the data of Figures 42 and 43 reveals that the peak difference between the standard gravity and reduced gravity appears at a slightly greater time with the 2 inch by 2 inch heater. This was caused by the timing of heater power cutoff by the universal timer. The data plotted in Figure 43 are related to the time from heater power termination, and this occurred on some tests prior to aeroshield release.

2 in. x 2 in. Heater

- 7,100 Btu/hr-ft², Heating Face Up
- 7,100 Btu/hr-ft², Heating Face Down
- △ 21,500 Btu/hr-ft², Heating Face Up
- 21,500 Btu/hr-ft², Heating Face Down

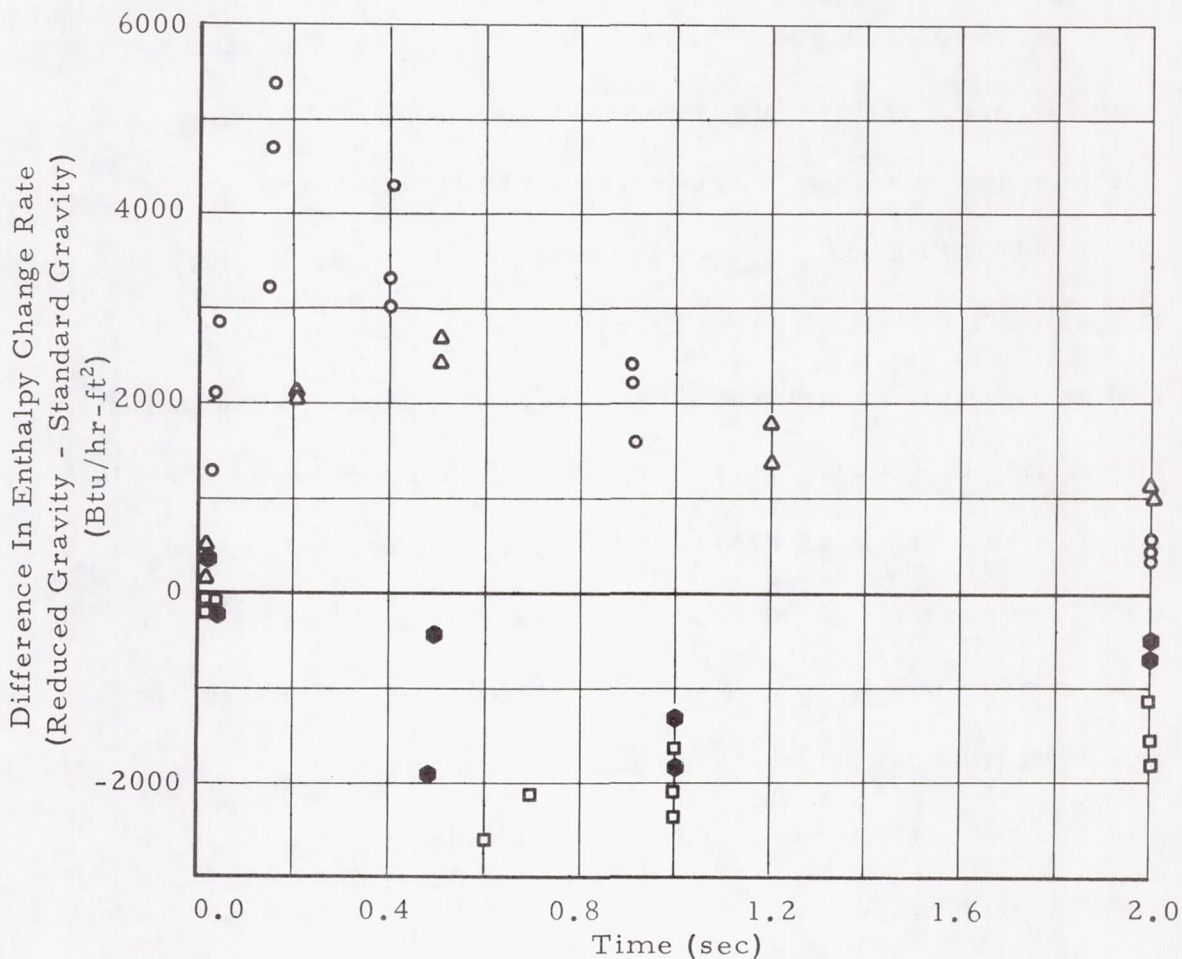


FIGURE 43. DIFFERENCE IN ENTHALPY CHANGE RATE BETWEEN REDUCED GRAVITY AND STANDARD GRAVITY VERSUS TIME FROM HEATER POWER TURN OFF (2 in. x 2 in. HEATER)

Standard Gravity Nucleate Boiling Data

In order to have a basis for comparison of the changes seen in the nucleate boiling curves for the various orientations between 1 g and low g, standard gravity boiling curves were created using the procedures outlined in the Test Procedures Section. The results for the 2 inch by 4 inch heater are presented in Figure 44 for the three orientations tested. The boiling curve is seen to shift in an upward direction as the heater orientation is changed from horizontal heating face upward to vertical to horizontal heating face downward. The results for the heater in the horizontal position with the heating face downward are contrary to what was expected. As can be seen from Figure 45, however, the same results were obtained for the 2 inch by 2 inch heater. The data for the two heaters are compared in Figure 46. Considering the fact that two different heaters are involved and that a deviation of the nucleate boiling curve is expected between different surfaces, the agreement of the two sets of data is quite satisfactory.

In obtaining the data for the horizontal heating face downward, the heater surface was normally only approximately 1.5 inches from the bottom of the test container. In order to determine whether the location of the surface with respect to the test container influenced the data, the distance was increased to the same level as the heater surface when tested in the horizontal heated face upward position. No significant change was seen in the results.

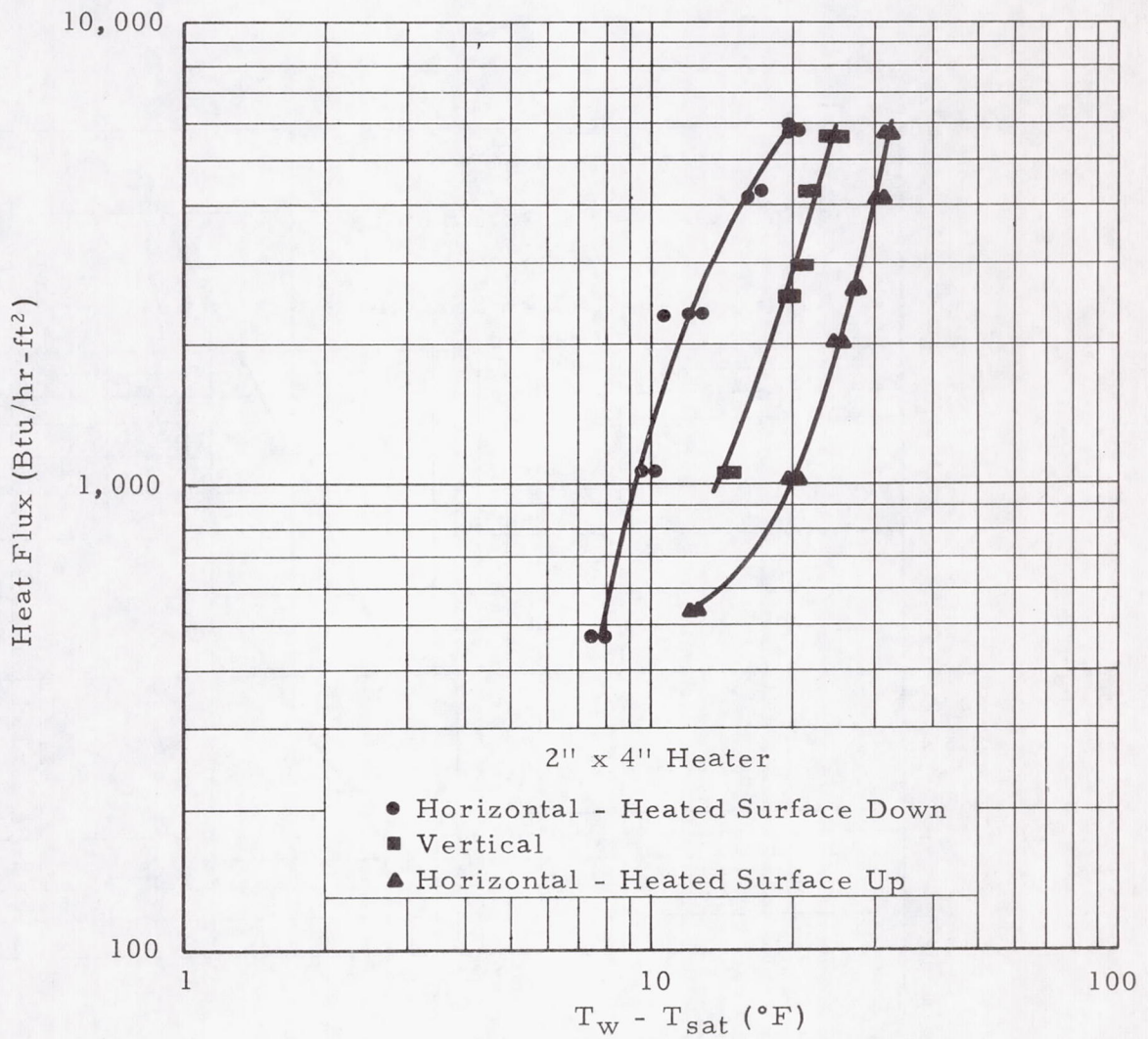


FIGURE 44. ONE g BOILING RESULTS VERSUS ORIENTATION (2'' x 4'' HEATER)

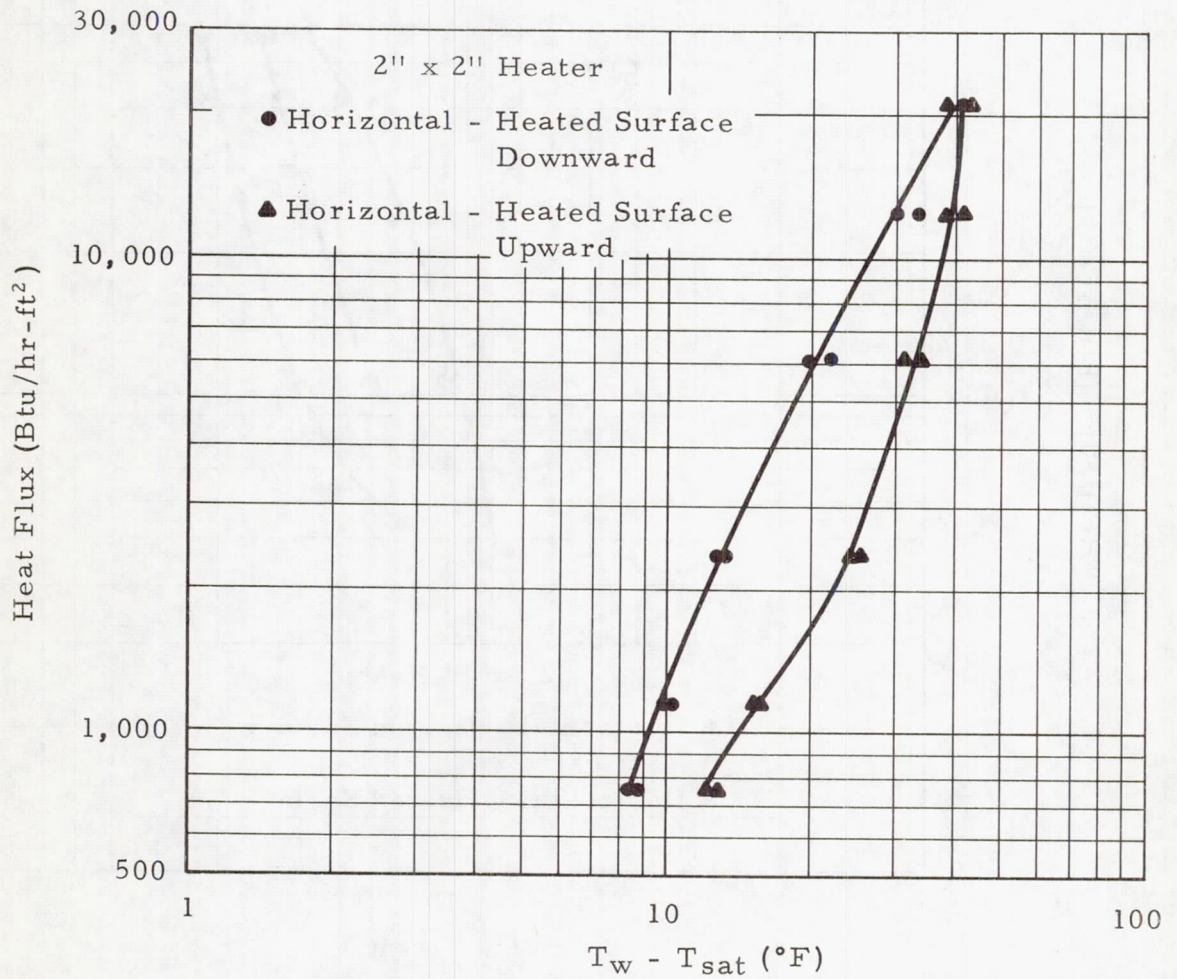


FIGURE 45. ONE g BOILING RESULTS VERSUS ORIENTATION (2'' x 2'' HEATER)

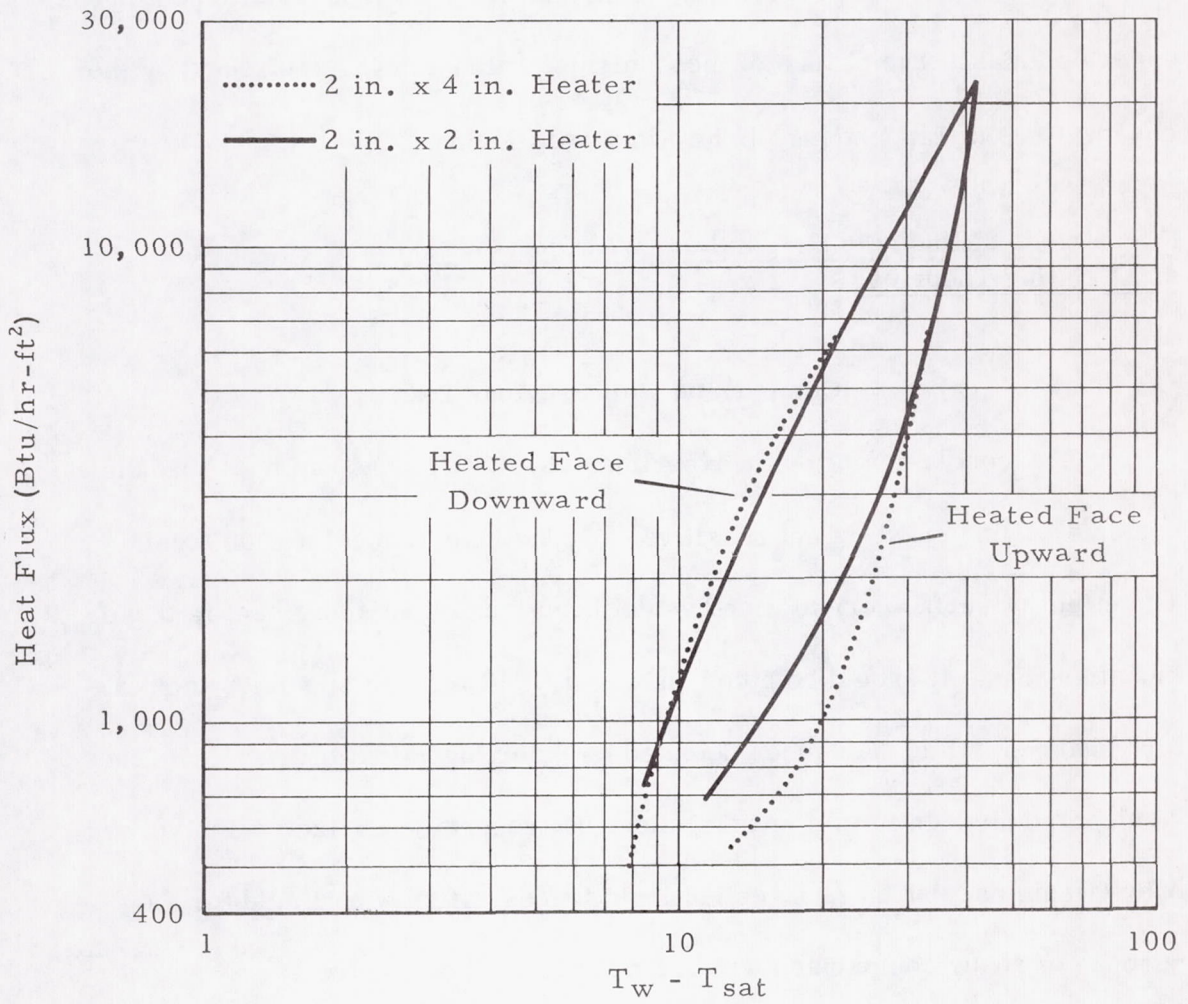


FIGURE 46. COMPARISON OF STANDARD GRAVITY DATA FOR HEATERS

An interesting feature of the data presented in Figure 45 is that as the heat flux is increased, the curves seem to merge for the two horizontal orientations. In the region where the curves come together, the mechanism of boiling on the surface is changing from that of isolated bubbles to continuous vapor columns. The change of mechanisms at this point is confirmed by the observations of Lippert [47] in his work with Freon 113.

Comparison of Nucleate Boiling Data With Previous Data and Existing Theories

Comparison with Previous Data

The conclusion of prior experimental investigators has been that the nucleate boiling curve is not sensitive to reductions in acceleration level. The effect of surface orientation has not been treated as significant in these investigations. It should be noted, however, that the test specimen temperature changes, which have been detected on prior investigations, indicate the same trend as seen in this investigation with respect to surface orientation. A brief summary of these investigation's trends will now be listed for the purpose of ready comparison with the results of this research.

1. Sherley [5] found that if a statistical line was drawn through data obtained for a horizontal plate, the direction of temperature shift for a given heat flux would be downward.

2. Clodfelter [7] detected a downward shift in temperature using horizontal wires and ribbons.

3. Siegel and Keshock [8] found a downward shift in temperature using horizontal wires and upward shift in temperature with vertical wires.

4. Schwartz's [4] data indicate a slight downward shift in temperature with a small horizontal surface.

5. Papell and Faber [11] found a downward shift in temperature with a small horizontal ribbon.

6. Merte and Clark [5] saw an upward shift in temperature with spheres.

It can be seen that the upward shift in temperature with vertical surfaces and the downward shift in temperature with horizontal surfaces with the heated face upward seen in the present investigation are in agreement with the trends of the previous investigations. No basis of comparison exists for the horizontal surface with the heated face downward.

As explained previously, the size of the surfaces used in some of the previous investigations has been approximately the same size as the bubbles at reduced gravity. For this reason, the small magnitude of shift in the nucleate boiling curve found by these investigators is subject to some question. However, this objection does not apply to the 2 square inch surface area used by Sherley.

The variation in the direction of the shift of the nucleate boiling curve at reduced gravity with surface orientation found in this investigation might possibly explain the relative insensitivity of the spheres of Merte and Clark to reductions in gravity level. It would seem that the sphere would effectively

average the variations seen over its surface and could yield an overall shift which is insignificant while relatively large positive and negative shifts of the nucleate boiling curve might exist on some areas of the sphere.

Comparison with Boiling Models

The nature of the results of this investigation does not permit direct comparisons with existing correlations and models. It is of interest, however, to compare the trends predicted by some of the more popular boiling models with respect to gravity level with the trends observed in this work. Some existing models are based on the stirring action of the bubble as it grows and departs from the heated surface. As explained by Zuber [1], this argument has some validity in the regime of isolated bubbles, but is questionable at higher heat fluxes where the growing bubbles interfere with each other and vapor columns and vapor patches come into existence. The validity of the argument in the lower heat flux range was verified somewhat by the work of Mixon, Chon, and Beatty [48] by generating gas bubbles electrolytically at a heated surface. It was found that the heat flux at a given temperature difference could be increased by a factor of 2 to 3. Even at a high generation rate of inert gas bubbles, however, the heat transfer coefficient was still in the nucleate boiling regime. The investigations of Rallis and Jawurak [49] and Schwartz [4] have both indicated that the contribution to total energy removal from a surface boiling in saturated water which could be attributed to latent heat increased as the heat flux to the surface increased.

In reporting his work on the effects of reduced gravity on boiling of saturated water, Schwartz analysed some of the existing models with respect to their predictions of the change of the nucleate boiling heat transfer coefficients with changes in acceleration level. The results obtained are pertinent to the present work and will be reviewed in the following paragraphs.

Zuber [50] suggests that the mechanism involved in energy removal in the isolated bubble region of the nucleate boiling curve is similar to that involved in turbulent natural convection from a horizontal surface since in both cases the heat transfer is caused by an "up-draught" circulation. The equations used in turbulent natural convection were used in the isolated bubble regime by making a suitable modification to the fluid density to include the vapor present. Schwartz has examined the terms of the equation resulting from the analysis and finds that, as would be expected from the analogy with free convection, the relationship is gravity dependent. In terms of the effect of gravity level, the equation is

$$h = a^{1/3} \left[\text{const} + \frac{C_4}{a^{3/4}} \right]^{1/3} \quad (22)$$

and, as pointed out by Schwartz, at low gravity levels,

$$h \sim C_5 a^{1/12} \quad (23)$$

The trend predicted by this relationship is opposite to the results found in the present investigation for a horizontal surface with the heated face upward.

This would be expected, however, since the free convection analogy was used

and this mechanism varies directly with acceleration level. It is interesting that the trend found by Merte and Clark [13], and other investigators in accelerated systems at low heat fluxes is consistent with the trend predicted but is in the opposite direction at high heat fluxes. The results at high heat fluxes are probably out of the isolated bubble regime and not compatible with Zuber's basic assumption.

Tien [51] has assumed that the flow field induced by the departing bubbles in the isolated bubble regime may be represented by an inverted stagnation flow. Solutions are available for the Navier-Stokes equations for plane flow representing this case and Tien used such a solution to obtain a heat transfer coefficient of the form

$$h = 1.32 \text{ Pr}^{0.33} \left(\frac{\Gamma n}{A} \right)^{0.5} k \quad (24)$$

As pointed out by Schwartz, the parameter Γ is defined as

$$\Gamma = \frac{a'}{\frac{nr}{A}} \quad (25)$$

and the constant, a' , appearing in this relationship is related to the velocity parallel to the wall

$$U = a'x \quad (26)$$

Since this velocity is a direct result of the rising bubbles, and since the bubble rise rate is gravity dependent, it would seem that the resulting heat

transfer coefficient is gravity dependent. The direction of the dependence would yield a decrease in heat transfer with a reduction in gravity level, since the bubble rise velocity decreases at reduced gravity. This is opposite to the direction of shift observed in the present work for the horizontal surface with the heated face upward. This is the only orientation used with which the model can be compared.

Han and Griffith [52] have proposed a model for the region of isolated bubbles which includes the natural convection from the area of the surface not influenced by growing and departing bubbles and a bulk convection term for the portion of the surface influenced by bubbles. The authors argue that when a bubble leaves the surface, it carries away the superheated thermal layer in contact with the heated surface within an influence circle, whose diameter is two times the diameter of the departing bubble. The energy removed in this manner was calculated using transient conduction results which were applied over the time of growth of the vapor bubble. The contribution due to the latent heat of the vapor inside the bubble was included in the bulk convection term and the authors argue that it is small in comparison to the other two terms. Schwartz has taken the expression derived and, neglecting the latent heat term, arranged it in a form such that the gravity dependence may be determined. The relationship in this form is

$$q \sim Nu + f D_d^2 \delta \quad . \quad (27)$$

Han and Griffith suggest that the thermal layer thickness $\delta \sim \left(\frac{1}{f}\right)^{1/2}$. At reduced gravity, the influences of natural convection may be neglected and the expression for q then becomes

$$q \sim f^{1/2} D_d^2 \quad (28)$$

For the present investigation, the bubble frequency, f , has been seen to vary approximately in proportion to a and the prediction for variation of bubble departure diameters by Fritz of $\frac{D}{D_0} \sim \left(\frac{a}{g}\right)^{1/2}$ seems reasonable. In terms of dependence on gravity level, the heat flux expression then becomes,

$$q \sim a^{-1/2} \quad (29)$$

In contrast to the two models described previously, the direction of shift of the nucleate boiling curve at reduced gravity for the horizontal surface with the heated face upward is predicted by the Han and Griffith model. The results of Merte and Clark for high acceleration at low heat flux might also be predicted since in this case the free convection term which was deleted above would have to be included and might overshadow the decrease predicted by the portion of the total expression represented by equation (29). A modification of this model might also explain the increased efficiency of nucleate boiling from vertical surfaces and horizontal surfaces with the heating face downward at standard gravity. In both cases, the vapor bubbles were seen to slide across the heated surface and a disruption of the thermal layer probably resulted

which could be analogous to the thermal layer removal portion of the Han and Griffith model.

In addition to the energy removal mechanisms involved in the foregoing models, the mass transport model postulated by Snyder and Robin [43] deserves consideration with respect to the results of this investigation. The model postulates that evaporation occurs from a thin film of liquid between the bubble vapor and the heated wall and is deposited simultaneously by condensation at the top of the vapor bubble. It was surmised by Snyder and Robin that the energy deposited by condensation at the top of the bubble was convected to the bulk fluid by turbulent eddies at the liquid-vapor interface. Photographic evidence for the existence of the proposed microlayer has been cited in a previous section, and measurements of rapid temperature fluctuations of the heated surface beneath growing bubbles [54, 55] support that evidence. Snyder and Robin [43] have shown experimentally that the mass transfer mechanism can be significant in turbulent subcooled forced convection nucleate boiling. They found that the energy transferred by a single bubble was from 10 to 100 times as great as the latent heat content of the vapor inside the bubble.

If the removal mechanism were present, the mass transport model could explain the increase in heat transfer coefficient seen in the current investigation for the horizontal surface with the heated face upward. For this model, most of the energy is assumed to come from a vaporizing liquid sublayer. As shown earlier, at reduced gravity, the bubble is significantly

larger than at standard gravity and more microlayer would be in contact with the heated surface. Recent work by McGrew [35] has shown that the velocity field associated with surface tension gradients around gas bubbles on a heated wall produces velocities of the same magnitude (0.2 ft/sec) as used by Snyder at the lower end of the velocity range in his experiments. Velocities of this magnitude produced energy transfer rates for bubbles of a factor of 10 greater than that of the latent energy content of the vapor of the bubble.

The recent work of Hospeti [56] has yielded some interesting data on microlayer vaporization. In his work, he found that the contribution to total energy removal by vaporization of the microlayer increased progressively for spherical, oblate, and hemispherical bubbles. The direction of increasing contribution of the microlayer is that of increasing surface area in contact with the heated surface, and this is the same phenomenon which occurs with a reduction in acceleration level. An increased heat transfer coefficient was also seen at standard gravity when the heated surface was turned from the heated face upward to the heated face downward orientation. It was noted that the bubble sizes increased by approximately an order of magnitude as a result of the change. Hospeti also found that the contribution of microlayer vaporization to total energy removal decreases with increasing heat flux. This observation is consistent with the finding of this investigation that the shift in the boiling curve with a reduction in gravity level decreases as heat flux is increased for the horizontal surface with the heated face upward. It is also consistent with the fact that the boiling curves for the heated face upward and

heated face downward at standard gravity merge at high heat fluxes (Figure 45).

Adelberg [56] has suggested that the criterion for gravity dependence of the boiling curve in the nucleate boiling regime is the relative magnitude of the boiling Froude number. The number is defined as the ratio of the dynamic force to the buoyancy force acting on the growing bubble where the force associated with the inertia of the liquid displaced by the growing bubble is defined as the bubble dynamic force. It was reasoned that for large Froude numbers, the relative influence of the buoyancy force would be small and the result would be that the nucleate boiling regime would be independent of acceleration level. Merte and Clark [6] calculated a Froude number of 452 for liquid nitrogen and 352 for liquid hydrogen, and the results, according to the theory of Adelberg, verify the lack of dependence on gravity seen by Merte and Clark [6] and Sherley [5] for liquid nitrogen and liquid hydrogen, respectively. However, the values of Froude number were obtained using a bubble radius of 0.005 inch and using the bubble growth equation of Forster and Zuber [27]. The relationship used contained R^{-3} . In calculating a Froude number for water using the same procedure, a value of 14,000 was obtained with the same bubble radius. Recent data provided by Schwartz indicate that the radii of bubbles departing in water at 1 g are approximately 0.035 inch. Using the maximum radius and growth time data presented by Schwartz [4], and the approximately relationship for Froude number (see Appendix C) presented by Adelberg [56], Froude numbers of from 0.13 to 0.915 were obtained for

g levels ranging from 0.04 g to 1 g. These values are consistent with values of approximately 0.5 reported in the work of Usiskin and Siegel [3] for water. The R^{-3} dependence of the relationship used by Merte and Clark could produce large errors if the bubble sizes assumed were incorrect and this, coupled with the theoretical growth rate equation, leaves the Froude numbers produced for liquid nitrogen and liquid hydrogen open to question.

The approximate technique for calculating the Froude number developed by Adelberg [56] was applied to bubble diameters and growth times for Freon 113 taken from the present investigation. At standard gravity, the values obtained varied from 0.16 to 0.71 which indicates a gravity dependence for Freon 113 in the nucleate boiling region, and such a dependence was found in the current work.

The downward shift of the nucleate boiling curve at reduced gravity with the heated surface in the vertical and horizontal heated face downward orientations seems to indicate that the energy removal mechanism present at standard gravity for these orientations has been reduced. This indicates that, even though the energy removal mechanism was enhanced for the horizontal surface with the heated face upward, a reduction of the acceleration level to zero and the resulting vapor accumulation on the horizontal upward facing surface might reverse the trend seen.

SUMMARY AND CONCLUSIONS

1. Bubble growth rates in saturated Freon 113 at atmospheric pressure are not predicted by existing theories. A new calculation procedure was outlined which allowed the bubble to grow through the thermal layer rather than moving it uniformly away from the wall and used some recently provided data on the thermal layer thickness and nature of bubbles growing on a heated surface. This calculation procedure predicted the bubble growth rates in Freon 113 better than existing theories and also predicted the growth rates for bubbles growing on a heated surface in saturated water quite well. The nature of the results in the latter growth stage supported the hypothesis that the bubble growth rate at reduced gravity during this stage is supported primarily by vaporization of a liquid microlayer between the bubble vapor and the heated wall.

2. Several types of bubble coalescence were discussed. It was observed that coalescence of bubbles sliding up a vertical surface at reduced gravity produced large vapor accumulations near the surface. At reduced gravity, the effective heat transfer coefficient for the vertical surface and for the horizontal surface with the heated face downward were seen to decrease, probably as a result of vapor accumulation.

3. A large scatter was seen in bubble departure diameters at reduced gravity. In general, the departure diameters were seen to fall between the values predicted by Fritz and those predicted by Zuber.

4. The location of the nucleate boiling curve in the isolated bubble region was found to be dependent on both effective acceleration level and on the orientation of the surface. At an acceleration level of 0.01 g, the boiling curve was seen to shift upward for the heated surface in the horizontal position with the heated face upward and shifted downward for the vertical surface and the horizontal surface with the heated face downward. The magnitude of the downward shift was greater for the heated face downward than for the vertical surface.

5. At standard gravity, the location of the nucleate boiling curve was found to be a function of the orientation of the heated surface with respect to the acceleration vector. The boiling curve was observed to shift upward as the surface orientation was changed from horizontal heated face upward to vertical and was shifted upward again when the surface orientation was changed to horizontal heated face downward. This shift was observed with both of the heaters used in the boiling curve investigation.

6. Previous investigations had found insignificant shifts of the boiling curve between standard and reduced gravity. However, the direction of the changes seen by previous investigators are the same as those observed in this study. The small magnitude of boiling curve change seen by some previous investigators might be explained by the fact that the heat transfer

surfaces used in most of the investigations were of the same relative size as the bubbles at reduced gravity. In other cases, the insignificant changes seen could have been a result of multiple orientations of heater surface with respect to acceleration vector and a resulting cancellation of the effects present for the various orientations.

7. A comparison of the trends predicted for shifting of the nucleate boiling curve by some of the existing nucleate boiling models for a reduction in acceleration level has shown that the models are not consistent. Of the models investigated, only the Han and Griffith enthalpy transport model indicated a shift in the direction found in this investigation. It was suggested that the mass transport model of Snyder might also explain the results of this work.

8. Even though the energy removal mechanism was enhanced at 0.01 g for the horizontal surface facing upward, the decrease in the boiling heat transfer coefficient for the vertical and horizontal surface facing downward orientations indicates that a reduction of acceleration level to zero and the resulting vapor accumulation might cause a decrease of the boiling curve for all orientations.

APPENDIX A
EXPERIMENTAL DATA

Preceding Page Blank

TABLE A-1. BOILING HEAT TRANSFER DATA

Test No. 10F20
Heated Surface Upward 2 × 4 in. Heater

Comments	Thermocouple No.	Time (sec)	Temperature (°F)	$T_w - T_{SAT}$ (°F)	Heater Enthalpy Change Rate ^a (BTU/hr ft ²)
Predrop No. 1, Initial Flux = 6210 BTU/hr ft ²	1	0	145.8	29.29	147.1
		1.0	145.65	29.14	990.9
		4.32	142.3	25.79	1044.7
		8.08	138.3	21.79	777.5
		10.48	136.4	19.89	701.5
Predrop No. 2, Initial Flux = 6280 BTU/hr ft ²	1	0	145.8	29.29	98.2
		1.0	145.7	29.19	1005.7
		4.32	142.3	25.79	1005.7
Predrop No. 3, Initial Flux = 6280 BTU/hr ft ²	1	0	145.8	29.29	0
		1.15	145.8	29.29	1084.3
		4.32	142.2	25.79	1409.49
		6.48	139.2	22.69	552.4
		8.08	138.3	21.79	818.4
		10.48	136.3	19.79	534.5
		13.42	134.7	18.19	534.5

^a Values in this column represent an average over the time interval bounded by the times shown on the data line and the succeeding line.

TABLE A-1. BOILING HEAT TRANSFER DATA (Continued)

Test No. 10F20 (Continued)

Comments	Thermocouple No.	Time (sec)	Temperature (°F)	$T_w - T_{SAT}$ (°F)	Heater Enthalpy Change Rate ^a (BTU/hr ft ²)
Reduced Gravity, Initial Flux = 5780 BTU/hr ft ²	1	0	146.0	29.5	3928.4
		0.25	145.0	28.5	2770.0
		0.64	143.9	27.4	1510.9
		1.94	141.9	25.4	880.2
		4.06	140.0	23.5	880.2
Predrop No. 1, Initial Flux = 6210 BTU/hr ft ²	2	0	147.6	31.1	0
		1.0	147.6	31.1	1209.8
		2.38	145.9	29.4	952.6
		6.71	141.7	25.2	735.4
		10.85	138.6	22.1	735.4
Predrop No. 2, Initial Flux = 6280 BTU/hr ft ²	2	0	147.8	31.3	0
		1.0	147.8	31.3	1057.7
		1.65	147.1	30.6	744.5
		4.42	145.0	28.5	1153.7
		7.91	139.9	24.4	722.6
		10.90	138.7	22.2	722.6

^a See note on page A-2.

TABLE A-1. BOILING HEAT TRANSFER DATA (Continued)

Test No. 10F20 (Continued)

Comments	Thermocouple No.	Time (sec)	Temperature (°F)	$T_w - T_{SAT}$ (°F)	Heater Enthalpy Change Rate ^a (BTU/hr ft ²)
Predrop No. 3, Initial Flux = 6280 BTU/hr ft ²	2	0	147.8	31.3	0
		1.0	147.8	31.3	1097.0
		2.88	145.7	29.2	959.5
		6.36	142.3	25.8	813.6
		9.86	139.4	22.9	503.6
		12.2	138.2	21.7	503.6
Reduced Gravity, Initial Flux = 6780 BTU/hr ft ²	2	0	148.1	31.6	3450.6
		0.37	146.8	30.3	2534.4
		0.68	146.0	29.5	1841.5
		1.16	145.1	28.6	1374.9
		1.66	144.4	27.9	801.7
		2.15	144.0	27.5	677.3
		3.02	143.4	26.9	677.3
Predrop No. 1, Initial Flux = 6210 BTU hr ft ²	3	0	146.8	30.3	0
		1.0	146.8	30.3	506.8
		2.55	146.0	29.5	1190.4
		5.85	142.0	25.5	914.4
		8.75	139.3	22.8	732.9
		12.1	136.8	20.3	732.9

^a See note on page A-2.

TABLE A-1. (Continued)

Test No. 10F20 (Continued)

Comments	Thermocouple No.	Time (sec)	Temperature (°F)	$T_w - T_{SAT}$ (°F)	Heater Enthalpy Change Rate ^a (BTU/hr ft ²)
Predrop No. 2, Initial Flux = 6280 BTU hr ft ²	3	0	146.8	30.3	0
		0.9	146.8	30.3	800.2
		2.25	145.7	29.2	1011.8
		5.55	142.3	25.8	942.8
		8.05	139.9	23.4	681.5
		10.05	138.2	21.7	681.5
Predrop No. 3, Initial Flux = 6280 BTU/hr ft ²	3	0	146.8	30.3	0
		1.0	146.8	30.3	954.0
		2.75	145.1	28.6	982.1
		7.65	140.2	23.7	757.6
		11.15	137.6	21.0	757.6
Reduced Gravity, Initial Flux = 5780 BTU/hr ft ²	3	0	147.5	31.0	4714.1
		0.25	146.3	29.8	2266.4
		0.77	145.1	28.6	1767.7
		1.27	144.2	27.7	1276.7
		2.27	142.9	26.4	589.3
		3.77	142.0	25.5	589.3

^a See note on page A-2.

TABLE A-1. (Continued)

Test No. 10F20 (Concluded)

Comments	Thermocouple No.	Time (sec)	Temperature (°F)	$T_w - T_{SAT}$ (°F)	Heater Enthalpy Change Rate ^a (BTU/hr ft ²)
Predrop No. 1, Initial Flux = 6210 BTU/hr ft ²	4	0	144.9	28.4	0
		0.82	144.9	28.4	958.5
		7.89	138.0	21.5	719.5
		10.62	136.0	19.5	569.8
		13.55	134.3	17.8	569.8
Predrop No. 2, Initial Flux = 6280 BTU/hr ft ²	4	0	145.0	28.5	0
		0.82	145.0	28.5	944.6
		7.89	138.2	21.7	755.5
		10.62	136.1	19.6	755.5
Predrop No. 3, Initial Flux = 6280 BTU/hr ft ²	4	0	145.1	28.6	0
		0.82	145.1	28.6	944.6
		7.89	138.3	21.8	791.4
		10.62	136.1	19.6	603.3
		13.55	134.3	17.8	603.3
Reduced Gravity, Initial Flux = 5780 BTU/hr ft ²	4	0	145.2	28.7	3535.5
		0.25	144.3	27.8	1762.8
		0.64	143.6	27.1	1592.6
		1.75	141.8	25.3	982.1
		2.25	141.3	24.8	982.1

^aSee note on page A-2.

TABLE A-1. (Continued)

Test No. 10F21
 Heated Surface Upward 2 × 4 in. Heater

Comments	Thermocouple No.	Time (sec)	Temperature (°F)	$T_w - T_{SAT}$ (°F)	Heater Enthalpy Change Rate ^a (BTU/hr ft ²)
Predrop No. 1, Initial Flux = 5710 BTU/hr ft ²	1	0	147.0	30.5	0
		1.0	147.0	30.5	877.8
		4.58	143.8	27.3	732.9
		5.92	142.8	26.3	554.4
		8.40	141.4	24.9	491.1
		10.40	140.4	23.9	491.1
Reduced Gravity, Initial Flux = 5540 BTU/hr ft ²	1	0	147.9	30.4	5524.4
		0.32	145.1	28.6	2769.9
		0.71	144.0	27.5	1855.1
		1.61	142.3	25.8	1383.2
		2.02	141.3	24.8	982.1
		3.72	139.9	23.4	982.1
Predrop No. 1, Initial Flux = 5710 BTU/hr ft ²	2	0	148.1	31.6	0
		1.0	148.1	31.6	785.7
		2.0	147.3	30.8	1178.5
		4.5	144.3	27.8	491.1
		6.5	143.3	26.8	491.1

^a See note on page A-2.

TABLE A-1. (Continued)

Test No. 10F21 (Continued)

Comments	Thermocouple No.	Time (sec)	Temperature (°F)	$T_w - T_{SAT}$ (°F)	Heater Enthalpy Change Rate ^a (BTU/hr ft ²)
Reduced Gravity, Initial Flux = 5540 BTU/hr ft ²	2	0	147.7	31.2	4752.1
		0.31	146.2	29.7	3819.3
		0.67	144.8	28.3	1853.0
		1.20	143.8	27.3	1467.5
		2.07	142.5	26.0	770.3
		3.60	141.3	24.8	770.3
Predrop No. 1, Initial Flux = 5710 BTU/hr ft ²	3	0	146.8	30.3	0
		0.7	146.8	30.3	861.5
		4.12	143.8	27.3	624.2
		6.48	142.3	25.8	692.1
		9.46	140.2	23.7	692.1
Reduced Gravity, Initial Flux = 5540 BTU/hr ft ²	3	0	145.4	28.9	3928.4
		0.3	144.2	27.7	2842.9
		0.68	143.1	26.6	1473.1
		1.28	142.2	25.7	1067.5
		2.2	141.2	24.7	876.9
		3.32	140.2	23.6	876.9

^a See note on page A-2.

TABLE A-1. (Continued)

Test No. 10F21 (Concluded)

Comments	Thermocouple No.	Time (sec)	Temperature (° F)	$T_w - T_{SAT}$ (° F)	Heater Enthalpy Change Rate ^a (BTU/hr ft ²)
Predrop No. 1, Initial Flux = 5710 BTU/hr ft ²	4	0	145.7	29.2	0
		0.8	145.7	29.2	982.1
		1.9	144.6	28.1	868.8
		4.5	142.3	25.8	565.2
		7.28	140.7	24.2	491.0
		10.48	139.1	22.6	491.0
Reduced Gravity, Initial Flux = 5540 BTU/hr ft ²	4	0	144.9	28.4	4637.7
		0.36	143.2	26.7	2104.5
		0.92	142.0	25.5	1381.1
		2.2	140.2	23.7	892.8
		3.52	139.0	22.5	892.8

^a See note on page A-2.

TABLE A-1. (Continued)

Test No. 10F22
Heated Surface Upward 2 × 4 in. Heater

Comments	Thermocouple No.	Time (sec)	Temperature (°F)	$T_w - T_{SAT}$ (°F)	Heater Enthalpy Change Rate ^a (BTU/hr ft ²)
Predrop No. 1, Initial Flux = 5880 BTU/hr ft ²	1	0	146.3	29.8	0
		0.75	146.3	29.8	1069.6
		2.77	144.1	27.6	892.8
		4.20	142.8	26.3	654.7
		5.70	141.8	25.3	346.6
		8.25	140.9	24.4	346.6
Predrop No. 2, Initial Flux = 5880 BTU/hr ft ²	1	0	146.3	29.8	0
		0.75	146.3	29.8	1152.4
		2.71	144.0	27.5	856.9
		4.2	142.7	26.2	883.9
		5.2	141.8	25.3	498.5
		7.17	140.8	24.3	498.5
Reduced Gravity, Initial Flux = 5670 BTU/hr ft ²	1	0	146.0	29.5	3437.3
		0.6	143.9	27.4	2160.6
		1.1	142.8	26.3	1964.2
		1.6	141.8	25.3	1374.9
		2.0	141.1	24.6	1374.9

^aSee note on page A-2.

TABLE A-1. (Continued)

Test No. 10F22 (Continued)

Comments	Thermocouple No.	Time (sec)	Temperature (°F)	$T_w - T_{SAT}$ (°F)	Heater Enthalpy Change Rate ^a (BTU/hr ft ²)
Predrop No. 1, Initial Flux = 5880 BTU/hr ft ²	2	0	147.3	30.8	0
		0.75	147.3	30.8	967.2
		2.07	146.0	29.5	998.7
		3.25	144.8	28.3	883.9
		4.25	143.9	27.4	628.5
		6.75	142.3	25.8	628.5
Predrop No. 2, Initial Flux = 5880 BTU/hr ft ²	2	0	147.7	31.2	0
		0.75	147.7	31.2	1152.7
		2.88	145.2	28.7	767.3
		4.80	143.7	27.2	552.4
		6.40	142.8	26.2	509.2
		7.75	142.1	25.6	509.2
Reduced Gravity, Initial Flux = 5670 BTU/hr ft ²	2	0	147.2	30.7	3928.3
		0.35	145.8	29.3	3055.4
		0.80	144.4	27.9	1543.3
		1.5	143.3	26.8	1540.3
		2.2	142.2	25.7	523.8
		2.95	141.8	25.3	523.8

^a See note on page A-2.

TABLE A-1. (Continued)

Test No. 10F22 (Continued)

Comments	Thermocouple No.	Time (sec)	Temperature (°F)	$T_w - T_{SAT}$ (°F)	Heater Enthalpy Change Rate ^a (BTU/hr ft ²)
Predrop No. 1, Initial Flux = 5880 BTU/hr ft ²	3	0	147.8	31.3	0
		0.5	147.8	31.3	785.7
		1.5	147.0	30.5	1113.1
		3.0	145.3	28.8	851.1
		4.5	144.0	27.5	687.5
		5.5	143.3	26.8	589.3
		7.5	142.1	25.6	589.3
Predrop No. 2, Initial Flux = 5880 BTU/hr ft ²	3	0	147.8	31.3	0
		0.5	147.8	31.3	801.7
		1.48	147.0	30.5	1104.9
		3.08	145.2	28.7	818.4
		4.4	144.1	27.6	785.7
		5.6	143.2	26.7	736.7
		7.6	142.0	25.5	736.7
Reduced Gravity, Initial Flux = 5670 BTU/hr ft ²	3	0	146.8	30.3	3571.3
		0.44	145.2	28.7	2370.6
		1.02	143.8	27.3	1964.2
		1.52	142.8	26.3	1178.5
		2.02	142.2	25.7	591.6
		2.85	141.7	25.2	591.6

^a See note on page A-2.

TABLE A-1. (Continued)

Test No. 10F22 (Concluded)

Comments	Thermocouple No.	Time (sec)	Temperature (°F)	$T_w - T_{SAT}$ (°F)	Heater Enthalpy Change Rate ^a (BTU/hr ft ²)
Predrop No. 1, Initial Flux = 5880 BTU/hr ft ²	4	0	145.1	28.6	0
		0.5	145.1	28.6	932.1
		3.45	142.3	25.8	692.2
		5.72	140.7	24.2	597.2
		7.2	139.8	23.3	392.8
		8.7	139.2	22.7	392.8
Predrop No. 2, Initial Flux = 5880 BTU/hr ft ²	4	0	145.3	28.8	0
		0.5	145.3	28.8	1043.5
		2.1	143.6	27.1	818.4
		3.3	142.6	26.1	785.7
		4.3	141.8	25.3	785.7
		5.3	141.0	24.5	982.1
6.8	140.0	23.5	982.1		
Reduced Gravity, Initial Flux = 5670 BTU/hr ft ²	4	0	146.6	29.1	5110.0
		0.2	144.3	27.8	2678.4
		0.75	142.8	26.3	1964.2
		1.25	141.8	25.3	1571.3
		1.75	141.0	24.5	1178.5
		2.75	139.8	23.3	1178.5

^a See note on page A-2.

TABLE A-1. (Continued)

Test No. 10F23
Heated Surface Upward 2 × 4 in. Heater

Comments	Thermocouple No.	Time (sec)	Temperature (°F)	$T_w - T_{SAT}$ (°F)	Heater Enthalpy Change Rate ^a (BTU/hr ft)
Predrop No. 1, Initial Flux = 5570 BTU/hr ft ²	1	0	145.8	29.3	0
		0.9	145.8	29.3	742.6
		5.0	142.7	26.2	736.6
		7.0	141.2	24.7	448.9
		10.5	139.6	23.1	448.9
Reduced Gravity, Initial Flux = 5570 BTU/hr ft ²	1	0	146.3	29.8	5401.6
		0.2	145.2	28.7	3055.4
		0.65	143.8	27.3	1571.3
		1.15	143.0	26.5	1374.9
		1.65	142.3	25.8	1080.3
		2.65	141.2	24.7	1080.3
Predrop No. 1, Initial Flux = 5570 BTU/hr ft ²	2	0	145.8	29.3	0
		0.5	145.8	29.3	589.3
		2.0	144.9	28.4	785.7
		3.5	143.7	27.2	667.8
		6.0	142.0	25.5	549.9
		8.5	140.6	24.1	549.9

^a See note on page A-2.

TABLE A-1. (Continued)

Test No. 10F23 (Continued)

Comments	Thermocouple No.	Time (sec)	Temperature (°F)	$T_w - T_{SAT}$ (°F)	Heater Enthalpy Change Rate ^a (BTU hr ft ²)
Reduced Gravity, Initial Flux = 5570 BTU/hr ft ²	2	0	145.8	29.3	3142.7
		0.25	145.0	28.5	2357.1
		0.75	143.8	27.3	1767.7
		1.25	142.9	26.4	1080.3
		2.25	141.8	25.3	1080.3
Predrop No. 1 Initial Flux = 5570 BTU/hr ft ²	3	0	145.3	28.8	0
		0.6	145.3	28.8	755.5
		2.55	143.8	27.3	811.3
		4.85	141.9	25.4	652.6
		6.35	140.9	24.4	549.8
		8.32	139.8	23.3	491.1
		10.32	138.8	22.3	491.1
Reduced Gravity, Initial Flux = 5570 BTU/hr ft ²	3	0	145.2	28.8	3928.4
		0.25	144.2	27.7	2291.6
		0.85	142.8	26.3	1964.2
		1.35	141.8	25.3	1178.5
		1.85	141.2	24.7	900.0
		2.35	140.8	24.3	785.7
		3.35	140.0	23.5	785.7

^a See note on page A-2.

TABLE A-1. (Continued)

Test No. 10F23 (Concluded)

Comments	Thermocouple No.	Time (sec)	Temperature (°F)	$T_w - T_{SAT}$ (°F)	Heater Enthalpy Change Rate ^a (BTU/hr ft ²)
Predrop No. 1, Initial Flux = 5570 BTU/hr ft ²	4	0	144.0	27.5	0
		0.5	144.0	27.5	762.6
		4.75	140.7	24.2	540.2
		6.75	139.6	23.1	392.8
		8.75	138.8	22.3	245.5
		10.75	138.1	21.8	245.5
Reduced Gravity, Initial Flux = 5570 BTU/hr ft ²	4	0	144.7	28.1	4715.8
		0.25	143.2	26.9	2357.1
		0.75	142.2	25.7	1374.9
		1.25	141.4	25.0	1080.3
		2.25	140.4	23.9	1080.3

^a See note on page A-2.

TABLE A-1. (Continued)

Test No. 10F24
Heated Surface Upward 2×4 in. Heater

Comments	Thermocouple No.	Time (sec)	Temperature (°F)	$T_w - T_{SAT}$ (°F)	Heater Enthalpy Change Rate ^a (BTU/hr ft ²)
Pretest No. 1, Initial Flux = 5570 BTU/hr ft ²	1	0	146.1	29.6	0
		1.0	146.1	29.6	841.7
		1.35	145.8	29.3	966.9
		4.6	142.6	26.1	736.6
		6.6	141.1	24.6	501.9
		11.1	138.8	22.3	501.9
Reduced Gravity, Initial Flux = 5150 BTU/hr ft ²	1	0	146.6	30.1	5106.8
		0.25	145.3	28.8	2678.4
		0.80	143.8	27.3	2031.9
		1.38	142.6	26.1	1178.5
		2.38	141.4	24.9	1178.5
Pretest No. 1, Initial Flux = 5570 BTU/hr ft ²	2	0	146.8	30.3	0
		0.6	146.8	30.3	982.1
		1.6	145.9	29.4	1178.5
		3.1	144.0	27.5	803.5
		5.1	142.2	25.7	1036.6
		7.1	140.3	23.8	510.7
		9.6	139.0	22.5	510.7

^aSee note on page A-2

TABLE A-1. (Continued)

Test No. 10F24 (Continued)

Comments	Thermocouple No.	Time (sec)	Temperature (°F)	$T_w - T_{SAT}$ (°F)	Heater Enthalpy Change Rate ^a (BTU/hr ft ²)
Reduced Gravity, Initial Flux = 5150 BTU/hr ft ²	2	0	146.8	30.3	3928.3
		0.2	146.0	29.5	3339.2
		0.7	145.3	27.8	1964.2
		1.2	143.3	26.8	1178.5
		1.7	142.7	26.2	982.1
		2.2	142.2	25.7	982.1
		2.7	141.7	25.2	982.1
Pretest No. 1, Initial Flux = 5570 BTU/hr ft ²	3	0	147.3	30.8	0
		0.6	147.3	30.8	613.8
		1.4	146.8	30.3	982.1
		3.4	144.8	28.3	883.9
		5.4	143.0	26.5	597.8
		8.85	140.8	24.4	540.2
		10.85	139.8	23.3	540.2
Reduced Gravity, Initial Flux = 5150 BTU/hr ft ²	3	0	146.8	30.3	4321.3
		0.25	145.7	29.2	3981.5
		0.62	144.2	27.7	1877.5
		1.3	142.9	26.4	1080.3
		2.3	141.8	25.3	1080.3

^a See note on page A-2.

TABLE A-1. (Continued)

Test No. 10F24 (Concluded)

Comments	Thermocouple No.	Time (sec)	Temperature (°F)	$T_w - T_{SAT}$ (°F)	Heater Enthalpy Change Rate ^a (BTU hr ft ²)
Pretest No. 1, Initial Flux = 5570 BTU/hr ft ²	4	0	145.0	28.5	0
		0.6	145.0	28.5	976.0
		3.85	141.8	25.3	716.6
		6.15	140.1	23.6	540.1
		8.15	139.0	22.5	294.6
		10.15	138.4	21.9	294.6
Reduced Gravity, Initial Flux = 5150/BTU hr ft ²	4	0	145.2	28.7	4714.0
		0.25	144.0	27.5	2749.9
		0.50	143.3	26.8	2553.4
		1.0	142.0	25.5	1374.9
		1.5	141.3	24.8	982.1
		2.0	140.8	24.3	785.7
		2.5	140.4	23.9	785.7

^aSee note on page A-2.

TABLE A-1. (Continued)

Test No. 10F30
Heated Surface Vertical 2 × 4 in. Heater

Comments	Thermocouple No.	Time (sec)	Temperature (°F)	$T_w - T_{SAT}$ (°F)	Heater Enthalpy Change Rate ^a (BTU/hr ft ²)
Predrop No. 1, Initial Flux = 5780 BTU/hr ft ²	1	0	143.0	26.5	982.1
		1.0	142.0	25.5	1425.6
		4.1	137.5	21.0	982.1
		5.6	136.0	19.5	982.1
Reduced Gravity, Initial Flux = 5780 BTU/hr ft ²	1	0	143.0	26.5	392.8
		0.5	142.8	26.3	589.2
		1.0	142.5	26.0	864.3
		2.25	141.4	24.9	864.3
Pretest No. 1, Initial Flux = 5780 BTU/hr ft ²	2	0	144.0	27.5	982.2
		0.2	143.8	27.3	982.1
		1.2	142.8	26.3	1374.9
		2.2	141.4	24.9	1080.3
		3.2	140.3	23.8	1080.3
Reduced Gravity, Initial Flux = 5780 BTU hr ft ²	2	0	144.2	27.7	516.9
		0.95	143.7	27.2	945.7
		2.3	142.4	25.9	945.7

^a See note on page A-2.

TABLE A-1. (Continued)

Test No. 10F30 (Concluded)

Comments	Thermocouple No.	Time (sec)	Temperature (°F)	$T_w - T_{SAT}$ (°F)	Heater Enthalpy Change Rate ^a (BTU/hr ft ²)
Pretest No. 1, Initial Flux = 5780 BTU/hr ft ²	3	0	142.2	25.7	736.6
		0.8	141.6	25.1	1243.9
		2.3	139.7	23.2	1276.7
		3.3	138.4	21.9	1276.7
Reduced Gravity, Initial Flux = 5780 BTU/hr ft ²	3	0	142.2	25.7	245.5
		0.4	142.1	25.6	589.2
		1.4	141.5	25.0	785.7
		2.4	140.7	24.2	785.7
Pretest No. 1, Initial Flux = 5780 BTU/hr ft ²	4	0	143.8	27.3	327.4
		0.6	143.6	27.1	1243.9
		2.1	141.7	25.2	1374.9
		3.6	139.6	23.1	1374.9
Reduced Gravity, Initial Flux = 5780 BTU/hr ft ²	4	0	143.3	26.8	0
		1.0	143.3	26.8	327.4
		1.6	143.1	26.6	982.1
		2.6	142.1	25.6	982.1

^a See note on page A-2.

TABLE A-1. (Continued)

Test No. 10F31
Heated Surface Vertical 2 × 4 in. Heater

Comments	Thermocouple No.	Time (sec)	Temperature (°F)	$T_w - T_{SAT}$ (°F)	Heater Enthalpy Change Rate ^a (BTU/hr ft ²)
Pretest No. 1, Initial Flux = 5670 BTU/hr ft ²	1	0	142.0	25.5	982.1
		0.6	141.4	24.9	1178.5
		1.6	140.2	23.7	1424.0
		3.6	137.3	20.8	1113.1
		5.1	135.6	19.1	1113.1
Reduced Gravity, Initial Flux = 5570 BTU/hr ft ²	1	0	142.8	26.3	196.4
		0.5	142.7	26.2	785.7
		1.0	142.3	25.8	883.9
		2.0	141.4	24.9	785.7
		2.5	141.0	24.5	785.7
Pretest No. 1, Initial Flux = 5670 BTU/hr ft ²	2	0	143.1	26.6	872.9
		0.9	142.3	25.8	1309.4
		2.4	140.3	23.8	1178.5
		3.4	139.1	22.6	1178.5
Reduced Gravity, Initial Flux = 5570 BTU/hr ft ²	2	0	142.9	26.4	491.1
		1.0	142.4	25.9	851.2
		2.5	141.1	24.6	851.2

^a See note on page A-2.

TABLE A-1. (Continued)

Test No. 10F31 (Concluded)

Comments	Thermocouple No.	Time (sec)	Temperature (°F)	$T_w - T_{SAT}$ (°F)	Heater Enthalpy Change Rate ^a (BTU/hr ft ²)
Pretest No. 1, Initial Flux = 5670 BTU/hr ft ²	4	0	141.6	25.1	491.0
		0.6	141.3	24.8	883.9
		1.6	140.4	23.9	1276.7
		2.6	139.1	22.6	1276.7
Reduced Gravity, Initial Flux = 5570 BTU/hr ft ²	4	0	142.8	26.3	0
		1.0	142.8	26.3	392.9
		1.5	142.6	26.1	883.9
		2.5	141.7	25.2	883.9

Test No. 10F32

Heated Surface Upward 2 × 4 in. Heater

Pretest No. 1 Initial Flux = 5610 BTU/hr ft ²	1	0	146.5	30.0	327.4
		0.6	146.3	29.8	720.2
		2.1	145.2	28.7	491.1
		4.1	144.2	27.7	1080.3
		7.1	140.9	24.4	746.4
		9.6	139.0	22.5	746.4

^a See note on page A-2.

TABLE A-1. (Continued)

Test No. 10F32 (Continued)

Comments	Thermocouple No.	Time (sec)	Temperature (°F)	$T_w - T_{SAT}$ (°F)	Heater Enthalpy Change Rate ^a (BTU/hr ft ²)
Reduced Gravity, Initial Flux = 5610 BTU/hr ft ²	1	0	146.5	30.0	6383.7
		0.2	145.2	28.7	3601.1
		0.5	144.1	27.6	2142.7
		1.05	142.9	26.4	1275.4
		1.85	141.9	25.4	572.1
		2.85	141.3	24.8	572.1
		Pretest No. 1, Initial Flux = 5610 BTU/hr ft ²	2	0	146.3
0.68	146.2			29.7	436.5
1.58	145.8			29.3	785.7
2.58	145.0			28.5	903.5
5.08	142.7			26.2	736.6
7.08	141.2			24.7	736.6
Reduced Gravity, Initial Flux = 5610 BTU/hr ft ²	2			0	146.2
		0.4	144.7	28.2	2291.5
		0.7	144.0	27.5	1767.8
		1.2	143.1	26.6	982.1
		2.7	141.6	25.1	982.1

^a See note on page A-2.

TABLE A-1. (Continued)

Test No. 10F32 (Continued)

Comments	Thermocouple No.	Time (sec)	Temperature (°F)	$T_w - T_{SAT}$ (°F)	Heater Enthalpy Change Rate ^a (BTU/hr ft ²)
Pretest No. 1, Initial Flux = 5610 BTU/hr ft ²	3	0	146.3	29.8	267.8
		1.1	146.0	29.5	628.5
		2.35	145.2	28.7	687.5
		4.35	143.8	27.3	736.6
		6.35	142.3	25.8	515.6
		10.35	140.2	23.7	515.6
Reduced Gravity, Initial Flux = 5610 BTU/hr ft ²	3	0	146.3	29.8	5401.6
		0.2	145.2	28.7	2946.3
		0.7	143.7	27.2	1747.7
		1.2	142.8	26.3	982.1
		1.7	142.3	25.8	687.5
		2.7	141.6	25.1	687.5
Pretest No. 1, Initial Flux = 5610 BTU/hr ft ²	4	0	146.3	29.8	267.8
		1.1	146.0	29.5	624.9
		2.2	145.3	28.8	1113.1
		3.7	143.6	27.1	1047.6
		5.2	142.0	25.5	785.7
		7.95	139.8	23.3	785.7

^a See note on page A-2.

TABLE A-1. (Continued)

Test No. 10F32 (Concluded)

Comments	Thermocouple No.	Time (sec)	Temperature (°F)	$T_w - T_{SAT}$ (°F)	Heater Enthalpy Change Rate ^a (BTU/hr ft ²)
Reduced Gravity, Initial Flux = 5610 BTU/hr ft ²	4	0	146.3	29.8	5647.0
		0.4	144.0	27.5	2357.1
		0.9	142.8	26.3	1571.3
		1.4	142.0	25.5	1178.5
		2.4	140.8	24.3	1178.5

Test No. 10F33

Heated Surface Downward 2 × 4 in. Heater

Pretest No. 1, Initial Flux = 5960 BTU/hr ft ²	1	0	138.0	21.5	736.6
		0.4	137.7	21.2	1848.6
		1.25	136.1	19.6	2258.8
		2.25	133.8	17.3	2258.8
		3.25	131.5	15.0	1669.6
		4.25	129.8	13.3	1669.6
		Reduced Gravity, Initial Flux = 5960 BTU/hr ft ²	1	0	137.7
0.65	138.2			21.7	280.6
1.0	138.1			21.6	930.4
1.95	137.2			20.7	982.1
2.45	136.7			20.2	982.1

^a See note on page A-2.

TABLE A-1. (Continued)

Test No. 10F33 (Continued)

Comments	Thermocouple No.	Time (sec)	Temperature (°F)	$T_w - T_{SAT}$ (°F)	Heater Enthalpy Change Rate ^a (BTU/hr ft ²)
Pretest No. 1, Initial Flux = 5960 BTU/hr ft ²	2	0	137.1	20.6	0
		0.5	137.1	20.6	1718.6
		1.7	135.0	18.5	2111.5
		3.7	130.7	14.2	1178.5
		4.7	129.5	13.0	1178.5
Reduced Gravity, Initial Flux = 5960 BTU/hr ft ²	2	0	137.1	20.6	-701.5
		0.7	137.6	21.1	122.7
		1.5	137.5	21.0	930.4
		2.45	136.6	20.1	930.4
Pretest No. 1, Initial Flux = 5960 BTU/hr ft ²	3	0	138.0	21.5	0
		0.45	138.0	21.5	1964.2
		1.35	136.2	19.7	2618.9
		2.40	133.4	16.9	2182.4
		3.30	131.4	14.9	1343.9
		4.25	130.1	13.6	1343.9

^a See note on page A-2.

TABLE A-1. (Continued)

Test No. 10F33 (Concluded)

Comments	Thermocouple No.	Time (sec)	Temperature (°F)	$T_w - T_{SAT}$ (°F)	Heater Enthalpy Change Rate ^a (BTU/hr ft ²)
Reduced Gravity, Initial Flux = 5960 BTU/hr ft ²	3	0	137.2	20.7	-982.1
		0.6	137.8	21.3	0
		1.25	137.8	21.3	654.7
		2.15	137.2	20.7	982.1
		2.65	136.7	20.2	982.1
Pretest No. 1, Initial Flux = 5960 BTU/hr ft ²	4	0	138.4	21.9	196.4
		0.5	138.3	21.8	1571.3
		1.0	137.5	21.0	1964.2
		2.0	135.5	19.0	1833.3
		3.5	132.7	16.2	1374.9
		4.5	131.3	14.8	1374.9
Reduced Gravity, Initial Flux = 5960 BTU/hr ft ²	4	0	137.8	21.3	-1160.0
		0.6	138.5	22.0	0
		1.4	138.5	22.0	392.8
		1.9	138.3	21.8	785.7
		2.4	137.9	21.4	785.7

^a See note on page A-2.

TABLE A-1. (Continued)

Test No. 10F34 Heated Surface Downward 2 × 4 in. Heater

Comments	Thermocouple No.	Time (sec)	Temperature (°F)	$T_w - T_{SAT}$ (°F)	Heater Enthalpy Change Rate ^a (BTU/hr ft ²)
Pretest No. 1 Initial Flux = 5900 BTU/hr ft ²	1	0	135.9	19.4	654.8
		0.45	135.6	19.1	1613.4
		1.85	133.3	16.8	2135.0
		3.0	130.8	14.3	1122.4
		4.75	128.8	12.3	1122.4
Reduced Gravity Initial Flux = 5900 BTU/hr ft ²	1	0	136.0	19.5	-491.0
		0.6	136.3	19.8	0
		1.45	136.3	19.8	613.8
		2.25	135.8	19.3	613.8
Pretest No. 1, Initial Flux = 5900 BTU/hr ft ²	2	0	135.8	19.3	218.3
		0.45	135.7	19.2	1262.7
		1.15	134.8	18.3	1964.2
		3.15	130.8	14.3	1473.2
		4.15	129.3	12.8	1473.2

^a See note on page A-2.

TABLE A-1. (Continued)

Test No. 10F34 (Continued)

Comments	Thermocouple No.	Time (sec)	Temperature (°F)	$T_w - T_{SAT}$ (°F)	Heater Enthalpy Change Rate ^a (BTU/hr ft ²)
Reduced Gravity, Initial Flux = 5900 BTU/hr ft ²	2	0	136.3	19.8	-420.8
		0.7	136.6	20.1	0
		1.65	136.6	20.1	808.7
		2.50	135.9	19.4	808.7
Pretest No. 1, Initial Flux = 5900 BTU/hr ft ²	3	0	136.6	20.1	491.0
		0.45	136.4	19.9	1502.0
		2.1	133.8	17.3	1800.5
		3.9	130.5	14.0	1352.2
		5.25	128.6	12.1	1352.2
Reduced Gravity, Initial Flux = 5900 BTU/hr ft ²	3	0	136.6	20.1	-613.8
		0.8	137.1	20.6	0
		1.65	137.1	20.6	654.7
		2.4	136.6	20.1	654.7
Pretest No. 1, Initial Flux = 5900 BTU/hr ft ²	4	0	135.6	19.1	0
		0.4	135.6	19.1	1669.6
		2.4	132.2	15.7	2020.3
		4.15	128.6	12.0	1402.9
		5.2	127.1	10.6	1402.9

^a See note on page A-2.

TABLE A-1. (Continued)

Test No. 10F34 (Concluded)

Comments	Thermocouple No.	Time (sec)	Temperature (°F)	$T_w - T_{SAT}$ (°F)	Heater Enthalpy Change Rate ^a (BTU/hr ft ²)
Reduced Gravity, Initial Flux = 5900 BTU/hr ft ²	4	0	135.0	18.5	-1190.0
		0.9	136.1	19.6	0
		2.0	136.1	19.6	294.6
		3.0	135.8	19.3	294.6

Test No. 10F36

Heated Surface Upward 2 × 2 in. Heater

Predrop No. 1, Initial Flux = 7100 BTU/hr ft ²	1	0	150.4	33.9	215.1
		1.0	150.2	33.7	322.6
		2.0	149.9	33.4	860.3
		3.0	149.1	32.6	752.7
		4.0	148.4	31.9	1182.9
		5.0	147.3	30.8	967.8
		6.0	146.4	29.9	1075.3
		7.0	145.4	28.9	1075.3
		8.0	144.4	27.9	1075.3

^a See note on page A-2.

TABLE A-1. (Continued)

Test No. 10F36 (Continued)

Comments	Thermocouple No.	Time (sec)	Temperature (°F)	$T_w - T_{SAT}$ (°F)	Heater Enthalpy Change Rate ^a (BTU/hr ft ²)
Predrop No. 1, Initial Flux = 7100 BUT/hr ft ²	2	0	146.0	29.5	0
		1.0	146.0	29.5	860.3
		2.0	145.2	28.7	860.3
		3.0	144.4	27.9	1290.4
		4.0	143.2	26.7	1075.3
		5.0	142.2	25.7	860.3
		6.0	141.4	24.9	654.2
		7.0	140.8	24.3	967.8
		8.0	139.9	23.4	967.8
Predrop No. 1, Initial Flux = 7100 BTU/hr ft ²	3	0	147.4	30.9	107.5
		1.0	147.3	30.8	860.3
		2.0	146.5	30.0	967.8
		3.0	145.6	29.1	967.8
		4.0	144.7	28.2	752.7
		5.0	144.0	27.5	860.3
		6.0	143.2	26.7	860.3
		7.0	142.4	25.5	654.2
		8.0	141.8	25.3	654.2

^a See note on page A-2.

TABLE A-1. (Continued)
 Test No. 10F36 (Continued)

Comments	Thermocouple No.	Time (sec)	Temperature (°F)	$T_w - T_{SAT}$ (°F)	Heater Enthalpy Change Rate ^a (BTU/hr ft ²)
Reduced Gravity, Initial Flux = 7100 BTU/hr ft ²	1	0	150.3	33.8	1433.8
		0.15	150.1	33.6	3441.1
		0.40	149.3	32.8	3226.0
		0.60	148.7	32.2	2867.6
		0.90	147.9	31.4	1613.0
		1.3	147.3	30.8	1228.9
		2.0	146.5	30.0	1228.9
Reduced Gravity, Initial Flux = 7100 BTU/hr ft ²	2	0	146.6	30.1	2867.5
		0.15	146.2	29.7	4731.5
		0.40	145.1	28.6	3226.0
		0.60	144.5	28.0	3584.4
		0.90	143.5	27.0	2150.6
		1.30	142.7	26.2	1689.8
		2.0	141.6	25.1	1689.8

^a See note on page A-2.

TABLE A-1. (Continued)

Test No. 10F36 (Concluded)

Comments	Thermocouple No.	Time (sec)	Temperature (°F)	$T_w - T_{SAT}$ (°F)	Heater Enthalpy Change Rate ^a (BTU/hr ft ²)
Reduced Gravity, Initial Flux = 7100 BTU/hr ft ²	3	0	147.6	31.1	2150.6
		0.15	147.3	30.8	5591.7
		0.40	146.0	29.5	4301.3
		0.60	145.2	28.7	2867.5
		0.90	144.4	27.9	1613.0
		1.30	143.8	27.3	1228.9
		2.0	143.0	26.5	1228.9
Reduced Gravity, Initial Flux = 7100 BTU/hr ft ²	4	0	150.3	33.8	1433.8
		0.15	150.1	33.6	3010.9
		0.40	149.4	32.9	3763.6
		0.60	148.7	32.2	2150.6
		0.90	148.1	31.6	2150.6
		1.30	147.3	30.8	921.7
		2.0	146.7	30.2	921.7

^a See note on page A-2.

TABLE A-1. (Continued)

Test No. 10F37
 Heated Surface Downward 2 × 2 in. Heater

Comments	Thermocouple No.	Time (sec)	Temperature (°F)	$T_w - T_{SAT}$ (°F)	Heater Enthalpy Change Rate ^a (BTU/hr ft ²)
Predrop No. 1, Initial Flux = 7100 BTU/hr ft ²	1	0	145.7	29.2	0
		1.0	145.7	29.2	2043.1
		2.0	143.8	27.3	2688.3
		3.0	141.3	24.8	2688.3
Reduced Gravity, Initial Flux = 7100 BTU/hr ft ²	1	0	144.4	27.9	0
		1.0	144.4	27.9	0
		1.5	144.4	27.9	0
		2.0	144.4	27.9	967.8
		2.5	143.95	27.5	967.8
Predrop No. 1, Initial Flux = 7100 BTU/hr ft ²	2	0	141.3	24.8	0
		0.6	141.3	24.8	2688.3
		1.0	140.3	23.8	2580.8
		2.0	137.9	21.4	2473.3
		3.0	135.6	19.1	2473.3

^a See note on page A-2.

TABLE A-1. (Continued)

Test No. 10F37 (Continued)

Comments	Thermocouple No.	Time (sec)	Temperature (°F)	$T_w - T_{SAT}$ (°F)	Heater Enthalpy Change Rate ^a (BTU/hr ft ²)
Reduced Gravity, Initial Flux = 7100 BTU/hr ft ²	2	0	140.9	24.4	0
		1.0	140.9	24.4	967.8
		1.5	140.45	23.9	1376.4
		2.0	139.8	23.3	1376.4
Predrop No. 1 Initial Flux = 7100 BTU/hr ft ²	3	0	142.4	25.9	0
		0.7	142.4	25.9	2150.6
		1.0	141.8	25.3	2473.3
		2.0	139.5	23.0	2688.3
		3.0	137.0	20.5	2688.3
Reduced Gravity, Initial Flux = 7100 BTU/hr ft ²	3	0	142.0	25.5	-107.5
		1.0	142.1	25.6	215.1
		1.5	142.0	25.5	860.3
		2.0	141.6	25.1	1290.4
		2.5	141.0	24.5	1290.4

^a See note on page A-2.

TABLE A-1. (Continued)

Test No. 10F37 (Concluded)

Comments	Thermocouple No.	Time (sec)	Temperature (°F)	$T_w - T_{SAT}$ (°F)	Heater Enthalpy Change Rate ^a (BTU/hr ft ²)
Predrop No. 1, Initial Flux = 7100 BTU/hr ft ²	4	0	144.5	28.0	0
		1.0	144.5	28.0	860.2
		2.0	143.7	27.2	2043.1
		3.0	141.8	25.3	2043.1
Reduced Gravity, Initial Flux = 7100 BTU/hr ft ²	4	0	143.3	26.8	0
		1.0	143.3	26.8	0
		2.0	143.3	26.8	107.5
		3.0	143.2	26.7	107.5

Test No. 10F39

Heated Surface Upward 2 × 2 in. Heater

Predrop No. 1, Initial Flux = 21,500 BTU/hr ft ²	2	0	151.7	35.2	0
		1.0	151.7	35.2	1397.9
		2.0	150.4	33.9	1075.3
		3.0	149.4	32.9	860.2
		4.0	148.6	32.1	752.7
		5.0	147.9	31.4	645.2
		6.0	147.3	30.8	860.2
		7.0	146.5	30.0	645.2
		8.0	145.9	29.4	645.2

^a See note on page A-2.

TABLE A-1. (Continued)
 Test No. 10F39 (Concluded)

Comments	Thermocouple No.	Time (sec)	Temperature (°F)	$T_w - T_{SAT}$ (°F)	Heater Enthalpy Change Rate ^a (BTU/hr ft ²)
Reduced Gravity, Initial Flux = 21,500 BTU/hr ft ²	2	0	153.3	36.8	0
		0.2	153.3	36.8	2150.6
		0.5	152.7	36.2	2457.9
		1.2	151.1	34.6	2795.8
		1.7	149.8	33.3	2150.6
		2.2	148.8	32.9	2150.6
Predrop No. 1, Initial Flux = 21,500 BTU/hr ft ²	3	0	154.3	37.8	0
		1.0	154.3	37.8	967.8
		2.0	153.4	36.9	967.8
		3.0	152.5	36.0	752.7
		4.0	151.8	35.3	967.8
		5.0	150.9	34.4	860.2
		6.0	150.1	33.6	645.2
		7.0	149.5	33.0	483.9
		8.0	149.05	32.5	483.9
Reduced Gravity, Initial Flux = 21,500 BTU/hr ft ²	3	0	154.5	38.0	537.6
		0.2	154.4	37.9	2150.6
		0.5	153.8	37.3	2765.1
		1.2	152.0	35.5	2795.9
		1.7	150.7	34.2	1935.6
		2.2	149.8	33.3	1935.6

^a See Note on page A-2.

TABLE A-1. (Continued)

Test No. 10F40
Heated Surface Downward 2 × 2 in. Heater

Comments	Thermocouple No.	Time (sec)	Temperature (°F)	$T_w - T_{SAT}$ (°F)	Heater Enthalpy Change Rate ^a (BTU/hr ft ²)
Predrop No. 1 Initial Flux = 21,500 BTU/hr ft ²	2	0	152.9	36.4	2365.7
		1.0	150.7	34.2	4408.9
		2.0	146.6	30.1	3441.1
		3.0	143.4	26.9	3441.1
Reduced Gravity, Initial Flux = 21,500 BTU/hr ft ²	2	0	156.1	39.6	2365.7
		0.5	155.0	38.5	1935.6
		1.0	154.1	37.6	2688.3
		2.0	151.6	35.1	2903.4
		3.0	148.9	32.4	2903.4
Predrop No. 1 Initial Flux = 21,500 BTU/hr ft ²	3	0	155.1	38.6	1720.5
		0.5	154.3	37.8	4086.2
		1.0	152.4	35.9	4086.2
		2.0	148.6	32.1	3548.6
		3.0	145.3	28.8	2688.3
		4.0	142.8	26.3	2688.3

^a See note on page A-2.

TABLE A-1. (Concluded)

Test No. 10F40 (Concluded)

Comments	Thermocouple No.	Time (sec)	Temperature (°F)	$T_w - T_{SAT}$ (°F)	Heater Enthalpy Change Rate ^a (BTU/hr ft ²)
Reduced Gravity, Initial Flux = 21,500 BTU/hr ft ²	3	0	157.1	39.6	2365.7
		0.5	156.0	38.5	1935.6
		1.0	155.0	37.6	2688.3
		2.0	152.0	35.1	2903.4
		3.0	149.2	32.4	2473.2
		4.0	147.2	30.1	2473.2

^aSee note on page A-2

TABLE A-2. BUBBLE GROWTH RATE DATA AT 1g

a/g	Time Seconds $\times 10^3$	Bubble Diameter inches	Site	Froude No.
1	2.5	0.014	1	0.71
	5.0	0.024		
	7.5	0.0285		
	10.0	0.0283		
	12.5	0.0285		
1	2.5	0.012	1	0.62
	5.0	0.020		
	7.5	0.025		
	10.0	0.026		
	12.5	0.025		
1	2.5	0.010	2	0.42
	5.0	0.018		
	7.5	0.025		
	10.0	0.028		
	12.5	0.030		
	15.0	0.031		
	17.5	0.033		
1	2.5	0.011	3	0.57
	5.0	0.022		
	7.5	0.022		
	10.0	0.023		
	12.5	0.023		
1	2.5	0.013	3	0.62
	5.0	0.018		
	7.5	0.021		
	10.0	0.025		
	12.5	0.025		

TABLE A-2. (Concluded)

a/g	Time seconds $\times 10^3$	Bubble Diameter inches	Site	Froude No.
1	2.5	0.010	4	0.35
	5.0	0.0175		
	7.5	0.022		
	10.0	0.023		
	12.5	0.025		
	15.0	0.025		
	17.5	0.027		
1	2.5	0.012	5	0.32
	5.0	0.019		
	10.0	0.021		
	15.0	0.022		
	17.5	0.025		
1	2.5	0.017	6	0.22
	5.0	0.018		
	10.0	0.021		
	15.0	0.023		
	17.5	0.026		
	22.5	0.028		
1	2.5	0.010	7	0.16
	5.0	0.018		
	7.5	0.022		
	17.5	0.024		
	25.0	0.026		

TABLE A-3. BUBBLE GROWTH RATE DATA AT LOW g

a/g	Time Seconds $\times 10^3$	Bubble Diameter inches	Site	Froude No.
0.02	2.5	0.023	8	0.2
	4.5	0.029		
	6.5	0.033		
	16.0	0.060		
	44.0	0.080		
	100.0	0.097		
	150.0	0.115		
	188.0	0.126		
	227.0	0.134		
	287.0	0.152		
	346.0	0.162		
	406.0	0.170		
0.02	2.5	0.020	9	0.27
	7.0	0.032		
	13.0	0.037		
	32.0	0.050		
	55.0	0.060		
	90.0	0.078		
	110.0	0.089		
	150.0	0.103		
	200.0	0.119		
	240.0	0.127		
	280.0	0.134		
	320.0	0.140		
0.02	2.5	0.021	10	0.43
	6.0	0.033		
	12.0	0.038		
	18.0	0.042		
	44.0	0.060		
	96.0	0.086		
	121.0	0.090		
	189.0	0.115		
	232.0	0.124		
273.0	0.132			

TABLE A-3. (Continued)

a/g	Time Seconds $\times 10^3$	Bubble Diameter inches	Site	Froude No.
0.02	2.5	0.023	9	0.35
	9.0	0.041		
	21.0	0.055		
	41.0	0.069		
	58.0	0.084		
	81.0	0.098		
	114.0	0.108		
	132.0	0.120		
	166.0	0.126		
	211.0	0.138		
	236.0	0.147		
	289.0	0.167		
306.0	0.165			
0.01	1.2	0.009	3	0.4
	8.1	0.016		
	11.2	0.017		
	21.0	0.029		
	41.0	0.044		
	53.0	0.054		
	67.0	0.058		
	100.0	0.066		
	134.0	0.080		
	183.0	0.094		
	215.0	0.102		
	279.0	0.108		
	311.0	0.120		
	342.0	0.128		
	357.0	0.129		

TABLE A-3. (Continued)

a/g	Time Seconds $\times 10^3$	Bubble Diameter inches	Site	Froude No.
0.01	10.0	0.018	4	9.5
	13.0	0.021		
	16.0	0.029		
	20.0	0.036		
	23.0	0.042		
	26.0	0.043		
	29.0	0.047		
	32.0	0.047		
	35.0	0.053		
	39.0	0.055		
	42.0	0.056		
	45.0	0.058		
	48.0	0.059		
	51.0	0.062		
0.01	10.0	0.025	5	1.6
	13.0	0.031		
	17.0	0.038		
	20.0	0.043		
	23.0	0.049		
	26.0	0.051		
	29.0	0.052		
	32.0	0.055		
	35.0	0.059		
	42.0	0.062		
	48.0	0.064		
	57.0	0.069		
	63.0	0.070		
	70.0	0.073		
	82.0	0.076		
	96.0	0.084		
	111.0	0.091		
	127.0	0.096		
142.0	0.100			
160.0	0.104			

TABLE A-3. (Concluded)

a/g	Time Seconds $\times 10^3$	Bubble Diameter inches	Site	Froude No.
0.01	1.2	0.015	6	2.5
	4.2	0.017		
	7.5	0.019		
	14.1	0.034		
	23.0	0.039		
	39.0	0.044		
	54.0	0.058		
	76.0	0.062		
	107.0	0.074		
0.01	1.2	0.015	7	1.3
	4.2	0.024		
	11.0	0.031		
	20.0	0.037		
	36.0	0.040		
	54.0	0.051		
	69.0	0.060		
	86.0	0.068		
	108.0	0.080		
	149.0	0.088		
164.0	0.090			

APPENDIX B
ERROR ANALYSIS

Heat Flux

Errors in the initial heat flux could be caused by uncertainties in the quantities measured to calculate the flux and by inaccuracies in the prediction of heat losses. The enthalpy change rate of the heater surface also contains errors due to uncertainties in reduced data and in measurements of the physical properties of the heater surface. In the following paragraphs, estimates will be made of the possible errors in these quantities.

The heat losses consist of energy conducted through the thermocouple wires and heater power wires and of losses through the polyurethane insulation behind the heater surface. The loss in the wires was estimated from

$$q_{\text{wire}} = \frac{k A_w}{L_w} (T - T_{\text{sat}}) \quad (1)$$

It was assumed that the wires were at the fluid saturation temperature after passing through the 2 inches of insulation. The total losses from the wires were determined to be insignificant with respect to the energy transferred by boiling at the heater surface.

The heat losses through the insulation were calculated by using the Chrysler Improved Numerical Differencing Analyzer (CINDA) digital computer program [57]. The program is capable of analyzing a three-dimensional lumped parameter representation of a physical system governed by the Fourier equation with an additional heat generation term. In order to use the program, the 2 inch by 4 inch by 2 inch piece of insulation was broken into 48 equal sized nodes. The arrangement consisted of 4 layers of 12 nodes each. The copper heater surface and heater wire were treated as one node with a heat generation source, and the Freon 113 was treated as a constant temperature node at saturation temperature. The heat leak from the surface to the insulation was integrated for the nodes adjoining the surface. For a steady state condition at a power level of 2000 BTU/hr-ft², approximately 1.1 percent of the energy was seen to pass through the insulation. At a power level of 20,000 BTU/hr-ft², the energy loss decreased to approximately 0.2 percent. The heat loss calculations are considered to be accurate to ±20 percent.

The uncertainties associated with the calculation of heat flux and enthalpy change rate will be estimated according to the method of Kline and McClintock [58] who define the uncertainty as

$$\omega_R = \left[\left(\frac{\partial R}{\partial v_1} \omega_1 \right)^2 + \left(\frac{\partial R}{\partial v_2} \omega_2 \right)^2 + \dots + \left(\frac{\partial R}{\partial v_n} \omega_n \right)^2 \right]^{1/2} \quad (2)$$

where R is the functional relationship being investigated, v_n are the independent variables, and ω_n the variation of the variables. For the heat flux calculation,

$$q = C \frac{V_h I}{LW} \quad (3)$$

and equation (2) in terms of the quantities of interest is

$$\Delta q = \left[\left(\frac{\partial q}{\partial I} \Delta I \right)^2 + \left(\frac{\partial q}{\partial V_h} \Delta V_h \right)^2 + \left(\frac{\partial q}{\partial W} \Delta W \right)^2 + \left(\frac{\partial q}{\partial L} \Delta L \right)^2 \right]^{1/2} \quad (4)$$

Performing the indicated operations and dividing by equation (3) to nondimensionalize,

$$\frac{\Delta q}{q} = \left[\left(\frac{\Delta I}{I} \right)^2 + \left(\frac{\Delta V_h}{V_h} \right)^2 + \left(\frac{\Delta W}{W} \right)^2 + \left(\frac{\Delta L}{L} \right)^2 \right]^{1/2} \quad (5)$$

The individual terms are estimated to be

$$\frac{\Delta I}{I} = 0.03$$

$$\frac{\Delta V_h}{V_h} = 0.03$$

$$\frac{\Delta L}{L} = 0.004$$

$$\frac{\Delta W}{W} = 0.008$$

Substituting these terms into equation (5), the uncertainty for heat flux is found to be 4.35 percent.

For the enthalpy change rate calculation,

$$\frac{q}{A} = \frac{Mc}{LW} \frac{dT}{dt} \quad (6)$$

Using equation (2) again,

$$\frac{\Delta(q/A)}{q/A} = \left[\left(\frac{\Delta M}{M} \right)^2 + \left(\frac{\Delta c}{c} \right)^2 + \left(\frac{\Delta L}{L} \right)^2 + \left(\frac{\Delta W}{W} \right)^2 + \left(\frac{\Delta \left(\frac{dT}{dt} \right)}{\frac{dT}{dt}} \right)^2 \right]^{1/2} \quad (7)$$

The individual terms are estimated to be

$$\frac{\Delta M}{M} = 0.001$$

$$\frac{\Delta c}{c} = 0.001$$

$$\frac{\Delta L}{L} = 0.004$$

$$\frac{\Delta W}{W} = 0.008$$

$$\frac{\Delta \left(\frac{dT}{dt} \right)}{\frac{dT}{dt}} = 0.1$$

Substituting these terms into equation (7), the uncertainty for enthalpy change rate is found to be slightly greater than 10 percent.

Surface Temperature

As a result of the calibration procedure described in the text, it is estimated that the accuracy of the thermocouples are within 0.2 °F. Due to the wide span used on the strip charts, it is believed that the thermocouple output trace was read within 0.1 °F. Considering these factors, it appears that an estimate of ±1 °F for the uncertainty of the absolute value of temperature is reasonable. The error associated with the temperature gradient should be no greater than the reading error for the charts.

It is estimated that the thermocouples were located in the center of the copper surface. The actual temperature of the surface can be found from

$$T_{tc} - T_w = \frac{q_w t_p}{2k} \quad (8)$$

Using this equation, the temperature at the point of measurement is found to deviate from the actual surface temperature by approximately 0.07 °F at a heat flux of 6000 BTU/hr-ft² and by 0.23 °F at a heat flux of 20,000 BTU/hr-ft².

Bubble Diameters

As explained in the text, the calibration readings for the probe used for a reference dimension in the bubble studies were always within 3 percent of each other. Considering the possibility of error in measuring the probe

prior to installation, it is estimated that a maximum error of 6 percent might be present in the bubble measurements.

APPENDIX C

FROUDE NUMBER CALCULATION

The expression used to calculate the Froude numbers in this work was derived using the method presented by Adelberg [56']. The bubbles in Freon 113 were found to be more nearly spherical than hemispherical, as was assumed by Adelberg. The Froude number expression is the same as found by Adelberg, however, due to the nature of the Froude number.

The Froude number is defined as the ratio of the bubble dynamic force, F_D , to the buoyancy force associated with the bubble, F_B . The force associated with the inertia of the mass of liquid displaced by the bubble growth with velocity \dot{R} is defined as the dynamic force. For a spherical bubble,

$$F_D = \frac{d}{dt} \left(\frac{4}{3} \rho_l \pi R^3 \dot{R} \right) = 4 \pi \rho_l \left(R^2 \ddot{R} + \frac{R^3 \dot{\dot{R}}}{3} \right) \quad (1)$$

The buoyancy force associated with the bubble is

$$F_B = \frac{4}{3} \pi R^3 g (\rho_l - \rho_v) \quad (2)$$

It has been found that \ddot{R} is generally quite small when compared to the growth rate, \dot{R} , and this can be seen to be especially true for Freon 113 at both standard and reduced gravity (Figures 22 and 23) in the latter growth

stage. The second term of the dynamic force equation may then be neglected. Since $\rho_l \ll \rho_v$, ρ_l will also be neglected. The expression for Froude number then becomes,

$$F = \frac{3\dot{R}^2}{Rg} \quad (3)$$

A further approximation was made by Adelberg by assuming that

$$\dot{R} = \frac{R_{\max}}{t_{\max}} \quad (4)$$

where R_{\max} is the radius of the bubble when it detaches from the surface and t_{\max} is the time from bubble nucleation to bubble departure. The final approximate expression for Froude number is then

$$F = \frac{3 R_{\max}}{g t_{\max}^2} \quad (5)$$

REFERENCES

1. Zuber, N.: Recent Trends in Boiling Heat Transfer Research, Part I: Nucleate Pool Boiling. *Applied Mechanics Review*, 17, No. 9, 1964.
2. Siegel, R., and Usiskin, C.: A Photographic Study of Boiling in the Absence of Gravity. *Trans. ASME, Series C, J. of Heat Transfer*, 81, 1959.
3. Usiskin, C., and Siegel, R.: An Experimental Study of Boiling in Reduced and Zero Gravity Fields. *Trans. ASME, Series C, J. of Heat Transfer*, 83, 1961.
4. Schwartz, S. H.: Saturated Pool Boiling of Water in a Reduced Gravity Environment. Ph.D. Thesis, University of Southern California, Los Angeles, California, 1966.
5. Sherley, J. E.: Nucleate Boiling Heat Transfer Data for Liquid Hydrogen at Standard and Zero Gravity. *Advances in Cryogenic Engineering*, Vol. 8, Plenum Press, 1963.
6. Merte, H., and Clark, J. A.: Boiling Heat Transfer with Cryogenic Fluids at Standard, Fractional, and Near-Zero Gravity. *Trans. ASME, Series C, J. of Heat Transfer*, 86, 1964.
7. Clodfelter, R. G.: Low Gravity Pool Boiling Heat Transfer. Air Force Aero Propulsion Laboratory, Wright Patterson Air Force Base, Ohio, Technical Documentary Report No. APL-TDR-64-19, 1964.
8. Siegel, R., and Keshock, E. G.: Nucleate and Film Boiling in Reduced Gravity from Horizontal and Vertical Wires. NASA Technical Report R-216, 1965.
9. Hedgepeth, L., and Zara, E.: Zero Gravity Pool Boiling. Aeronautical Systems Division, Wright-Patterson Air Force Base, Ohio, Technical Report ASD-TDR-63-706, 1963.

REFERENCES (Continued)

10. Rex, J., and Knight, B. A.: An Experimental Assessment of the Heat Transfer Properties of Propane in a Near-Zero Gravity Environment. Royal Air Force Establishment Technical Note No. 69, Ministry of Aviation, London, England, 1964.
11. Papell, S. S., and Faber, O. C., Jr.: Zero and Reduced Gravity Simulation on a Magnetic Colloid Pool Boiling System. NASA Technical Note TN D-3288, 1966.
12. Graham, R. W., and Hendricks, R. C.: A Study of the Effect of Multi-G Accelerations on Nucleate Boiling Ebullition. NASA Technical Note TN-D1196, 1963.
13. Merte, H., and Clark, J. A.: Pool Boiling in an Accelerating System. Trans. ASME, Series C, J. of Heat Transfer, August 1961.
14. Costell, C. P., and Tuthill, W. E.: Effects of Acceleration on Nucleate Pool Boiling. Chemical Engineering Symposium Series, Vol. 57, No. 32, 1961.
15. Graham, R. W., Hendricks, R. C., and Ehlers, R. C.: Analytical and Experimental Study of Pool Heating of Liquid Hydrogen Over a Range of Accelerations. NASA Technical Note D-1883, 1964.
16. Githinji, P. M., and Sabersky, R. H.: Some Effects of Orientation of the Heating Surface in Nucleate Boiling. Trans. ASME, Series C, J. of Heat Transfer, 85, No. 4, 1963.
17. Marcus, B. D., and Dropkin, D.: The Effect of Surface Configuration on Nucleate Boiling Heat Transfer. Int. J. of Heat Mass Transfer, 6, 1963.
18. Coeling, K. J.: Incipient Boiling of Cryogenic Liquids. Ph.D. Thesis, University of Michigan, Ann Arbor, Michigan, 1967.
19. Class, C. R., DeHann, J. R., Piccone, M., and Cost, R. B.: Boiling Heat Transfer to Liquid Hydrogen from Flat Surfaces. K. D. Timmerhaus, Advances in Cryogenic Engineering, 5, Plenum Press, 1960.

REFERENCES (Continued)

20. Bosnjakovic, F.: Verdampfung und Flussigkeitsuberhitzung. Tech. Mech. und Therm., Bd. 1, 1930.
21. Jacob, M.: Kondensation and Verdampfung. Zetschr. d. Ver. Deutsch. Ingr., Bd. 76, 1932.
22. Fritz, W., and Ende, W.: Verdampfungsvorgang nach Kinematographischen Aufnahmen an Dampfblasen. Phys. Zeitsh, 37, 1936.
23. Siegel, R., and Keshock, E. G.: Effects of Reduced Gravity on Nucleate Boiling Bubble Dynamics in Saturated Water. AIChE Journal, 10, No. 4, July 1964.
24. Plesset, M. S. and Zwick, S. A.: The Growth of Vapor Bubbles in Superheated Liquids. Journal of Applied Physics, 25, No. 4, April 1954.
25. Dergarabedian, P.: The Rate of Growth of Vapor Bubbles in Superheated Water. Journal of Applied Mech., 20, 1953.
26. Hewitt, H. C., and Parker, J. D.: Bubble Growth and Collapse in Liquid Nitrogen. ASME Paper No. 67-WA/HT-10.
27. Forster, H. K., and Zuber, N.: Growth of a Vapor Bubble in a Superheated Liquid. Journal of Applied Physics, 25, No. 4, 1954.
28. Zuber, N.: Hydrodynamic Aspects of Boiling Heat Transfer. Ph.D. Thesis, University of California, Los Angeles, 1959.
29. Griffith, P.: Bubble Growth Rates in Boiling. Trans. ASME, Series C, J. of Heat Transfer, 80, 1958.
30. Bankoff, S. G., and Mikesell, R. D.: Growth of Bubbles in a Liquid of Initially Nonuniform Temperature. ASME, Paper 58-A-105, 1959.
31. Hsu, Y. Y., and Graham, R. W.: An Analytical and Experimental Study of the Thermal Boundary Layer and Ebullition Cycle in Nucleate Boiling. NASA TN D-594, May 1961.

REFERENCES (Continued)

32. Cochran, T. H., Aydelott, J. C., and Frysinger, T. C.: The Effect of Subcooling and Gravity Level on Boiling in the Discrete Bubble Region. NASA Technical Note TN D-3449, 1966.
33. Rehm, T. R.: Gravity as a Removal Force in Nucleate Boiling. AIChE, Symposium on Effects of Zero Gravity on Fluid Dynamics and Heat Transfer - Part II, Houston, Texas, Preprint 24b, 1965.
34. Keshock, E. G., and Siegel, R.: Forces Acting on Bubbles in Nucleate Boiling Under Normal and Reduced Gravity Conditions. NASA Technical Note TN D-2299, 1964.
35. McGrew, J. L., and Larkin, B. K.: Cryogenic Liquid Experiments in Orbit: Volume II, Bubble Mechanics, Boiling Heat Transfer, and Propellant Tank Venting in a Zero-Gravity Environment. NASA Contractor Report CR-652, 1966.
36. Fritz, W.: Berechnung des Maximalvolumens von Dampfblasen. Physik Zeitschrift, 36, 1935.
37. Jacobs, J. D., and Shade, A. H.: Measurement of Temperatures Associated with Bubbles in Subcooled Pool Boiling. ASME Paper 68-HT-47.
38. Lippert, T. E., and Dougall, R. S.: A Study of the Temperature Profiles Measured in the Thermal Sublayer of Water, Freon 113, and Methyl Alcohol During Pool Boiling. ASME Paper 68-HT-7.
39. Sharp, R. R.: The Nature of Liquid Film Evaporation During Nucleate Boiling. NASA TN D-1997.
40. Torikai, K., and Yamazaki, T.: Dry State in a Contact Area of a Boiling Bubble on a Heating Surface. Bull. JSME, Vol. 38, April 1967.
41. Moore, F. D., and Mesler, R. B.: Microlayer Vaporization - A New Hypothesis About Nucleate Boiling Based on Recent Experimental Evidence. AIChE Journal, Vol. 7, 1961.
42. Rogers, T. F., and Mesler, R. B.: An Experimental Study of Surface Cooling by Bubbles During Nucleate Boiling of Water. AIChE Journal, September 1964.

REFERENCES (Continued)

43. Synder, N. W., and Robin, T. T.: Mass-Transfer Model in Subcooled Nucleate Boiling. ASME Paper 68-HT-51.
44. McAdams, W. H.: Heat Transmission. 3rd. Ed., New York, McGraw-Hill Book Company, Inc., 1954.
45. Bashford, F., and Adams, J. C.: An Attempt to Test Theories of Capillary Action by Comparing the Theoretical and Measured Forms of Drops of Fluid. Cambridge University Press, 1883.
46. Goldsmith, A., Waterman, T. E. and Hirschorn, H. J.: Handbook of Thermophysical Properties of Solid Materials, Volume I: Elements. The Macmillan Co., New York, 1961.
47. Lippert, T. E.: An Experimental Investigation of the Role of Thermal Fluctuations on Nucleate Boiling in the Region of Isolated Bubbles. MS Thesis, University of Pittsburgh, 1967.
48. Mixon, F. O., Jr., Chon, W. Y., and Beatty, K. O., Jr.: The Effect of Electrolytic Gas Evolution on Heat Transfer. Chem. Engr. Progr. Symposium Series, No. 30, 56, 1960.
49. Rallis, G. J., and Jawurek, H. K.: Latent Heat Transfer in Saturated Nucleate Boiling. Int. J of Heat and Mass Transfer, 7, 1964.
50. Zuber, N.: Nucleate Boiling. The Region of Isolated Bubbles and the Similarity with Natural Convection. Int. Journal of Heat and Mass Transfer, Vol. 6, 1963.
51. Tien, C. L.: A Hydrodynamic Model for Nucleate Pool Boiling. International Journal of Heat and Mass Transfer, Vol. 5, 1962.
52. Han, Chi-Yeh, and Griffith, P.: The Mechanism of Heat Transfer in Nucleate Pool Boiling - Part II. International Journal of Heat and Mass Transfer, Vol. 8, No. 6; 1965.

REFERENCES (Concluded)

53. Moore, F. D., and Mesler, R. B.: The Measurements of Rapid Surface Temperature Fluctuations During Nucleate Boiling of Water. American Institute of Chemical Engineers Journal, Vol. 7, No. 4, 1961.
54. Hendricks, R. C., and Sharp, R. R.: Initiation of Cooling Due to Bubble Growth on a Heating Surface. NASA TN D-2290, Lewis Research Center, 1964.
55. Hospeti, N. B.: Investigation of Microlayer Vaporization Mechanism in Pool Boiling of Water at Atmospheric Pressure. Ph.D. Thesis, University of Kansas, 1966.
56. Adelberg, M.: Gravitational Effect Upon Nucleate Boiling Heat Transfer. Advances in the Astronautical Sciences, Vol. 14, American Astronautical Society, 1963.
57. Chrysler Improved Numerical Differencing Analyzer. Space Division, Chrysler Corporation Technical Note TN-AP-66-15.
58. Kline, S. J., and McClintock, F. A.: The Description of Uncertainties in Single Sample Experiments. Mechanical Engineering, Vol. 75, 1953.

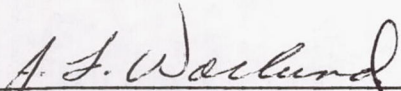
NUCLEATE POOL BOILING OF SATURATED FREON 113
IN A REDUCED GRAVITY ENVIRONMENT

By

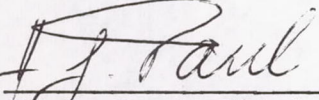
Jerrold Wayne Littles

The information in this report has been reviewed for security classification. Review of any information concerning Department of Defense or Atomic Energy Commission programs has been made by the MSFC Security Classification Officer. This report, in its entirety, has been determined to be unclassified.

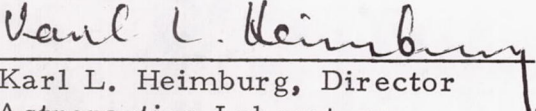
This document has also been reviewed and approved for technical accuracy.



A. L. Worlund, Chief
Fluid Mechanics and Dynamics Branch



H. G. Paul, Chief
Propulsion and Thermodynamics Division



Karl L. Heimburg, Director
Astronautics Laboratory

DISTRIBUTION

S&E-ASTN-DIR

S&E-ASTN-P

S&E-ASTN-PL

S&E-ASTN-PT

S&E-ASTN-PF

S&E-ASTN-RM

A&TS-MS-IP

A&TS-MS-IL (8)

A&TS-TU (6)

A&TS-MS-H

PAT

PM-PR

Mr. Heimburg

Dr. Head

Mr. Paul

Mr. Wood

Mr. Hopson

Mr. Moses

Dr. Littles (10)

Mr. Vaniman

Mr. Worlund

Mr. Hastings

Miss Scott

Scientific and Technical Information Facility (25)

P. O. Box 33

College Park, Maryland 20740